NUMERICAL ANALYSIS OF PHASE CHANGE MATERIAL FOR ENERGY STORAGE SYSTEM

WAN KHAIRUL MUZAMMIL B ABDUL RAHIM

FACULTY OF ENGINEERING
UNIVERSITY OF MALAYA
KUALA LUMPUR

2012

NUMERICAL ANALYSIS OF PHASE CHANGE MATERIAL FOR ENERGY STORAGE SYSTEM

WAN KHAIRUL MUZAMMIL B ABDUL RAHIM

RESEARCH REPORT SUBMITTED IN PARTIAL FULFILMENT OF THE REQUIREMENT FOR DEGREE OF MASTER OF ENGINEERING

FACULTY OF ENGINEERING
UNIVERSITY OF MALAYA
KUALA LUMPUR

2012

UNIVERSITI MALAYA

ORIGINAL LITERARY WORK DECLARATION

Name of Candidate: WAN KHAIRUL MUZAMMIL B ABD RAHIM (I.C/Passport No:)

Registration/Matric No: KGH100032

Name of Degree: M.Eng. MECHANICAL ENGINEERING

Title of Project Paper/Research Report/Dissertation/Thesis ("this Work"):

NUMERICAL ANALYSIS OF PHASE CHANGE MATERIAL
FOR ENERGY STORAGE SYSTEM

Field of Study: ENERGY

I do solemnly and sincerely declare that:

(1) I am the sole author/writer of this Work;
(2) This Work is original;
(3) Any use of any work in which copyright exists was done by way of fair dealing and for permitted purposes and any excerpt or extract from, or reference to or reproduction of any copyright work has been disclosed expressly and sufficiently and the title of the Work and its authorship have been acknowledged in this Work;
(4) I do not have any actual knowledge nor do I ought reasonably to know that the making of this work constitutes an infringement of any copyright work;
(5) I hereby assign all and every rights in the copyright to this Work to the University of Malaya ("UM"), who henceforth shall be owner of the copyright in this Work and that any reproduction or use in any form or by any means whatsoever is prohibited without the written consent of UM having been first had and obtained;
(6) I am fully aware that if in the course of making this Work I have infringed any copyright whether intentionally or otherwise, I may be subject to legal action or any other action as may be determined by UM.

Candidate's Signature Date

Subscribed and solemnly declared before,

Witness's Signature Date

Name:
Designation:

ACKNOWLEDGEMENT

I hereby would like to express my utmost gratitude towards my supervisor and mentor; Prof. Dr. T.M.I. Mahlia for his continuous guidance, motivation, patience and help during the entire period of this research report was written. To my dearly loved wife, for her constant inspiration, encouragement and strength which helps me to cope with all the challenges during my course of study. And to my beloved parents and sisters, anchors of my life; thank you for giving me the courage to face the unknown.

ABSTRACT

A numerical method based on the effective heat capacity method was studied to solve the phase change heat transfer problems of a phase change material in a cylindrical latent heat thermal energy storage device during the charging (melting) process of the material. The commercial software COMSOL Multiphysics was employed to run the numerical simulations. The effective heat capacity method was used to characterize the fusion heat of melting of the phase change material and the moving boundary of solid-liquid interface. An analytical tool was used to validate the phase change heat transfer process in which the results show a good agreement between the numerical and analytical analysis. Subsequently, the effects of fins and various heat transfer velocities on the thermal behavior of the PCM were studied numerically using the software. Generally, the results obtained from the analysis show that the heat transfer rate increases as the number of fins and HTF velocities were increased. For small number of fins configurations, the effect of increasing the HTF velocities are not so significant, as the thermal resistance of the phase change material is high. However, the effect is more evident as the number of fins increases; due to the decreasing thermal resistance on the PCM side.

ABSTRAK

Suatu kaedah berangka berdasarkan kaedah muatan haba berkesan telah dikaji untuk menyelesaikan masalah pemindahan haba bagi suatu bahan ubah fasa di dalam alat penyimpan tenaga haba pendam berbentuk silinder semasa proses pelakuran bahan tersebut. Perisian komersial *COMSOL Multiphysics* telah digunakan untuk menjalankan simulasi berangka berdasarkan kaedah muatan haba berkesan. Kaedah tersebut digunakan untuk menggambarkan ciri-ciri pelakuran bahan ubah fasa dan pergerakan sempadan antara fasa-fasa pepejal dan cecair. Analisa ke atas bahan ubah fasa telah dilakukan untuk pengesahsahihan proses ubah fasa. Pengiraan yang dibuat telah menunjukkan hasil yang baik antara kaedah berangka dan kaedah analisa yang digunakan. Seterusnya, suatu ujikaji ke atas kesan penambahan sirip dan pengunaan bendalir pindah haba berlainan halaju telah dilakukan menggunakan perisian *COMSOL*. Secara amnya, hasil daripada ujikaji yang dijalankan menunjukkan bahawa kadar pemindahan haba meningkat dengan bertambahnya jumlah bilangan sirip dan peningkatan halaju bendalir pindah haba di dalam alat penyimpan tenaga haba pendam tersebut. Bagi jumlah konfigurasi sirip yang kecil, kesan peningkatan halaju bendalir pindah haba adalah tidak signifikan kerana rintangan terma di dalam bahan ubah fasa adalah tinggi. Walaubagaimanapun, rintangan terma itu berkurangan apabila jumlah sirip bertambah.

Table of Contents

List of Tables

List of Figures

List of Symbols and Abbreviations

SYMBOL	
C_{ap}	Average specific heat between T_i and T_f (J/kg.K)
C_k	Specific heat of phase k in PCM (J/kg.K)
C_p	Specific heat (J/kg.K)
$C_{p,eff}$	Effective heat capacity (J/kg.K)
$C_{p,l}$	Liquid PCM specific heat (J/kg.K)
$C_{p,pcm}$	Modified heat capacity (J/kg.K)
$C_{p,s}$	Solid PCM specific heat (J/kg.K)
C_{lp}	Average specific heat between T_m and T_f (J/kg.K)
C_{sp}	Average specific heat between T_i and T_m (J/kg.K)
f	Melt fraction
$flc2hs$	COMSOL function
g	Acceleration of gravity (m/s^2)
H	Total volumetric enthalpy (J/m^3)
h	Sensible volumetric enthalpy (J/m^3)
$\bar{h}$	Prescribed function of $t > 0$
Δh_m	Heat of fusion per unit mass (J/kg)
Δh_r	Endothermic heat of reaction
k	Thermal conductivity (W/m.K)
k_k	Thermal conductivity of phase k in PCM (J/kg.K)
L	Latent heat of fusion (J/kg)
m	Mass (kg)
$\vec{n}$	Normal to
P	Pressure (Pa)
Q	Energy stored (J)
q	Heat flux (W/m^2)
R,r	Cylindrical coordinate (m)
r	Radius (m)
$S(t)$	Location of solid-liquid interface as a function of time (m)
Ste	Stefan number
T	Temperature (K)
t	Time (s)
u	Velocity (m/s)
X,x	Space coordinate (m)
Z,z	Space coordinate (m)

GREEK LETTERS

α	Thermal diffusivity of PCM (m^2/s)
α_m	Fraction melted
α_r	Fraction reacted
β	Constant
η	Similarity variable
θ	Angle (°)
ρ	Density (kg/m^3)
μ	Dynamic viscosity ($N.s/m^2$)
ν	Kinematic viscosity (m^2/s)
ϕ	Viscous dissipation (m^2/s^2)

SUBSCRIPT

f	Final
i	Initial
in	Inlet
l	Liquid
m	Melting
r	In the radial direction
s	Solid
w	Wall

GENERAL

DOF	Degree of freedom
FEM	Finite element method
HTF	Heat transfer fluid
LHTES	Latent heat thermal energy storage
PCM	Phase change material
SHS	Sensible heat storage
SHZ	Slow Heating Zone
TES	Thermal energy storage

CHAPTER 1

INTRODUCTION

1.1 Background of study

In the interest of reducing energy usage in a wide variety of industrial and commercial applications, many efforts have been initiated to utilize renewable energy sources and to enhance the usage of waste energy. One way to solve the issue of wasted energy is by storing the excess energy into thermal energy storage (TES) which would increase the efficiency of energy consumption and production. TES can be categorized as sensible, latent, or the combination of these two types of heat systems. Between these two types of thermal energy storage systems; latent heat thermal energy storage (LHTES) system is a more attractive technology due to its higher density of energy storage capabilities. Furthermore, as comparison to the conventional sensible heat thermal energy storage system, LHTES system has smaller volume and less weight for a given amount of energy stored.

Latent heat storage using phase change materials (PCMs) have been gaining much attention over the last few decades due to its capability to store heat of fusion at a constant or near constant temperature which corresponds to the solid-liquid phase change material. During the charging (or melting) process, the thermal energy is stored in phase change materials, and recovered during the discharging (or freezing) process (Zalba et al., 2003, Sharma et al., 2009, Benli and Durmus, 2009). Various industrial, commercial and laboratorial

applications have adopted the use of latent heat thermal energy storage system such as in solar energy heating system (Saman et al., 2005, Shukla et al., 2009, Hasnain, 1998), waste heat recovery (Azpiazu et al., 2003, Go et al., 2004) and conservation of energy in building (Kuznik et al., 2008, Tyagi and Buddhi, 2007, Liu and Chung, 2005).

For the current study, the latent heat thermal energy storage can be applied in a solar hot water system application as shown in Fig. 1.1. When solar energy is available, the cold heat transfer fluid (HTF) is pumped to the solar collector whilst the isolation valve connecting the hot and cold pipes is closed. The high temperature fluid from the solar collector then flows through the latent heat thermal energy storage device and melts (charging process) the PCM inside. The high temperature fluid continues to flow into the water tank, heating the cold water supply. At night, when there is no solar energy available the valves leading to and from the solar collector are closed, and the isolation valve between the hot and cold pipes is opened; creating a shorter route for the HTF. The discharging process occurs where the thermal energy from the PCM is transferred to the HTF, increasing its temperature and then flows into the water tank. The discharging/solidification process however is not included in the scope of research. On the other hand, the focus of the study is to investigate the effects of fins and HTF velocities on the thermal behavior of the PCM in the LHTES device.

1.2 Statement of problem

For this study, an investigation of a phase change material; namely paraffin wax is used in a cylindrical latent heat thermal energy storage device to analyze the effects of fins in the system and the velocities of heat transfer fluids on the melting of PCM.

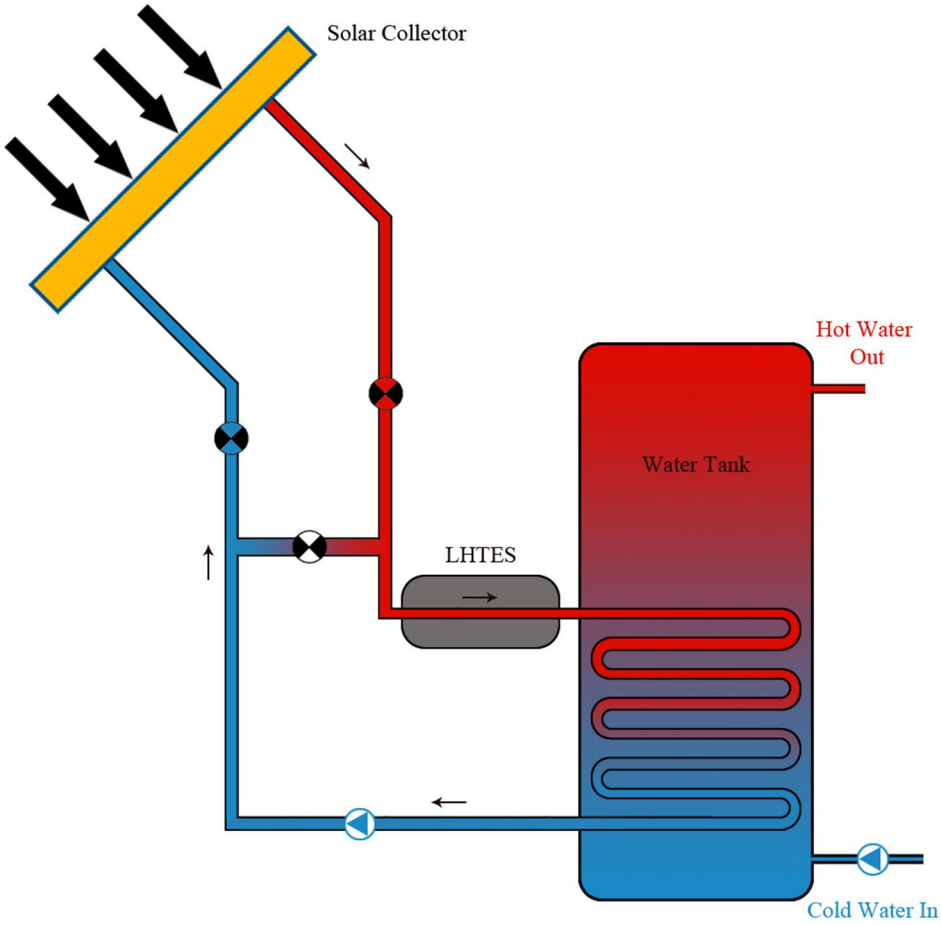

Fig. 1.1. Schematic diagram of a solar water heater system with LHTES.

1.3 Objectives of study

The objectives of this research study are as follows:-

1. To study a method of numerical analysis pertaining to phase change heat transfer problems in a cylindrical latent heat thermal energy storage device during the charging process through the use of commercial software COMSOL Multiphysics.
2. To investigate the effects of thermal enhancers or fins in cylindrical latent heat thermal energy storage device as well as the effects of heat transfer fluid velocities on the thermal behavior of phase change material.

1.4 Research scope

The scope of this study mainly focuses on the effects of the addition of fins and heat transfer velocities on the thermal behavior of the phase change material. The geometry of the thermal storage device is translated into the COMSOL software where various mathematical equations and boundary conditions are solved numerically through the use of finite element analysis method in the software. Validation on the numerical study results of the phase change process (Stefans problem) for a semi-infinite slab is carried out using analytical tool. Afterwards, study on the effects of fins and the velocities of the thermal fluid are presented in the subsequent chapters where the latent heat thermal energy storage system numerical results are summarized and discussed.

1.5 Research methodology

The research methodology can be simply explained with the following steps:

Step 1: Selection of geometry, fins and dimensions of the LHTES.

Step 2: Translate the desired geometry into COMSOL Multiphysics.

Step 3: Materials for the system are assigned to its individual parts.

Step 4: Meshing of the geometry.

Step 5: Carry out the finite element analysis through the use of COMSOL.

Step 6: Extract the relevant data and discuss.

Step 7: Present the conclusions of the study.

1.6 Organization of research report

Chapter 1

This chapter consists of a background of study of the research project. Furthermore, a simple discussion on an overview of the project methodology is presented as well as the outline of the study.

Chapter 2

The second chapter consists of literature review on the study of the latent heat thermal energy storage where various geometries used in recent researches are presented as well as discussion on different phase change materials.

Chapter 3

This chapter includes the discussions on the geometrical arrangement, dimensions and the materials used for the numerical studies on the LHTES device. Also in this chapter, the governing physical equations and mathematical formulations used in the study are presented.

Chapter 4

The fourth chapter describes about an analytical validation of the numerical results data obtained from the simulation of heating a semi-infinite paraffin slab.

Chapter 5

The results and discussion obtained from the numerical study of an axisymmetric 2D latent heat thermal energy storage is presented in the fifth chapter.

Chapter 6

This chapter concludes the main findings of the research report.

CHAPTER 2

LITERATURE REVIEW

2.1 Thermal energy storage systems

Renewable energy has become one of the most important topics recently which has seen various developments and critical breakthroughs in technological advancement in order to optimize the use of energy more efficiently. The high level of greenhouse gas emissions and the ever increasing of fuel prices played a major and yet destructive role to realize the importance of utilizing energy as efficient as possible to reduce the waste of energy into the environment. There are many new and renewable energy methods that can be utilized to extract energy from the wasted or exhausted energy sources. Energy storage devices are one of the most widely used technique that can be implemented in most industrial and commercial applications. The disparity between demand and supply can be reduced through the use of energy storage. Furthermore, the reliability and performance of energy systems can be enhanced which can be an advantage to conserve the energy used (Garg et al., 1985).

In the past few decades, the use of phase change materials to store thermal energy has been used in many researches due to its great prospect and commercial values (Dutil et al., 2011, Agyenim et al., 2010, Sharma et al., 2009, Nayak et al., 2006, Anica, 2005, Rosen and Dincer, 2003). Thermal energy storage systems can be used to collect energy at a certain period and deliver it in a later time, increase the efficiency of a refrigerator (Cheng et al.,

2011) or to provide output stability for any plants in areas with cloudy weather conditions. The types of thermal energy storage can be classified by the different forms of the change in internal energy of the materials used in the devices. A summary of the different types of thermal energy storage is illustrated in Fig. 2.1 (Baylin, 1979).

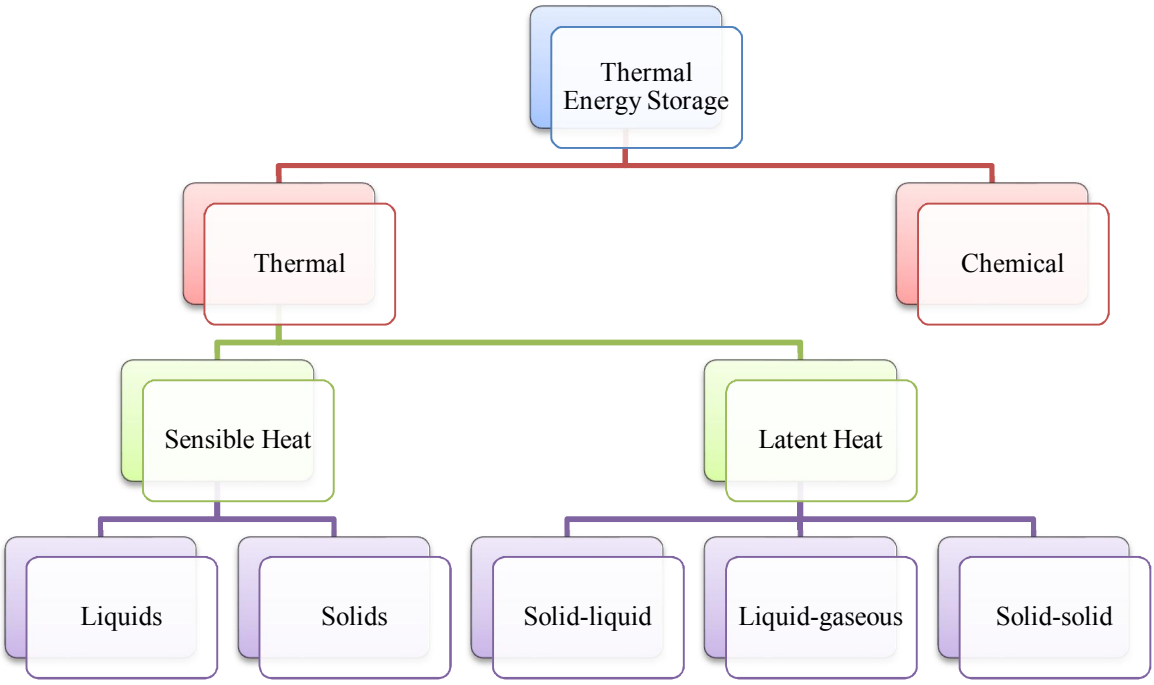

Fig. 2.1. Various types of thermal energy storage.

2.1.1 Sensible heat energy storage

Sensible heat storage (SHS) involves the storing of energy by raising the temperature of a medium (solid or liquid) with high heat capacity. The storage medium can be water, bricks, sand, rock beds, oil or soil. Together with a container, and input/output device is attached to it to provide thermal energy for any intended application. Most commonly used in dwellings, SHS is used as heat storage to provide hot water for houses and offices. The system depends heavily on the heat capacity and the change in the temperature of the

medium during the charging and discharging process. Furthermore, the amount of total energy that can be stored in the system depends on the specific heat of the medium, the volume of the material used and the temperature change (Lane, 1983). Hence, the total energy stored in a sensible heat energy storage system can be calculated by using the following equation:

$$Q = \int_{T_i}^{T_f} mC_p dT \tag{2.1}$$

$$Q = mC_{ap}(T_f - T_i) \tag{2.2}$$

Where T_f and T_i denote the final and initial temperatures; whereas C_{ap} denotes the average specific heat between the initial and final temperatures. However, SHS systems have a few disadvantages. There are: (i) Non-isothermal behavior during charging (storing of heat) and discharging (releasing of heat) processes, and (ii) Low heat storage capacity per unit volume of the medium.

2.1.2 Thermochemical heat energy storage

In thermochemical energy storage system, the energy is stored after a breaking or dissociation reaction of chemical bonds at molecular level which releases energy and then recovered in a completely reversible chemical reaction. The thermochemical energy storage system process can be illustrated by the following equation which describes the amount of heat that can be stored is directly dependent on the amount of storage material, the extent of conversion and the endothermic heat of reaction (Sharma et al., 2009):

$$Q = a_r m \Delta h_r \tag{2.3}$$

where Δh_r is the endothermic heat of reaction, m is the mass of heat storage medium and a_r is the fraction reacted. To date, thermochemical heat energy storage has not yet been used in practical applications due to a few economical and technical aspects that needed to be improved before it becomes viable (Agyenim et al., 2010).

2.1.3 Latent heat energy storage

Latent heat storage system is based on the high latent heat of a phase change material which stores the released energy through the phase change process of the storage medium that occurs at specific temperature range. The phase change process can either be from solid to liquid, liquid to gas or vice versa. The storage capacity of any latent heat energy storage system is given by (Lane, 1983):

$$Q = \int_{T_i}^{T_m} mC_p \mathrm{d}T + ma_m \Delta h_m + \int_{T_m}^{T_f} mC_p \mathrm{d}T \tag{2.4}$$

$$Q = m\left[C_{sp}(T_m - T_i) + a_m \Delta h_m + C_{lp}(T_f - T_m)\right] \tag{2.5}$$

Where T_m denotes the melting temperature, a_m is the melted fraction, Δh_m is the heat of fusion per unit mass, C_{sp} is the average specific heat between T_i and T_m, whereas C_{lp} denotes the average specific heat between T_m and T_f. From the various thermal heat storage methods discussed in the previous subsections, latent heat thermal energy storage system offers better and attractive prospects due to its larger heat storage density at constant or nearly constant temperature that corresponds to the phase-transition temperature of the PCM (Sharma et al., 2009). The phase change processes can be in many forms: solid-solid,

solid-liquid, solid-gas, liquid-gas and vice versa. However, solid-liquid phase transitions have been proved to be more economically viable for thermal energy storage applications.

2.2 Phase change materials used in latent heat energy storage

Phase change materials or PCM are specifically used in latent heat energy storage systems, and thus PCM can also be called latent heat storage material. As discussed previously, the thermal energy transfer of PCM occurs during the charging or discharging process at which the state or phase of the material changes from solid to liquid, or liquid to solid. At the start of the heating of the material, the PCM temperature rises as it absorbs the thermal energy. When the material reaches a specific temperature range; it will start to melt as the material begins to experience a phase transition from solid to liquid state. However, unlike sensible heat storage materials; during the phase transition process the PCM releases or absorbs heat at a constant or nearly constant temperature.

In many studies conducted previously; it has been proved that in comparison latent heat energy storage has lower storage volume than sensible heat energy storage system. Studies by Ghoneim (Ghoneim, 1989) and Morrison and Abdel-Khalik (Morisson and Abdel-Khalik, 1978) show that sensible heat storage material or a rock requires more than 5 times the storage mass of medicinal paraffin, 7 times that of Paraffin 116 Wax (P116-Wax) and 8 times that of $Na_2SO_4.10H_2O$ to store the same amount of energy from a unit collector area.

2.2.1 Desirable properties of phase change materials

Many authors have experimented with different types of PCMs, subdividing them into organic, inorganic and eutectic types. There are several properties that governs the selection of phase change materials which are describe as follows (Abhat, 1983):

Thermal properties

i. Suitable melting temperature range for a particular application.
ii. High latent heat of fusion per unit mass to reduce the amount of material and thus minimizing the physical size of the thermal energy storage device.
iii. High specific heat in order to provide additional sensible heat storage effects.
iv. High thermal conductivity for assisting in the charging and discharging processes.

Physical properties

i. Stability of phase transition in molecular levels ensures better heat storage.
ii. Small volume changes during phase transition allows for simple container and heat exchanger geometry.
iii. Low vapor pressure at operating temperatures helps to increase the safety of the operators during the charging process.

Kinetic properties

i. The material used must exhibit little or no supercooling during freezing. Supercooling affects proper heat extraction from the material.

Chemical properties

i. The material used must posses chemical stability and compatibility with construction materials of the container.
ii. The material must be non-toxic, non-flammable and non-explosive for safety concerns.

Economic aspect

i. The material is available in abundance and low-cost.

2.2.2 Classification of PCMs

There are many types of phase change materials for a given temperature range. Fig. 2.2 shows the classification of PCMs that are subdivided into three different classes namely organic, inorganic and eutectic (Sharma et al., 2009).

These various types of PCMs as illustrated Fig 2.2 have different thermal and physical properties from one another. The selection of suitable phase change material depends on the desirable properties as discussed in the previous subsection. However, majority of the phase

change material do not possess the recommended properties for an ideal thermal energy medium and thus thermal enhancers are used to improve any disadvantages that the medium may have. The following discusses the properties of each subclass of the phase change material.

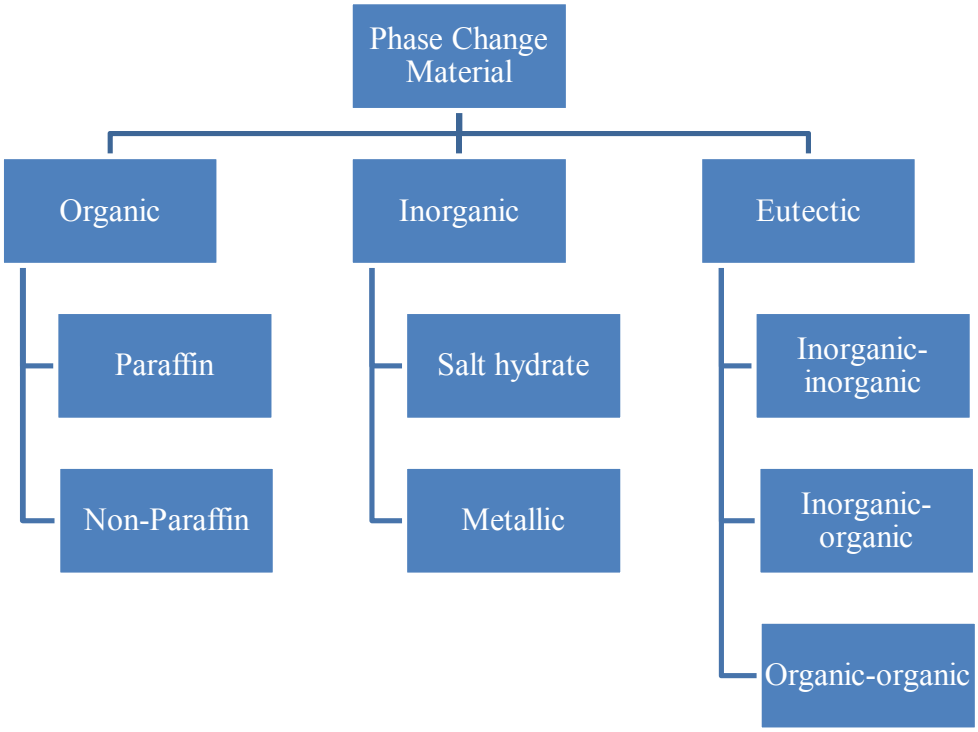

Fig. 2.2. Classification of phase change materials.

Inorganic materials

Inorganic materials can be further subdivided into salt hydrate and metallics. These materials do not show degradation in their latent heats of fusion with cycles of freezing and melting. Furthermore, they do not supercool noticeably.

i. Salt hydrate

The most commonly used inorganic compounds are the hydrated salts. Suitable to be used in a wide range of applications, salt hydrates are the most important group of PCMs and have been studied comprehensively in latent heat thermal energy storage systems. Salt hydrates are mostly consisting of salt and water, which mixtures form a crystalline matrix when they solidify. Salt hydrates may be combined with other components to form eutectic solutions. They have high latent heats of fusion and high thermal conductivity. Their availability and low cost made them commercially attractive for heat storage applications. Salt hydrates have a sharp melting point which increases the efficiency of a heat storage system and have a lower volume change during melting.

The melting behavior of the salt hydrates can be identified into three types, which are: (a) congruent, (b) incongruent and (c) semi-congruent melting. The main problem when using salt hydrates as a medium in thermal energy storage is the behavior of the melted salt hydrate once it melted incongruently. As the salt is not entirely soluble in its water of hydration during melting, some of the salt settles down at the bottom of the container. As a result some fractions of the salts are not able to recombine with water during the freezing/discharging process and thus reducing the active volume available for heat storage. This cycle continues with each melting-freezing process cycle. Fortunately, this problem can be resolved by encapsulating the phase change material to reduce separation (Lane and Rossow, 1976), mechanical stirring (Lane, et al., 1978), using gelled or thickening agents (Telkes, 1975), modifying the chemical

composition of the system (Charlsson et al., 1979, Alexiades and Solomon, 1992) or using excess water to prevent supersaturation (Biswas, 1977).

ii. Metallic

Metallic materials; which include low melting metals and metal eutectics are not widely used due to their heavy weights. Thermal energy storages that employ metallics however might have an advantage on their physical sizes as metallic materials have high heat of fusion per unit volume, apart from their higher thermal conductivities compared to other types of PCMs.

Organic materials

In the past, organic materials such as polyethylene glycol, fatty acid and paraffin were not favorable due to them being costlier than common salt hydrates and low heat storage capacity per unit volume. However, the strong advantage of the organic materials over inorganic materials compensates its disadvantages. Organic materials can melt congruently in which the constant melting and freezing cycle of the material does not cause any degradation of its latent heat of fusion and phase segregation in the material. Furthermore, organic materials can self-nucleate in which the crystallization of the material happens with little or no supercooling. Organic materials can be further classified into paraffin and non-paraffin.

i. Paraffin

Paraffin wax is a mixture of n-alkanes that has a general formula of C_nH_{2n+2} and falls within the $20 \leq n \leq 40$ range (Freund et al., 1982). It is mostly made up of straight chain n-alkanes CH_3-(CH_2)-CH_3. As the hydrocarbon chain increases, the melting temperature and heat of fusion of the paraffin wax increase with longer chain length (Suwondo et al., 1994). Through petroleum distillation, commercial grade paraffin wax can be obtained and may be used as PCMs in latent heat thermal energy storage systems. The reliability, predictability, non-corrosiveness, abundant and easily available at low-cost made paraffin wax an attractive material to be used in latent thermal energy storage system. They are chemically inert and stable below 500°C although it can undergo slow oxidation when exposed to oxygen; thus requiring closed containers (Lane, 1983). Paraffin wax does not show any degradation in its properties even after 1500 cycles (Liu and Chung, 2005). For containers that are made up of plastic, some care should be taken during experiments as paraffin waxes have a tendency to soften some plastics (Lane, 1983).

Although paraffin waxes show favorable characteristics, they also have a few unwanted properties. Paraffin waxes have low thermal conductivity in their solid state and are moderately flammable. These unwanted properties can be alleviated with modifying the wax and also by using proper container (Sharma et al., 2009). Furthermore, paraffin waxes are not compatible to some plastic containers. However, acrylic plastics are chemically resistant of paraffinic hydrocarbons (Schwartz, 2002).

ii. Non-paraffin

Unlike paraffin, non-paraffin organic phase change materials have various properties with their own each distinction. Buddhi and Sawhney (Buddhi and Sawhney, 1994) and Abhat et al. (Abhat, et al., 1981) have studied, compiled and identified various types of fatty acids, esters, glycols and alcohols that are suitable for thermal energy storage systems. These non-paraffin organic materials are further subdivided into other non-paraffin organic materials and fatty acids (Sharma et al., 2009). Although these organic materials have high heat of fusion, they also have high inflammability which can easily be ignited when exposed to flames, low flash points, unpredictability at high temperatures and varying level of toxicity which renders them unsafe if not handled carefully.

Eutectics

A eutectic system is a mixture of two or more chemical compounds or elements, which has a single chemical composition when mixed in a particular ratio and has a minimum-melting composition that corresponds to two or more components, each of which melts and freezes congruently forming a mixture of the component crystals during crystallization (George, 1989). Since eutectic melts and freezes without segregation, the components are not easy to be separated. The unpredictability of the life expectancy and separation of eutectic compounds hinders them from being widely used thermal energy storage application.

2.3 Geometry of thermal energy storage systems

In this section, a review of various geometrical configurations is presented. These include rectangular, spherical, cylindrical and finned geometries that have been studied extensively in the past.

2.3.1 Rectangular geometry

Studies on the use of rectangular geometry for phase change thermal energy storage was first initiated by Shamsundar and Sparrow (Shamsundar and Sparrow, 1975, Shamsundar and Sparrow, 1976) by applying fully implicit finite-difference method to the resolution of the enthalpy equation in square geometry. Studies by (Wang et al., 1999, Hamdan and Elwerr, 1996, Benard et al., 1985) have shown that the effects of free convection in the melting layers of PCM in rectangular enclosure are significant. Stritih (Stritih, 2004) compared the heat-transfer characteristics of a finned rectangular latent heat storage unit with a plain latent heat storage unit. It was found that during melting and solidification, the finned unit has an increase in heat transfer rate compared to the plain unit. The author also noted the effects of natural convection on the increased rate of heat transfer during melting. The use of fins in rectangular geometry has always been employed to improve the low thermal conductivities of most PCMs. The PCMs are often used in a thin plate configuration similar to that of a heat exchanger (Farid and Husian, 1990, Farid et al., 1998, Halawa et al., 2005).

Works by Lacroix et al. (Lacroix, 1989, Binet and Lacroix, 1998, Lacroix, 2001) showed that the fusion and natural convection effects in a rectangular cavity can be solved by using

a technique similar to the moving mesh method. The simulation studies also show that the melted fraction from close-contact melting at the bottom of the cavity (dominated by natural convection) is larger than the melted fraction due to conduction at the top. The authors noted that the melting process is fundamentally governed by the magnitude of Stefan number. A study on the effects of convection in close-contact melting of high Prantdl number substances has also been carried out (Groulx and Lacroix, 2007). Liu and Groulx (Liu and Groulx, 2011) studied the effects of fins in a rectangular geometry using octadecane as the phase change material. They found out that the positioning and length of the fin can increase the heat transfer rate of the PCM in a free convection driven melting process.

2.3.2 Spherical geometry

The use of spherical geometry in thermal energy storage is often employed in packed beds where spherical capsules are used as containers for PCMs to increase storage density and efficiency (Regin et al., 2008). A study on the spherical geometry found that spherical capsules with small diameters are dominated by conduction heat transfer (Saitoh and Moon, 1998). The authors further noted that for large diameter and high Stefan number cases, the combined natural convection and close-contact melting effects are significant. Ettouney et al. (Ettouney et al., 2005) experimented on the heat transfer of paraffin wax in spherical shells during melting and solidification. They found that the Nusselt number for melting is greatly influenced by the sphere diameter, low dependency on the air temperature and the air velocity effects however can be neglected. Furthermore, the authors noted that spheres with larger volumes allow for free motion inside the shells where the cooler and hotter

molten wax is freely moving. This is attributed to the increase of natural convection cells in the PCM.

A study to enhance the heat transfer performance of PCMs in spherical geometry has also been carried out by Ettouney et al. (Ettouney et al., 2006). Together with paraffin wax; metal beads were filled into the spherical capsule. A single capsule is then placed in a stream of hot/cold air. A comparison study between capsules with pure paraffin wax and paraffin mixed with metal beads was performed. It was found that the enhancement technique by using metal beads shows a reduction of melting and solidification times by up to 15%.

2.3.3 Cylindrical geometry

Cylindrical geometry in various practical applications such as food processing, casting processes and thermal storage systems is deemed to be significantly convenient (Jones et al., 2006). Since the beginning of computer age and the rapid increase of computing power, numerical simulations based on fixed or moving grid methods have been used to solve solid-liquid phase change problems (Brent et al., 1988, Simpson and Garimella, 1998, Beckett et al., 2001). Experimental data on a coolant-carrying tube analysis (Sparrow and Hsu, 1981) has also been compared to a numerical validation done by Zhang and Faghri (Zhang and Faghri, 1996) in which the results were found to be in good agreement. Jones et al. (Jones et al., 2006) employed photographic and digital image processing techniques along with enthalpy method to study the melting of a moderate-Prandtl-number material in a cylindrical enclosure which aims to set up a benchmark experimental measurements in order to validate numerical codes. Validation of a numerical model based on particle-

diffusive model and the enthalpy method in the melting of particle-laden slurry in a cylinder was performed (Suna et al., 2009). Analysis between the numerical study and experiment shows a reasonable agreement. The authors also noted that the flow and heat transfer characteristics of the melt are influenced by the solid particles and the migration of particles during melting cannot be sufficiently described by the particle-diffusive model alone.

Prakash et al. studied a solar water heater storage unit which contains a layer of phase change material at the bottom (Prakash et al., 1985). Due to the low thermal conductivities of most PCMs, Farid (Farid, 1986) proposed a method of using many layers of PCMs with different melting temperatures in order to improve the performance of thermal energy storage devices for solar heating applications. Works by Farid and Kanzawa (Farid and Kanzawa, 1989) and Farid et al. (Farid et al., 1990) applied the proposed method by developing a heat storage module which consists of vertical tubes filled with materials having different melting temperatures. Jian-you (Jian-you, 2008) performed an experimental and numerical investigation of a thermal energy storage device that has a triplex concentric tube with PCM filled in the middle channel and hot/cold heat transfer fluids are filled in the other two channels. Furthermore, a temperature and thermal resistance iteration method was developed by the author to analyze the melting and solidification of PCM in the triplex concentric tube in which when compared to experimental data shows a good agreement.

2.3.4 Finned geometry

There have been numerous studies conducted in order to improve the performance of phase change materials due to most of the available PCMs have unsatisfactorily low thermal conductivity. This leads to the slow melting and solidification process in thermal energy storage devices, and in turn reducing the efficiency of the system. Due to the low cost of construction, simplicity and ease in fabrication; most of heat enhancement techniques studied in the literatures are based on the configurations of fins embedded in the PCM side. Lamberg and Siren (Lamberg and Siren, 2003) studied a simplified analytical model for melting in a semi-infinite PCM storage with an internal fin to predict the solid-liquid interface location and temperature distribution of the fin. The results show a good agreement between analytical and numerical results. Reddy (Reddy, 2007) analyzed a double rectangular enclosure for solar water heating system with PCM. The system performance with 4, 9 and 19 fins inside the PCM was investigated. The author observed that the system with 9 fins shows an optimal performance with 95% of the PCM has melted during the study. For other literatures, Table 2.1 summarizes some studies on finned geometry thermal energy storage devices.

Table 2.1: Studies on finned geometry of thermal energy storage devices.

Reference	System geometry	Geometry/configurat-ion of fins	Process	Remarks
(Lamberg and Siren, 2003)	Rectangular	Rectangular/placed between two vertical heated surfaces	Melting	An analytical model was presented to predict the position of the mushy region during melting of PCM.
(Lacroix and Benmadda, 1998)	Rectangular	Rectangular/ vertically emerged from bottom of heated surface	Melting	Melting is enhanced with increasing Rayleigh number. For a given Rayleigh number, melting time is minimized with an optimal distance between the fins.
(Reddy, 2007)	Rectangular	Rectangular/emerge from the top of an inclined heated surface	Melting	An optimum performance with 9 fins configuration was observed with 95% of PCM was melted.
(Seeniraj et al., 2002)	Shell and tube	Annular/circling the HTF tube	Melting	Numerical study using enthalpy based method shows a considerable increase in the energy storage with the addition of fins.
(Zhang and Faghri, 1996)	Shell and tube	Rectangular/internal, longitudinal	Melting	Melting volume fraction can be increased significantly with the increase of thickness, height and number of fins.
(Liu et al., 2005)	Shell and tube	Spiral twisted tape/spans and circling the HTF tube	Solidifi-cation	The new fin improves conduction and natural convection of the PCM by up to 250% during solidification. A fine fin results in more effective enhancement.

2.4 Heat transfer in phase change materials

This section describes the heat transfer characteristics of heat transfer process in phase change materials used in latent heat thermal energy storage systems.

2.4.1 Stefan problem

Stefan (Stefan, 1891) studied the melting of ice as to investigate the phenomenon of heat conduction or diffusion involving a phase change or a moving boundary problem. This type of problem has been collectively referred to Stefan problem. Solving the Stefan problem involves determining the location of solid-liquid interface boundary that changes with time. Consider a one-dimensional heat conducting material which occupies a semi-infinite half space $0 < X < \infty$ that can exist either in solid or liquid state. Initially, the material is in solid state and at its melting temperature T_m. At time $t = 0$ thermal energy in the form of constant wall boundary temperature $T_w (> T_m)$ is supplied at $X = 0$. Therefore, the material melts and the solid-liquid interface $S(t)$ moves away from $X = 0$ as the melting process occurs. The temperature distribution of $T(X, t)$ in the molten region $0 < X < S(t)$ is governed by the heat conduction equation given by (Esen and Kutluay, 2004):

$$\rho C \frac{\partial T}{\partial t} = k \frac{\partial^2 T}{\partial X^2}, \ 0 < X < S(t), \ t > 0 \tag{2.6}$$

With boundary conditions given as:

$$k \frac{\partial T}{\partial X} = -\bar{h} T_w, \ X = 0, \ t > 0 \tag{2.7}$$

$$T(S(t),t) = T_m,\ X = S(t),\ t > 0 \tag{2.8}$$

where k and ρ is the liquid thermal conductivity and density respectively (assumed constant), C is the specific heat capacity and $\bar{h}$ is the prescribed function of $t > 0$. The right hand side term of Eq. (2.6) describes the heat flux in the decreasing temperature direction and thus it has a positive magnitude due to the heat flow which moves in the positive X direction, $0 < X < \infty$.

The heat balance equation governs the location of the moving solid-liquid interface. It is also known as the Stefan condition and can be described as (Esen and Kutluay, 2004, Dutil et al., 2011):

$$L\rho\left[\frac{dS(t)}{dt}\right] = k_s\left(\frac{\partial T_s}{\partial X}\right) - k_l\left(\frac{\partial T_l}{\partial X}\right), \qquad X = S(t), \qquad t > 0 \tag{2.9}$$

where L is the latent heat of fusion of the material, $S(t)$ is the location of solid-liquid interface as a function of time, the subscripts *s* and *l* denote the solid and liquid phases of the material. At $t = 0$, the material is in the solid state only. Therefore no liquid region exists in the material, $S(0) = 0$.

2.4.2 Solving the Stefan problem

The behavior of the phase change materials during melting or solidification proves to be difficult to solve due to the non-linear nature of the moving solid-liquid interface and different thermophysical properties of the two phases. Classical approach on the Stefan

problem only involves pure conduction in semi-infinite medium (Carslaw and Jager, 1973, Lauardini, 1981) before natural convection effects are considered in later years. Analytically, techniques such as isothermal migration (Keung, 1980), heat balance integral (Goodman, 1958, Yeh and Chung, 1975), source and sink method (Buddhi, et al., 1988) have been used to solve Stefan problem. However, these techniques are limited to one-dimensional problem as they are proven to be very complicated when applied to multi-dimensional analyses. Through numerical methods, either by using finite element or finite difference has been shown to be more powerful in solving the Stefan problem. In general, there are two numerical approaches of solving the moving boundary problems: (a) Adaptive mesh or (b) fixed grid technique.

Adaptive mesh technique

The element sizes used in numerical analysis may be refined to increase the model grid density in order to improve the accuracy of the calculation. This technique may be used to increase the grid density in areas of the numerical domain where the melting or solidification process is taking place. However, the highly refined mesh elements may not be needed in other areas of the domain. A local mesh refinement method, called the *h*-method is used to add or remove grid points subjected to the required accuracy on a uniform grid for every iteration (Provatas et al., 1999, Ainsworth and Oden, 2000). Another method, called the *r*-method (relocation method); also known as the moving mesh method starts with a uniform mesh in the domain. The mesh points are then moved, keeping the mesh topology and number of mesh points fixed as the solution evolves. The deformation of grid is done by tracking the rapid evolution of the solution or one of its higher order derivatives (Mackenzie and Mekwi, 2007, Tan et al., 2007).

Fixed grid technique

Through the use of an enthalpy method, the phase change problem is simplified since the governing equation is similar for the two solid/liquid phases, the solid-liquid interface condition is automatically achieved and the method creates a mushy zone between the two phases. The mushy zone allows for smooth continuity between the solid-liquid phases during the numerical analysis. The enthalpy formulation has been used extensively and is one of the most popular fixed grid methods for solving the phase change problem. The enthalpy function *h* as a function of temperature is given by (Voller, 1990):

$$\frac{\partial H}{\partial t} = \nabla[k_k(\nabla T)] \tag{2.10}$$

where *H* is the total volumetric enthalpy and k_k is the thermal conductivity of phase *k* in PCM. Eq. (2.10) describes the energy conservation of a phase change process in terms of the total volumetric enthalpy and temperature for constant thermophysical properties. *H* is the sum of sensible and latent heats, and can be given as:

$$H(T) = h(T) + \rho_l f(T) L \tag{2.11}$$

The enthalpy h is defined as:

$$h = \int_{T_m}^{T} \rho_k C_k dT \tag{2.12}$$

For isothermal phase change process, the liquid fraction f is given by:

$$f = \begin{cases} 0, \ T < T_m & \text{(solid)} \\ 0 - 1, \ T = T_m & \text{(mushy)} \\ 1, \ T > T_m & \text{(liquid)} \end{cases} \tag{2.13}$$

An alternative form of Eq. (2.10) can be produced by using Eqs. (2.11) and (2.12). For a two-dimensional heat transfer in the PCM is given by:

$$\frac{\partial H}{\partial t} = \frac{\partial}{\partial x}\left(\alpha \frac{\partial h}{\partial x}\right) + \frac{\partial}{\partial y}\left(\alpha \frac{\partial h}{\partial y}\right) - \rho_l L \frac{\partial f}{\partial t} \tag{2.14}$$

where α is the thermal diffusivity of the material and ρ is the density of the material.

A study to compare simulation methods for a phase change model in a rectangular cavity was performed by Lacroix and Voller (Lacroix and Voller, 1990). They conclude that the use of moving mesh method is limited due to the need of coordinate generator at each time increment. The fixed grid technique on the other hand must be finer for a unique melting temperature material. Bertrand et al. (Bertrand et al., 1999) have also carried out a comparison study between moving and fixed grid methods. They found out that the adaptive mesh method performs better than the fixed grid technique. However, a scenario where the solidification occurs at macroscopic surface level is better suited for the enthalpy method.

CHAPTER 3

METHODOLOGY: GEOMETRICAL DESIGN AND GOVERNING MATHEMATICAL EQUATIONS

This chapter includes the discussions on the geometrical arrangement, dimensions and the materials used for the numerical studies on the LHTES. Also in this chapter, the governing physical equations and mathematical formulations used by COMSOL Multiphysics software for the thermophysical processes that are used in the numerical studies are presented in the following subsections.

3.1 Latent heat thermal energy storage device geometrical arrangement, dimensions and materials

The drawing of the cylindrical LHTES device used for the numerical studies is shown in Fig. 3.1. The full geometrical dimensions of the LHTES are tabulated in Table 3.1; together with the list of materials used for each component. Also, the materials' properties are presented in Table 3.2.

Table 3.1: Latent heat thermal energy storage device dimensions and materials.

Component	Material	Outer radius, mm	Inner radius, mm	Thickness, mm	Length, mm
Tube	Copper	40	30	10	1000
Fin	Copper	240	40	5	-
Container	Acrylic plastic	290	280	10	1000

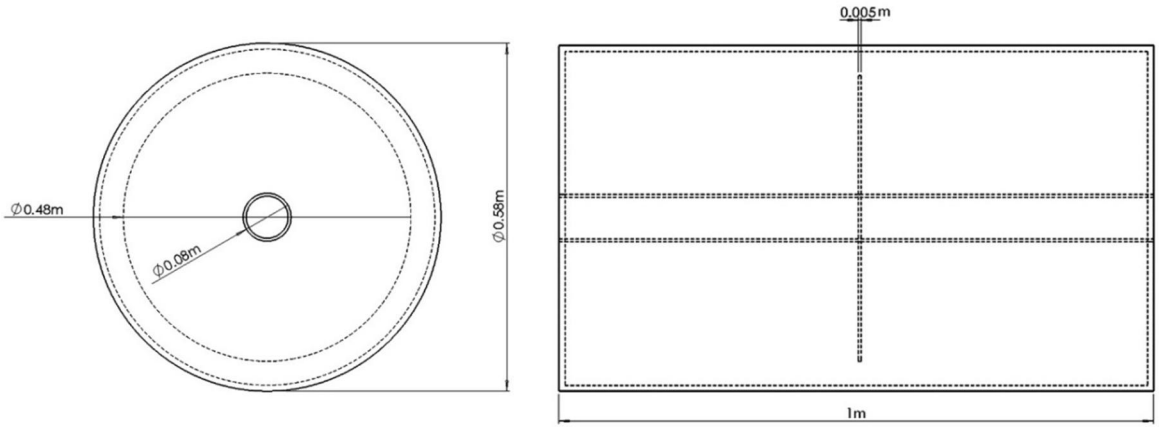

Fig. 3.1. Front and top side drawings of the LHTES with single fin configuration.

Table 3.2: Properties of the materials used (Benenson et al., 2000, Groulx and Ogoh, 2009).

Material	Heat capacity, kJ/kg.K	Thermal conductivity, W/m.K	Latent heat of fusion, kJ/kg	Density, kg/m^3
Acrylic plastic	1.470	0.19	-	1160
Copper	0.385	400	-	8700
Paraffin wax	2.400	0.21	174	750

A few examples of the arrangement of fins are presented in Fig. 3.2. The radial fins are evenly spaced to allow for uniform heat distribution into the PCM and hence permitting it to melt homogeneously. The cylindrical type LHTES has a copper pipe in the center in which a heat transfer fluid (or water) that has a higher temperature than the copper pipe flows through it, distributing thermal energy as it passes the device. The thermal enhancer or the circular fin increases the amount of surface area in contact between the paraffin and the copper which helps to distribute the thermal energy from the pipe deeper into the PCM regions, therefore increasing the heat transfer rate of the device.

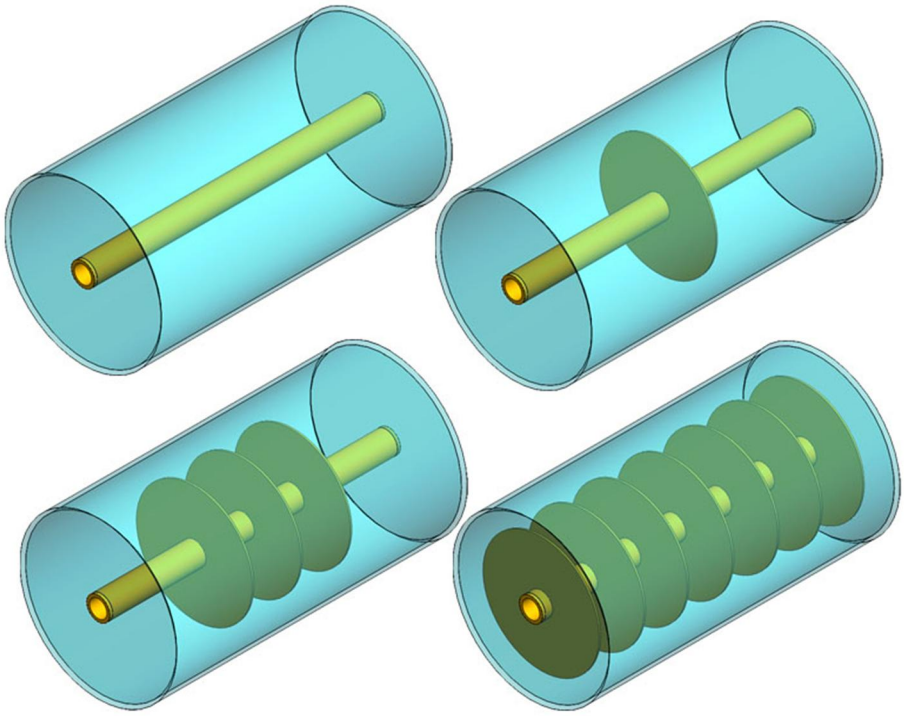

Fig. 3.2. Geometrical representations of 0, 1, 3 and 7 fins configuration of LHTES.

3.1.1 Selection of fins

To support the weight of the PCM in between fins, the circular fin is chosen to have the thickness of 5 mm and has the outer radius of 240 mm, leaving a 40 mm gap between the container and the fin. The effects of the thickness of the fin and the gap may result in a different outcome for different thicknesses and gap lengths. However, these two variables are not in the scope of study for this research.

3.2 Heat transfer, fluid flow and phase change processes

The following subsections cover the fundamental thermophysical laws that govern the system. The boundary and initial conditions are also presented in order for each of the processes to be solved.

3.2.1 Heat transfer process

Convection heat transfer by thermal fluid

When the thermal fluid or water flows through the tube pipe, convection mechanism transfers the heat from within the fluid to the wall of the copper pipe. Temperature distribution in any system can be obtained by solving the energy equation that governs the system. In the case of a pipe, the energy equation in cylindrical coordinates for constant properties is given by (Deborah and Michael, 2005, Jiji, 2009b):

$$\rho C_p \left(\frac{\partial T}{\partial t} + \upsilon_r \frac{\partial T}{\partial r} + \frac{\upsilon_\theta}{r}\frac{\partial T}{\partial \theta} + \upsilon_z \frac{\partial T}{\partial z}\right) = k\left[\frac{1}{r}\frac{\partial}{\partial r}\left(r\frac{\partial T}{\partial r}\right) + \frac{1}{r^2}\frac{\partial^2 T}{\partial \theta^2} + \frac{\partial^2 T}{\partial z^2}\right] + \mu\phi \qquad (3.1)$$

Where υ denotes the velocity of the fluid; subscripts *r*, θ and *z* represent the radial, angular and z-direction components of the system, C_p and k are the specific heat and thermal conductivity of the fluid. The heat generated by viscous dissipation $\mu\phi$ is trivial for the current study. The flow field of the thermal fluid can be solved using the Navier-Stokes and continuity equations which are heavily discussed by (Jiji, 2009b). Together with Eq. (3.1),

the convection heat transfer problem can be solved by the following boundary and initial conditions:

$$T(r, z, t = 0) = T_0 \tag{3.2}$$

$$T(r, z = 0, t) = T_{in} \tag{3.3}$$

$$\left.\frac{\partial T}{\partial r}\right|_{r=0} = 0 \qquad \text{(axial symmetry)} \tag{3.4}$$

Conduction heat transfer

In the current study, the heat transfer in the PCM is assumed to only be in the conduction mode; in which the free convection effects due to the liquid PCM is neglected to reduce computing time. Furthermore, at higher number of fins configuration the volume of PCM between the fins is small, reducing the effects of the natural convection. Nevertheless, the general axisymmetric energy equation in cylindrical coordinate for constant properties can be given by (Deborah and Michael, 2005, Jiji, 2009b):

$$\rho C_p \frac{\partial T}{\partial t} = k\left[\frac{1}{r}\frac{\partial}{\partial r}\left(r\frac{\partial T}{\partial r}\right) + \frac{\partial^2 T}{\partial z^2}\right] \tag{3.5}$$

Eq. (3.5) can be solved by using the initial condition given by Eq. (3.2) at $t = 0$. The exterior of the container is insulated and therefore the boundary condition for the surface of

the system is governed by $\partial T/\partial \vec{n} = 0$, where $\vec{n}$ describes the fluid flow normal to the outside surface.

3.2.2 Fluid flow process

As discussed earlier, the flow field of the thermal fluid is governed by the Navier-Stokes and continuity equations. For an incompressible axisymmetric flow, the continuity equation in cylindrical coordinates is given by (Deborah and Michael, 2005, Jiji, 2009b, Flandro et al., 2011):

$$\frac{1}{r}\frac{\partial}{\partial r}(rv_r) + \frac{\partial}{\partial z}(v_z) = 0 \tag{3.6}$$

The incompressible axisymmetric Navier-Stokes equations in the radial and z-direction components are given by (Deborah and Michael, 2005, Jiji, 2009b, Flandro et al., 2011):

$$r\text{:}\ \rho\left(\frac{\partial v_r}{\partial t} + v_r\frac{\partial v_r}{\partial r} + v_z\frac{\partial v_r}{\partial z}\right) = -\frac{\partial P}{\partial r} + \mu\left[\frac{1}{r}\frac{\partial}{\partial r}\left(r\frac{\partial v_r}{\partial r}\right) + \frac{\partial^2 v_r}{\partial z^2} - \frac{v_r}{r^2}\right] + \rho g_r \tag{3.7}$$

$$z\text{:}\ \rho\left(\frac{\partial v_z}{\partial t} + v_r\frac{\partial v_z}{\partial r} + v_z\frac{\partial v_z}{\partial z}\right) = -\frac{\partial P}{\partial r} + \mu\left[\frac{1}{r}\frac{\partial}{\partial r}\left(r\frac{\partial v_z}{\partial r}\right) + \frac{\partial^2 v_z}{\partial z^2}\right] + \rho g_z \tag{3.8}$$

where P denotes the pressure and g is the gravity acceleration. The initial and boundary conditions are given as:

$$v_z(z, t = 0) = u_0 \tag{3.9}$$

$$v_z(z = 0, t) = u_0 \tag{3.10}$$

$$v_r = 0 \qquad \text{(no-slip at the wall)} \tag{3.11}$$

$$\left.\frac{\partial v_z}{\partial r}\right|_{r=0} = 0 \qquad \text{(axial symmetry)} \tag{3.12}$$

Where u_0 is the initial inlet velocity of the thermal fluid. Since there is no velocity relative to the boundary, the thermal fluid in the copper pipe has a no-slip condition at the wall.

3.2.3 Phase change heat transfer process

During the phase change heat transfer process, or melting of the phase change material; the conduction occurs in the phase change can be described as a moving boundary or free boundary problems. The transfer of energy during this process must be accounted for to analyze the amount of energy that can be stored during the simulation. The general interface energy equation is given by (Jiji, 2009a, Naterer, 2003):

$$k_s \frac{\partial T_s}{\partial x} - k_l \frac{\partial T_l}{\partial x} = \rho L \frac{dX}{dt} \tag{3.13}$$

Where *X* denotes the position of the melting front and *L* denotes the latent heat of fusion. Therefore, Eq. (3.13) describes the balance between the difference of solid and liquid phases' heat fluxes with the latent heat absorbed by the PCM during the melting process.

3.3 Numerical analysis

The application of computer simulation through the use of finite element method (FEM) has become a vital part of engineering and science. Developing new products and optimizing designs by digitally analyzing the components have accelerated innovations and breakthroughs over the recent years. This part of the chapter explains the use of COMSOL Multiphysics to numerically simulate the thermal behavior of the latent heat thermal energy storage system having transient partial differential equations, either linear or non-linear thermophysical systems that govern the various processes in the LHTES.

3.3.1 Numerical model

The geometry of the numerical model is first created in the COMSOL Multiphysics space environment by applying the 2D axisymmetrics model configuration. The physics of the study are then determined. For the current study, the conjugate heat transfer physics interface in the heat transfer module is selected during the set-up of the model; which combines the heat transfer analysis of solid and fluid systems. The module also includes turbulent flow model including fast moving fluids that have a high Reynolds number. Afterwards, the initial and boundary conditions of the physics applied to the geometry are determined. The geometry computational domains are discretized into triangular mesh elements and time-steps are carefully selected. Lastly, the numerical study is executed by running the simulation.

All of the heat transfer and fluid flow governing equations are solved by COMSOL Multiphysics software during the simulation by applying the initial and boundary conditions that are defined earlier. The following subsections describe the numerical model and the conditions that are applied for the numerical simulation.

Initial conditions for the system

The initial values node in the model builder of the COMSOL software is used to define the initial conditions for the velocity field, pressure and temperature as well as for the turbulence variables and radiosity, if applicable (COMSOL, 2011). The following are the applied initial conditions for the study:

$$u_z = u_0 \tag{3.14}$$

$$T = T_0 \tag{3.15}$$

Where u_z denotes the velocity field in the z-direction and u_0 denotes the initial thermal fluid velocity.

Heat transfer module

Heat transfer in solids node: The node adds the heat equation for conductive heat transfer in solids. It essentially uses the same heat conduction equation of Eq. (2.6).

Temperature node: The temperature node defines the thermal fluid inlet temperature boundary condition which is given as (COMSOL, 2011):

$$T = T_{in} \tag{3.16}$$

Heat continuity node: The continuity node prescribes that the temperature field is continuous across different domains where the boundaries are matched. This heat continuity boundary condition permits the heat flux to travel from one internal boundary to another, simulating the continuous heat flow from the source and finally to the phase change material. The governing mathematical equation is given as (COMSOL, 2011):

$$\vec{n}.(q_1 - q_2) = 0 \tag{3.17}$$

Where q_1 and q_2 denote the calculated heat fluxes of two adjacent mesh elements. The heat flux q is defined as (COMSOL, 2011):

$$q = -k\vec{\nabla}T \tag{3.18}$$

Thermal insulation node: The node is the default boundary condition for all heat transfer interfaces. Naturally, the insulation boundary equation describes the temperature gradient across the boundary to be zero at which the temperatures for adjacent boundaries are equal. The thermal insulation boundary equation is given as (COMSOL, 2011):

$$\vec{n}.\left(k\vec{\nabla}T\right) = 0 \tag{3.19}$$

Fluid flow module

Inlet node: The node defines the boundary condition of a fluid flow at an inlet. The normal inflow velocity is selected and its governing equation is given as (COMSOL, 2011):

$$\vec{u} = -u_0\vec{n} \tag{3.20}$$

Wall node: The node denotes the wall boundaries in a fluid-flow simulation. As explained earlier, the thermal fluid velocity in the radial component is zero; hence a no-slip condition exists at the pipe wall. The boundary condition is given as (COMSOL, 2011):

$$\vec{u}_r = \vec{0} \tag{3.21}$$

The Wall node represents wall boundaries in a fluid-flow simulation. It includes several options to describe different type of walls. The default condition is that for a smooth wall.

Outlet node: The node denotes boundaries with outwards flow in a fluid-flow simulation. The node can be used to define the boundary condition of the thermal fluid in terms of its pressure, velocity or stress condition. For the current study, "pressure, no viscous stress" is applied for the outlet boundary condition. This condition specifies vanishing viscous stress along with a Dirichlet condition on the pressure which gives total control of the pressure level at the entire boundary. The mathematical governing equations are given as (COMSOL, 2011):

$$P = P_0 = 0 \tag{3.22}$$

$$\mu\left[\vec{\nabla}u + (\vec{\nabla}u)^T\right]\vec{n} = 0 \tag{3.23}$$

Modeling the phase change process

Energy is needed in large quantity during the phase change process to melt the PCM. Furthermore, the position of the melting interface during the solid-liquid phase change process must be recognized and solved. These two factors can be solved numerically using the effective heat capacity method. The effective heat capacity, $C_{p,eff}$ of the paraffin wax can be defined by (Lamberg et al., 2004):

$$C_{p,eff} = \frac{L}{(T_2 - T_1)} + \frac{C_{p,s} + C_{p,l}}{2} \tag{3.24}$$

Where L denotes the latent heat of fusion, T_1 is the temperature at the start of the phase change and T_2 is the temperature when the phase change process ends. Knowing that the solid and liquid heat capacities for paraffin have the same values, the modified heat capacity can be written as (Lamberg et al., 2004):

$$C_{p,pcm}\begin{cases} 2.4\ \mathrm{kJ/(kg.K)} & T < T_1 \\ 60.5\mathrm{kJ/(kg.K)} & T_1 < T < T_2 \\ 2.4\ \mathrm{kJ/(kg.K)} & T > T_2 \end{cases} \tag{3.25}$$

A continuous step function is created in the COMSOL software to incorporate Eq. (3.25) in order to solve the phase transition problem numerically. By adopting the method introduced by Groulx and Ogoh (Groulx and Ogoh, 2009); the following function is used in the material node of the COMSOL software (COMSOL, 2011):

$$C_{p,pcm} = C_p + C_{p,eff} * (flc2hs(T - T_1, scale) - flc2hs(T - T_2, scale)) \quad (3.26)$$

Where $flc2hs$ is a smoothed step transition function in COMSOL Multiphysics.

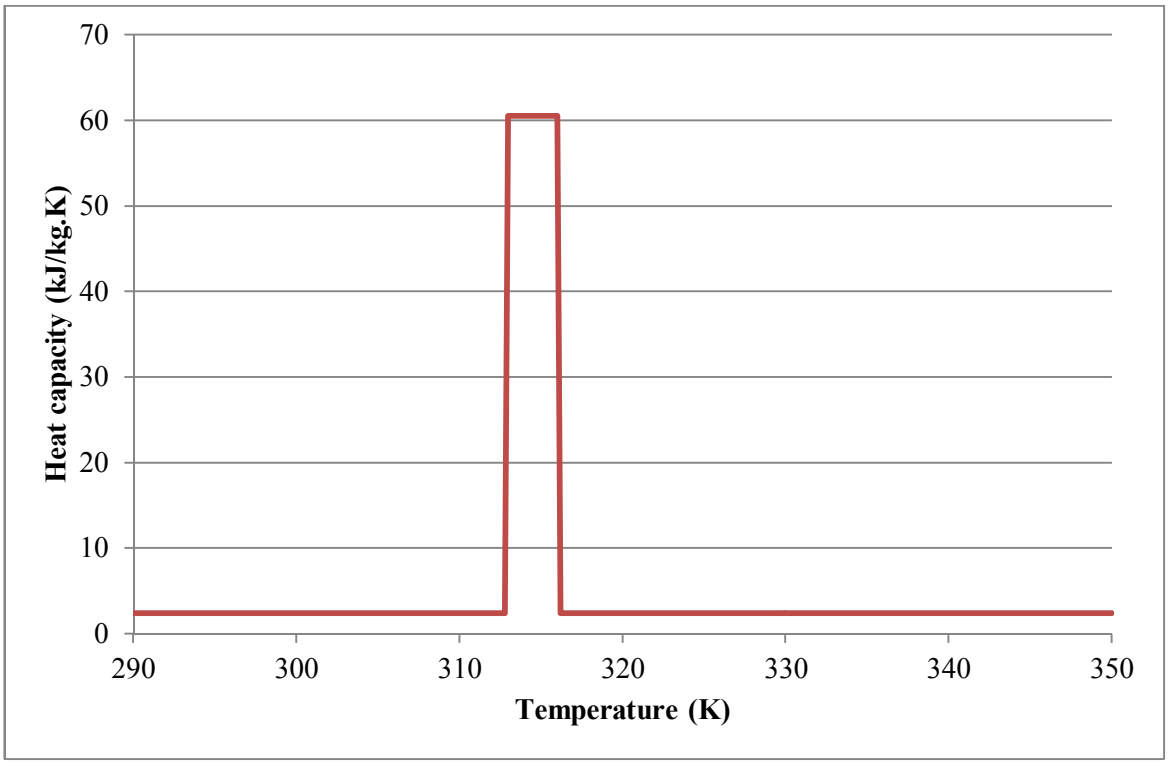

Fig. 3.3. The modified heat capacity of the paraffin wax defined from temperature range of 290 K to 350 K.

The graph shown in Fig. 3.3 illustrates the modified heat capacity of the paraffin wax after applying Eq. (3.25) into Eq. (3.26) which can then be written as (Groulx and Ogoh, 2009, COMSOL, 2011):

$$C_{p,pcm} = 2.4 + 60.5 * (flc2hs(T - 313, 0.02) - flc2hs(T - 316, 0.02)) \quad (3.27)$$

The plot shown in Fig. 3.3 illustrates the non-linear characteristic of the modified heat capacity that changes its value during the melting of the PCM. This method forces the COMSOL software to change the heat capacity value of the PCM from a constant value of 2.4 kJ/kg.K in the solid (T < 313K) and liquid state (T > 316K) to 60.5 kJ/kg.K in the melting phase (313K < T < 316K).

CHAPTER 4

VALIDATION OF PHASE CHANGE PROCESS

This chapter describes about an analytical validation of numerical results data obtained from the simulation of heating a semi-infinite paraffin slab. The numerical study is done to simulate the phase change process of paraffin taking place inside the thermal energy storage. It is important to validate the data analytically in order to support the results obtained through the numerical studies on the latent heat thermal energy storage system in the next chapter. For greater accuracy, a mesh convergence study is performed to assure better numerical results obtained from the simulations.

4.1 Analytical Study

Phase change heat transfer that occurs in any PCM thermal energy storage is a well-known problem that can be encountered naturally in many thermophysical processes such as melting of ice, freezing of foods, solidification of metals and other various natural reactions. It is a transient, non-linear phenomenon in which a moving solid-liquid interface exists in the material during the phase change process. This moving boundary problem, or also known as Stefan problem, requires solving the fusion or heat conduction in an unknown region during the melting or solidification process. Furthermore, the nonlinearity of the process poses some difficulty in mathematical formulations and therefore simpler analytical solution in a simple system and geometry having simple boundary conditions is always favorable in any analysis. For a one-dimensional free and moving boundary

problem, Neumann presented an analytical solution to the classical Stefan's problem in a very simple formulation (Gupta, 2003).

Fig. 4.1 shows the schematic diagram of a simplified one-dimensional analytical model that was analyzed. The model is used in the analytical validation of the numerical results data obtained for a one-dimensional transient solid-liquid phase change process. The semi-infinite model of a paraffin wax slab is initially assumed to be at its melting temperature point, T_m. As such, an increase in its temperature will change its current solid state to liquid state.

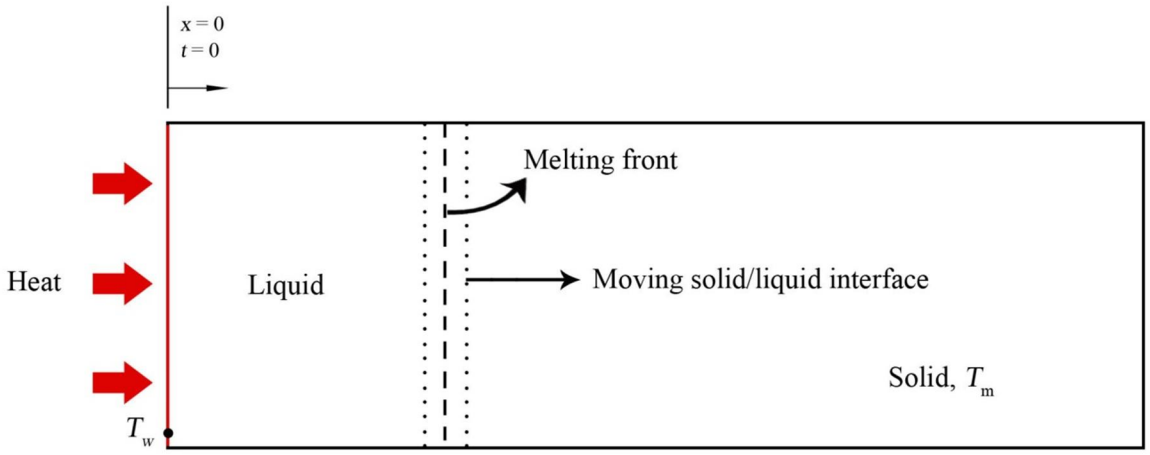

Fig. 4.1. One-dimensional analytical moving boundary phase change problem.

The following assumptions were made for the analysis, in which Stefan's problem is defined. The assumptions are made similar for the numerical analysis:

1. The wall temperature, T_w and the phase change material temperature in its solid state are assumed to be at the melting temperature of the PCM, thus $T_w = T_m$.
2. The only heat transfer mechanism during the melting of the PCM is conduction.
3. The entire walls of the PCM are insulated, except for the heated wall.

4. Distribution of temperature is one-dimensional and in the x-direction.
5. The thermophysical properties of the PCM material are independent of temperature, in which for the current study the heat capacities for solid and liquid phases are equal.

The boundary conditions are given as follow (Gupta, 2003):

1. Wall temperature: $T(x = 0, t > 0) = T_w$ (4.1)
2. Melting front temperature: $T(x = X(t), t > 0) = T_m$ (4.2)

where $X(t)$ is the solid-liquid melting interface position.

During melting, the transient energy equation in the liquid phase is governed by (Gupta, 2003, Massoud, 2002, Jiji, 2009a):

$$\frac{\partial T_l}{\partial t} = \frac{1}{\alpha_l}\frac{\partial^2 T_l}{\partial x^2} \tag{4.3}$$

where α_l is the liquid thermal diffusivity, which can be defined as $(\rho_l C_{p,l})/k_l$.

The moving solid-liquid interface in the system is influenced by the heat flux of the liquid phase at the melting interface and the magnitude of latent heat of the phase change material. The following equation defines the melting front energy balance (Gupta, 2003, Massoud, 2002, Jiji, 2009a):

$$-\rho_l L\frac{dX(t)}{dt} = k_l\frac{\partial T_l(X,t)}{\partial x} \tag{4.4}$$

where L is the latent heat of fusion of the material.

By solving Eqs. (4.1) to (4.4), the transient temperature distribution in the liquid phase can be obtained from the following equation (Gupta, 2003, Massoud, 2002) :

$$\frac{T_l(x,t) - T_w}{T_m - T_w} = \frac{erf\left[\frac{x}{2\sqrt{\alpha_l t}}\right]}{erf(\beta)} = \frac{erf(\eta)}{erf(\beta)} \tag{4.5}$$

The similarity variable η is defined as:

$$\eta = \frac{x}{2\sqrt{\alpha_l t}} \tag{4.6}$$

Whereas, the constant β can be obtained by referring to Eq. (4.4) (Gupta, 2003, Massoud, 2002):

$$\beta e^{\beta^2}\,\mathrm{erf}(\beta) = \frac{Ste_l}{\sqrt{\pi}} = \frac{C_{p,l}(T_w - T_m)}{L\sqrt{\pi}} \tag{4.7}$$

Referring to Eq. (4.7), the Stefan number, Ste_l is defined as the following equation:

$$Ste_l = \frac{C_{p,l}(T_w - T_m)}{L} \tag{4.8}$$

For further validation purposes, the position of the melting front as a function of time, measured from the wall at $x = 0$, can be calculated by using the following equation (Massoud, 2002):

$$X(t) = 2\eta\sqrt{\alpha_l t} \tag{4.9}$$

The rate of energy stored through the phase change process due to the heat transferred at the melting interface can be given as (Massoud, 2002):

$$q[X(t)] = k_l \frac{\partial T_l}{\partial x} = -\rho_l L \frac{\eta\sqrt{\alpha_l}}{\sqrt{t}} = -\rho_l L u_m(t) \tag{4.10}$$

where $u_m(t)$ is the melting front velocity obtained from Eq. (4.9).

4.2 Numerical Study

The numerical simulation in this section attempts to solve Stefan problem through the use of pure conduction modeling method. The transient study simulates a 21 hour long heating of a paraffin wax slab. Fig. 4.2 shows the meshed diagram of a 2D semi-infinite slab of the PCM which has the dimension of 0.3 m in width and 0.1 m in height. Similar to the previous section, the PCM was initially set to the melting temperature of 313 K to instantly melt the material when there is an increase of temperature. The thermal boundary conditions of the slab are defined in such a way that only the left wall is heated with temperature of 350 K while the other wall surfaces are insulated. As previously defined, the latent heat of fusion at the melting interface is solved by using the modified heat capacity as shown in Eq. (3.27).

Before the numerical results data from the simulation can be analyzed, a mesh convergence study was carried out to increase the accuracy of the results and independent of the mesh element sizes. Six different element sizes were tested and their sizes, numbers, degrees of freedom and simulation times are illustrated in Table 4.1. During the transient study, the

time step is carefully chosen to ensure that the simulated temperature increase does not overshoot the phase change region, where the melting process is taking place. As shown in Eq. (3.27), the modified heat capacity forces the COMSOL software to solve the system non-linear. Thus, by adopting the COMSOL time-step technique introduced by (Groulx and Ogoh, 2009), the time step for the transient study must be less than 350 seconds, for a total simulated time of 75000 seconds or 21 hours.

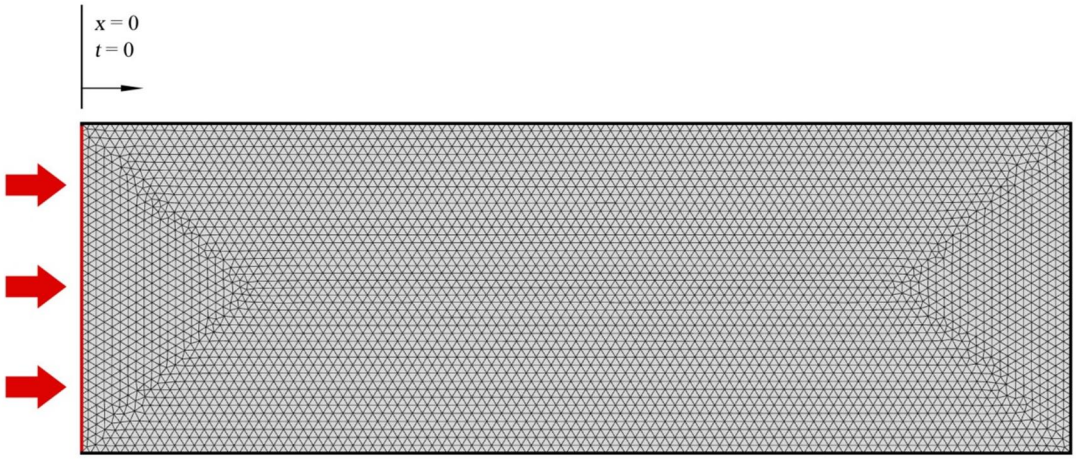

Fig. 4.2. Schematic diagram of the 2D slab of paraffin wax.

Table 4.1: Various mesh element sizes used for the simulation.

Element size (mm)	No. of elements	Number of DOFs	Simulation time (s)
20	188	417	12 s
10	790	1661	17 s
5	3036	6233	26 s
3	8470	17209	43 s
0.6	229910	461155	274 s
0.5	313020	627641	384s

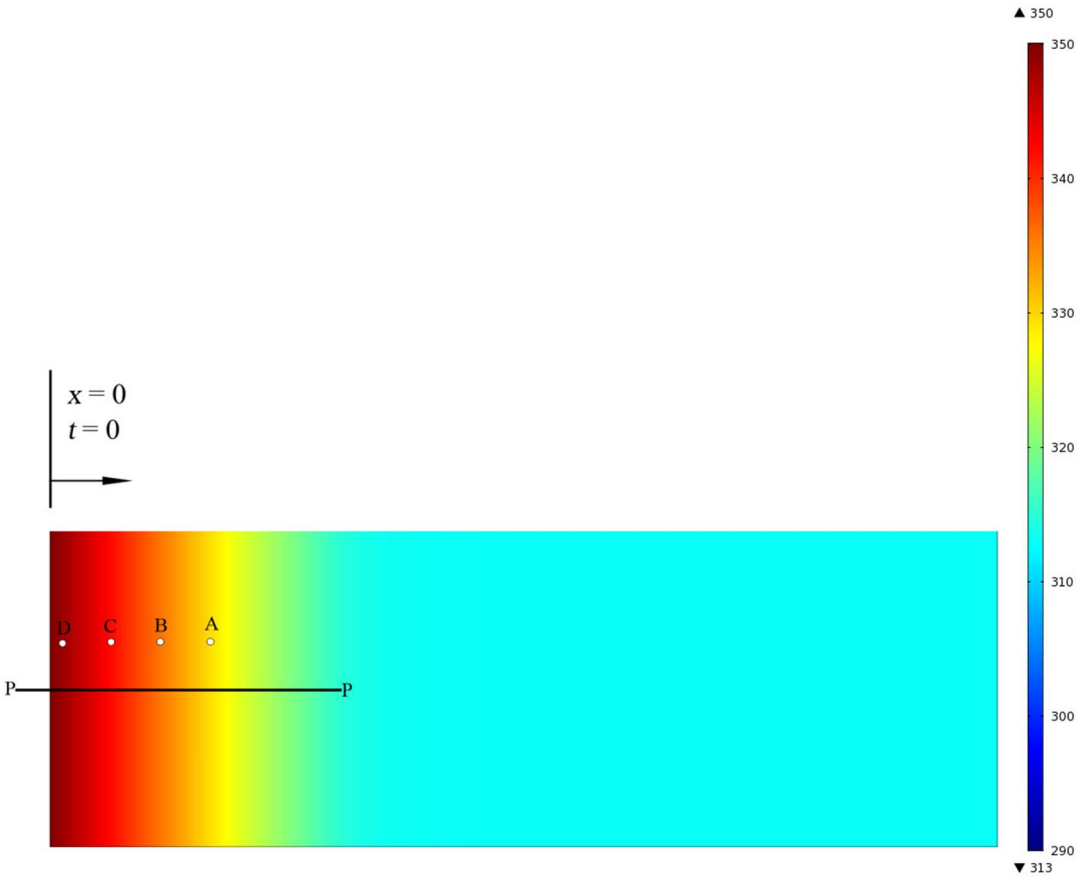

Fig. 4.3. Simulated 2D surface temperature plot. Simulated time: 21 hours.

The numerical solution after 21 hours of simulated time is presented in the Fig. 4.3. The horizontal line P-P, 0.12 m in length; is the linear region at which the analytical temperature profile will be compared to the numerical temperature profile. The geometrical dimension of the slab is justified as only about a quarter of the whole system experiences temperature changes, therefore simulating a semi-infinite system.

Fig. 4.4 shows the temperature distribution profile along the linear region of line P-P after a simulated time of 3 hours using various mesh element sizes. The convergence study shows that the results converge at element size of 0.6 mm; with reduction of element size to 0.5

mm displays no noticeable changes and therefore element size of 0.6 mm is chosen for simulation.

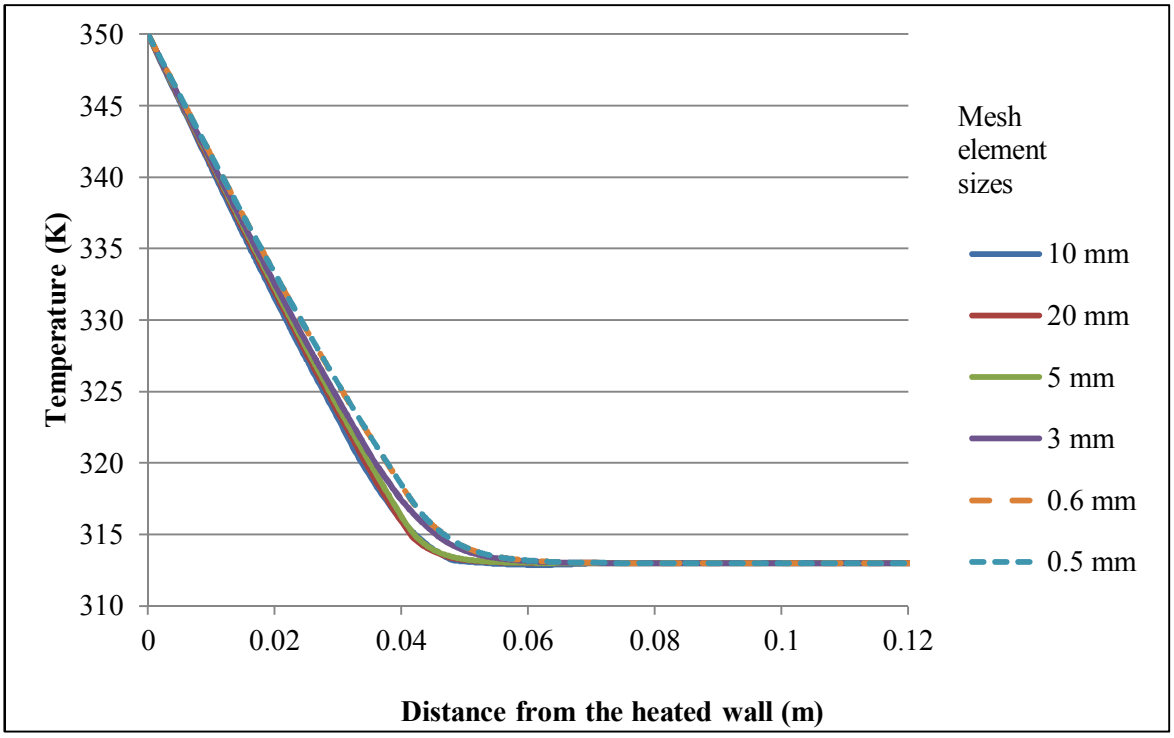

Fig. 4.4. Temperature distribution profile along section P-P for various mesh element sizes. Simulated time: 3 hours.

The temperature history of points A, B, C and D (with distances from the heated wall 0.035 m, 0.025 m, 0.015 m and 0.005 m respectively) after a simulated time of 18 hours is shown in Fig. 4.5. The figure shows that the four different points demonstrate proper phase change processes. As previously defined, the paraffin wax melts over a 3 K temperature range. At point A, melting process starts at the temperature of 313 K and increases until 316 K for duration of 3 hours at which after the period an inflexion point is observed. This is expected for a phase change material undergoing a phase change process. However, the inflexions on the other temperature graphs of point B, C and especially D are less noticeable as the

distance between the heated wall and the points are reduced; the rate of temperature increase is higher.

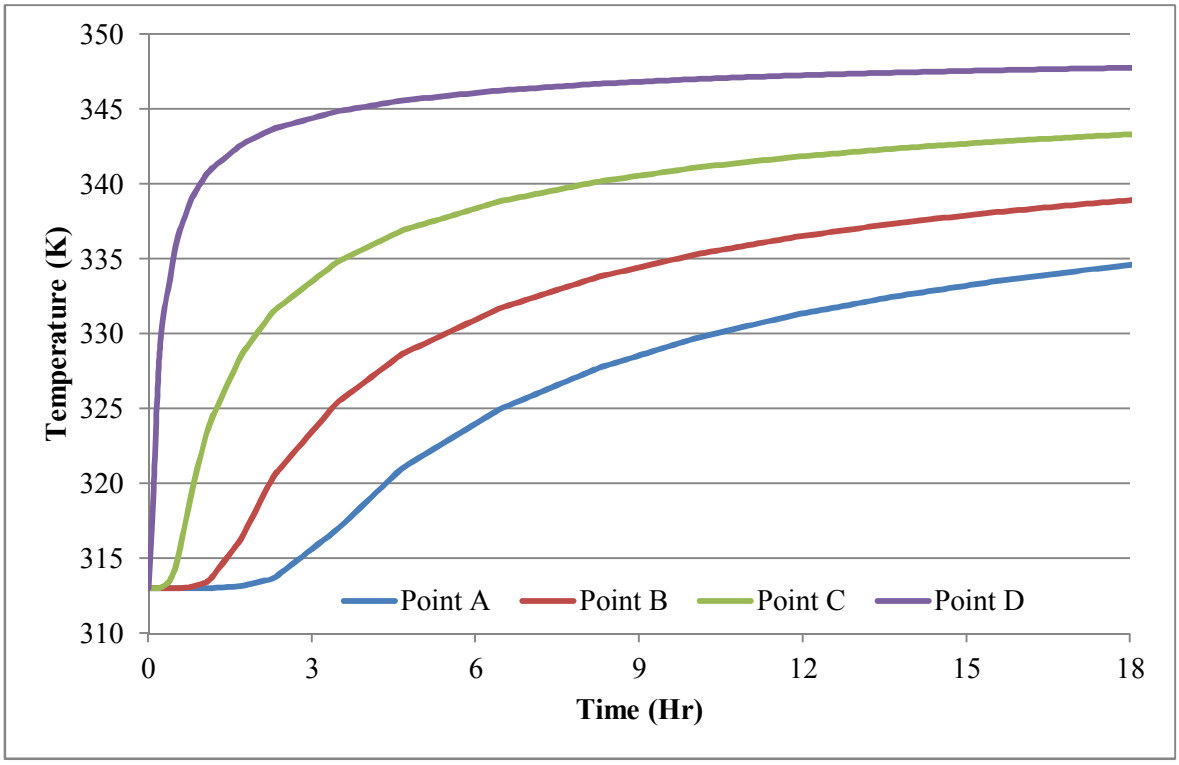

Fig. 4.5. Temperature history of points A, B C and D. Simulated time: 18 hours.

Fig. 4.6 shows the temperature distribution along section P-P after simulated times of 0.8, 3, 6, 9, 12, 15 and 18 hours. The numerical results show that 0.017, 0.034, 0.049, 0.060, 0.068, 0.076 and 0.082 m of the phase change material were fully melted ($T > 316$ K) during these 7 time periods respectively. This validates an accurate simulation of heat conduction along the length of the melted PCM.

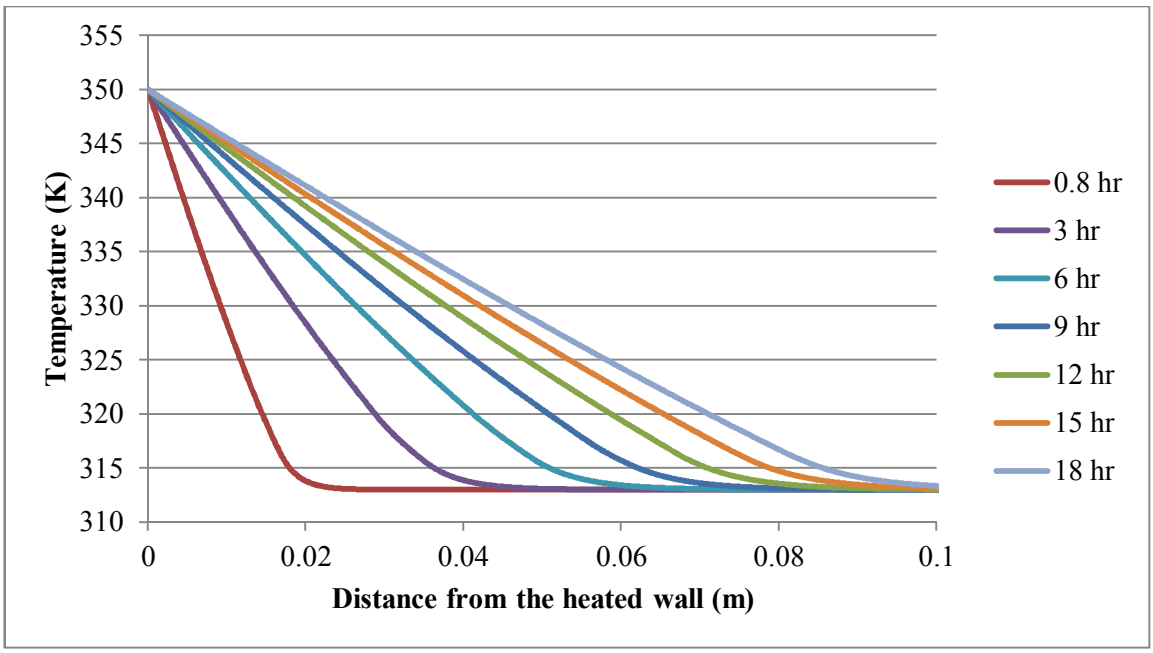

Fig. 4.6. Temperature distribution profile for various simulated time.

4.3 Validation

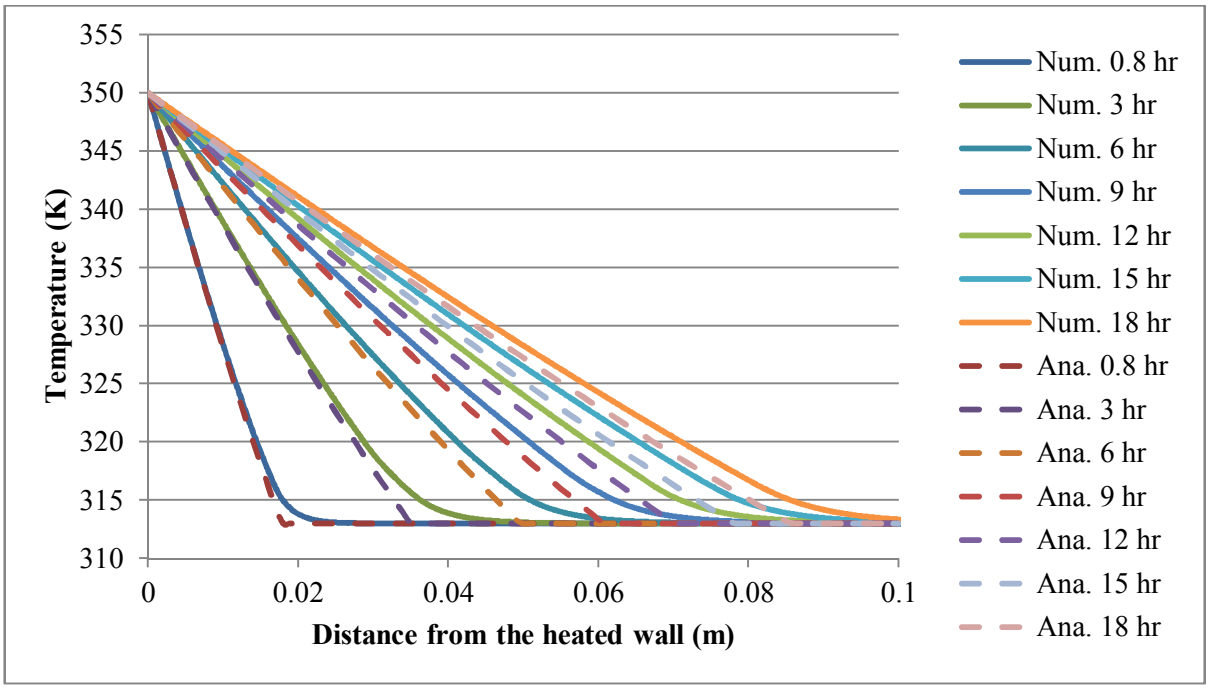

Fig. 4.7. Comparison of numerical and analytical temperature distribution profiles for various simulated times.

Fig. 4.7 shows the comparison between the analytical and numerical temperature profiles for various simulated time. By using Eqs. (4.5) to (4.7), the analytical results obtained from the calculation of these equations show a good agreement with the numerical results obtained from the simulations. However, the analytical results for longer periods of time (6, 9, 12, 15 and 18 hours) tend to under predict the numerical results data. This is due to the under prediction of the total heat flux which reduces the melting rate for the analytical calculation, and thus resulting in lower temperature compared to the numerical simulation. This can be simply explained through the different mathematical approach of both of these models in which the analytical analysis uses a single constant temperature difference during melting process (T_w-T_m), whereas the simulation melts the PCM over a 3 K temperature range (313K to 316K).

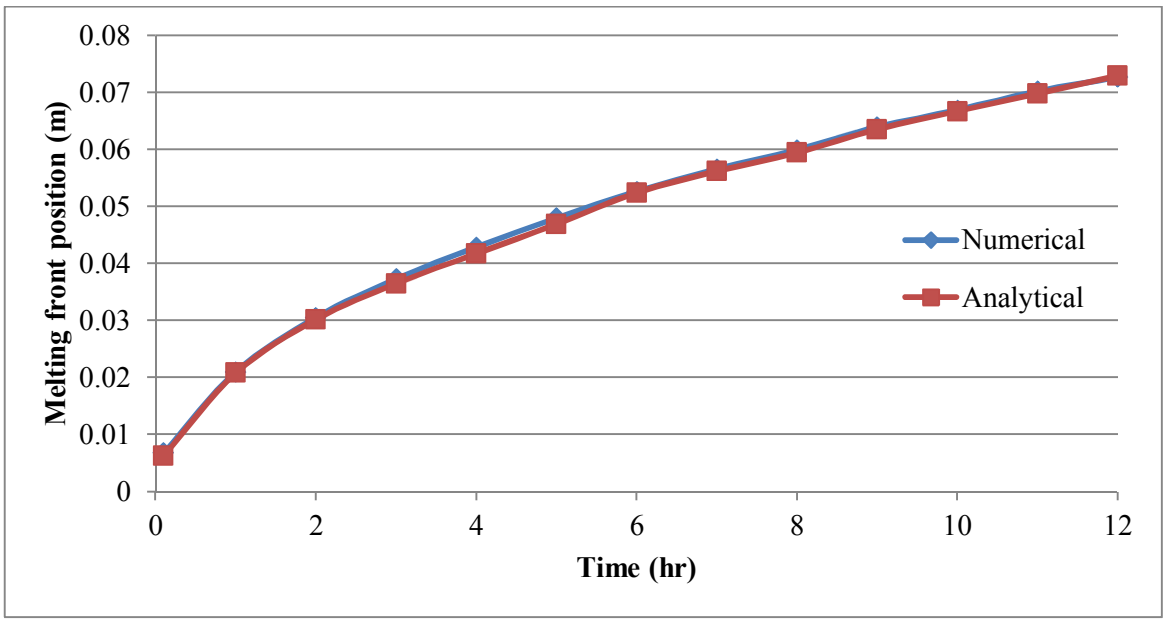

Fig. 4.8. Melting front position obtained from numerical and analytical studies.

Simulated time: 12 hours.

The plots in Fig. 4.8 demonstrate a comparison of the melting front positions as a function of time for numerical and analytical studies. The mushy region in the solid-liquid interface exists between the temperature ranges of 313 K to 316 K, where the melting front position can be assumed to be in the middle of this mushy region and therefore the temperature of 314.5 K is chosen to represent the position of the melting front. By using Eq. (4.9), the results of both numerical and analytical data show a good agreement and thus confirming the simulation of the phase change process.

CHAPTER 5

LATENT HEAT THERMAL ENERGY STORAGE: NUMERICAL ANALYSIS RESULTS AND DISCUSSION

The analytical validation presented in the previous chapter shows that COMSOL Multiphysics software can sufficiently simulate the phase change process with the use of the modified heat capacity method. In the following sections of this chapter, the results obtained from the numerical study of an axisymmetric 2D latent heat thermal energy storage will be presented and discussed in detail. Before any simulations are carried out, a mesh convergence study is performed to obtain optimum mesh element size and to achieve results with the highest possible accuracy from the numerical studies. The numerical studies are then carried out to investigate the effects of the heat transfer fluid velocities and the number of the thermal enhancers or fins on the phase change process occurring inside the LHTES. Furthermore, the maximum possible energy that can be stored in various configurations of the LHTES is also calculated.

5.1 Numerical analysis – Mesh convergence study

An axisymmetric 2D latent heat thermal energy storage system with similar dimensions and materials presented in Chapter 3 are illustrated in Fig. 5.1. The mesh convergence study was set in the beginning to the boundary and initial conditions shown in Table 5.1. These conditions can be easily set up in the COMSOL software.

Table 5.1: Boundary and initial conditions used in the convergence study.

	Initial	Inlet (water)	Outlet	Channel wall	Outer surfaces
Thermal parameters	293.15K	350K	Convective flux	Thermal continuity	Insulated
Fluid parameters	0.05 m/s	0.05 m/s	No viscous stress, P_o=0	No slip	-

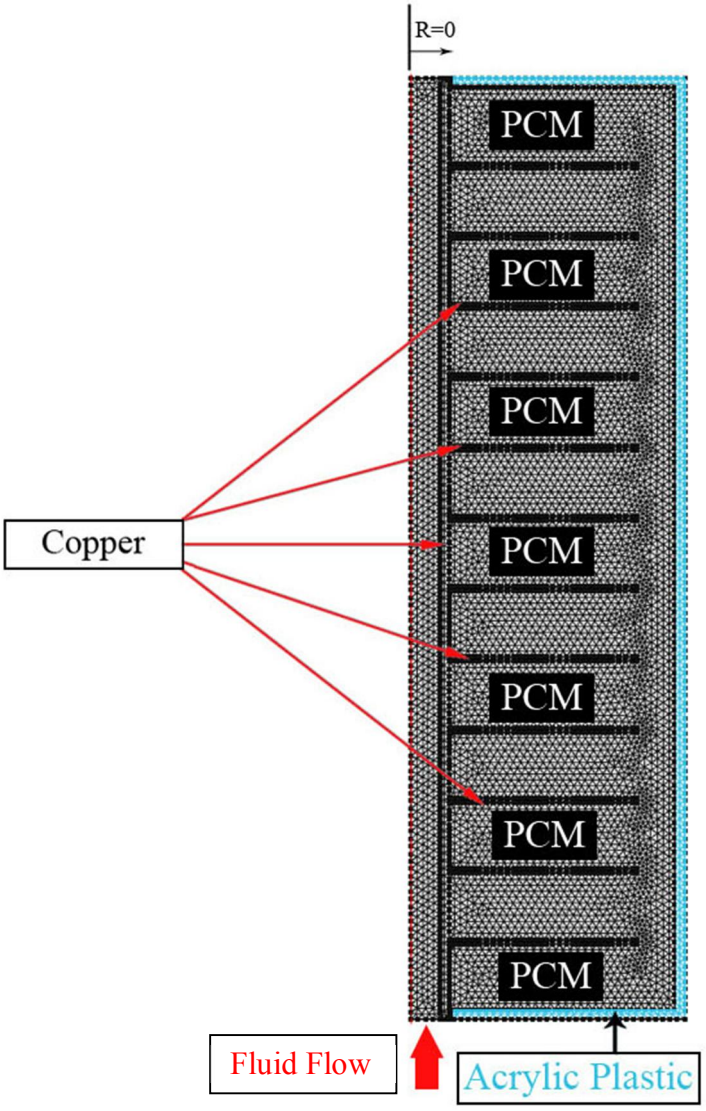

Fig. 5.1. A meshed axisymmetric 2D model of the LHTES used in the numerical studies.

The outer surfaces of the model are thermally insulated.

Similar to the mesh convergence study carried out in the previous chapter, changes to the mesh element size are performed and refined until converging results can be obtained. The time-step configuration is also similar to the study done in Chapter 3. The following Table 5.2 shows the various element sizes and the data collected from the 21 hours simulated time study.

Table 5.2: Various element sizes used in the convergence study and their data.

Element size (mm)	No. of elements	Number of DOFs	Simulation time (s)
20	4405	3521	357s
16	5248	4281	876s
12	6915	5728	5975s
8	12963	10047	9327s
5	31368	23043	12832s

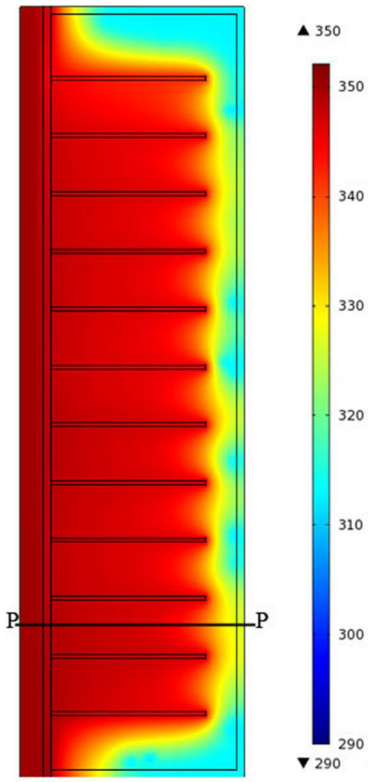

Fig. 5.2. A 12 fins configuration LHTES with its 2D surface temperature plot used in the convergence study. Simulated time: 21 hours.

Fig. 5.2 shows the temperature plot of a 12 fins configuration LHTES after 21 hours simulated time. The line P-P shows the region at which the convergence study is carried out for various mesh element sizes; from 0.02 m down to the smallest size of 0.005 m. The results of the study are illustrated in the temperature profile plot as shown in Fig. 5.3. As shown in the figure, the mesh element sizes of 0.02, 0.016 and 0.012 m recorded higher temperature profile plots compared to the plots of mesh element sizes of 0.005 and 0.008 m. The figure also shows that the temperature is independent of the 0.005 and 0.008 element sizes; which means further reduction in the size of element does not change the numerical results. Thus, to save time; mesh element size of 0.008 m is chosen for the subsequent simulation runs.

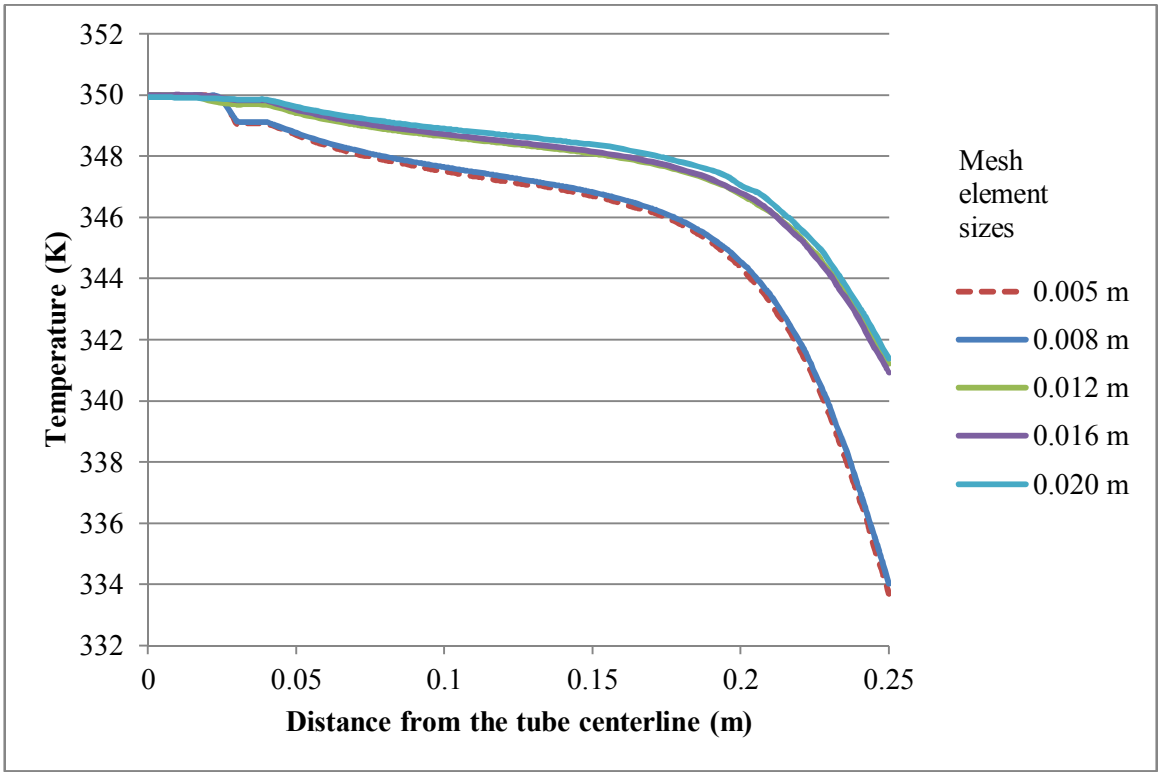

Fig. 5.3. Temperature profile plots for various mesh element sizes at line P-P.

Simulated time: 21 hours.

5.2 Energy stored in LHTES: Integrating COMSOL functions

In order to calculate the possible amount of energy stored in the LHTES device during the charging (melting) period, volume integration on the phase change material domain is carried out. The integration calculation is performed on the modified heat capacity $C_{p,pcm}$ (which is in the function of the temperature) multiplied with the temperatures in the PCM region, divided by total volume of the phase change material:

$$E_{total} = m_{pcm} \frac{\iiint C_{p,pcm}(T(r,\theta,z) - T_i).r\ drd\theta dz}{\iiint (r,\theta,z).r\ drd\theta dz} \tag{5.1}$$

Through the finite element analysis simulation, temperature data from every point of the whole system can be extracted out. Knowing this, the sensible and latent heat contributions for each temperature range can also be calculated and translating all the information into COMSOL requires special functions. By restricting the integration on known temperature ranges for the solid-liquid phase transformation process, the following COMSOL functions describe the total, sensible and latent energy stored in the LHTES (Groulx and Ogoh, 2009):

$$\begin{aligned} E_{sensible} = \rho[&(C_p * (1 - flc2hs((T - 313)[1/K], dD[1/K])) * (T - (293[K]))) \\ &+(C_p * (flc2hs((T - 313)[1/K], dD[1/K]) - flc2hs((T \\ &\quad - 316)[1/K], dD[1/K])) * (20[K])) \\ &+(C_p * (flc2hs((T - 316)[1/K], dD[1/K])) * (T - (296[K])))] \end{aligned} \tag{5.2}$$

$$E_{latent} = \rho[(C_{p,eff} * (flc2hs((T - 313)[1/K], dD[1/K]) - flc2hs((T - 316)[1/K], dD[1/K])) * (T - (313[K])))$$
$$+(C_{p,eff} * (flc2hs((T - 316)[1/K], dD[1/K])) * (3[K]))] \quad (5.3)$$

$$E_{total} = E_{sensible} + E_{latent} \quad (5.4)$$

The equation of Eq. (5.2) describes the sensible energy stored in the solid (T < 313 K) and liquid phase (T > 316 K). Whereas, equation of Eq. (5.3) describes the latent energy stored by the PCM (313 K < T < 316 K).

5.3 Effects of HTF velocities

Simulations on LHTES with fin configurations of 0, 1, 2, 3, 4, 5, 6, 7, 9, 12, 15, 18, 21 and 24 fins were carried out to investigate the effects of various velocities of the HTF on the thermal behavior of the PCM in the thermal energy storage system. Heat transfer fluid velocities of 0.01, 0.03, 0.05 and 0.1 m/s (equivalent to mass flow rates of 0.0275, 0.0825, 0.1375 and 0.275 kg/s respectively) were used for the study. The range of mass flow rates between 0.0825 and 0.1375 kg/s are typically used in solar storage systems. The boundary and initial conditions used in the numerical studies have been presented in Table 5.1. Also, only the initial condition of the inlet flow velocity of the HTF is changed accordingly.

The following Figs. 5.4 and 5.5 show the temperature distribution plots for 7 and 15 fins configuration LHTES with different fluid inlet velocities after 12 hours of simulated time. Additionally, the Reynolds numbers for each inlet fluid velocity are also presented.

Appendix A shows all the temperature distribution plots studied for various number of fins and the four different HTF velocities.

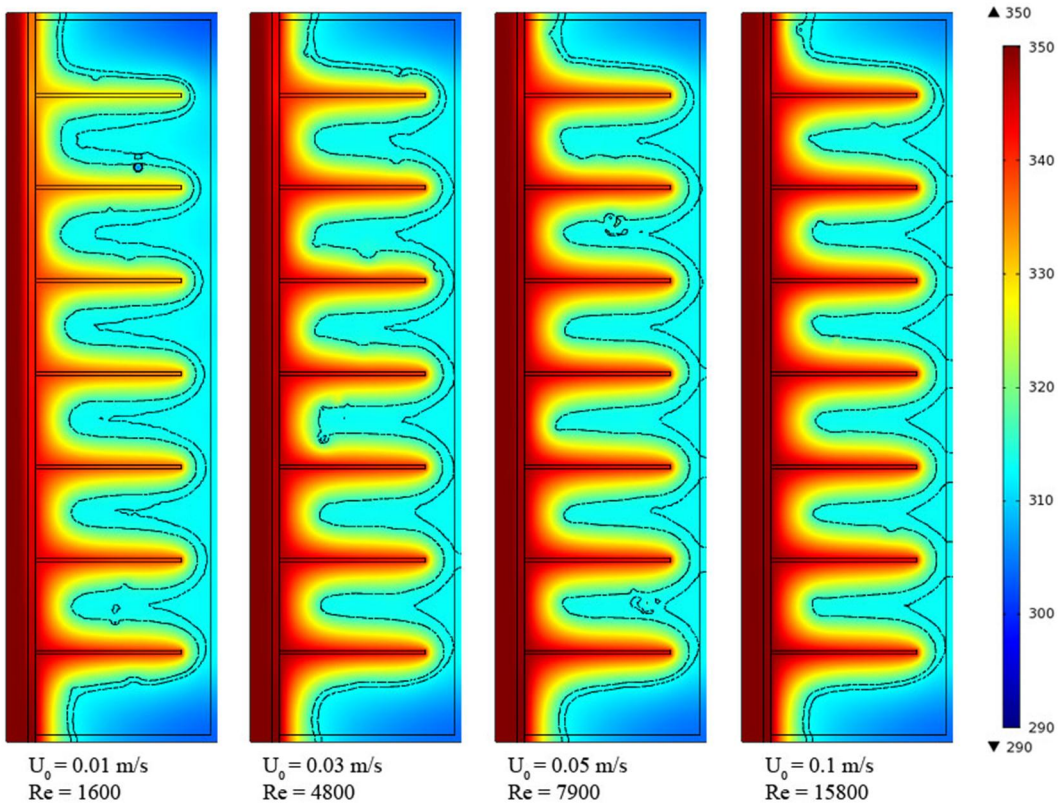

Fig. 5.4. Temperature distribution plots for the 7 fins configuration LHTES with various HTF velocities and their Reynolds numbers. Simulated time: 12 hours.

As can be seen from both Figs. 5.4 and 5.5, the heat from the thermal fluid (or water) is transferred by the conduction heat transfer mechanism through the copper tube and finally distributed into the phase change material. The heat is largely congregating around the fins nearer to the inlet, as can be clearly seen in the low thermal fluid velocity of 0.01 m/s. The heat transferred from the HTF to the fins produces higher temperature regions surrounding the fins nearer to the inlet. Furthermore, in Figs. 5.4 and 5.5; as the thermal fluid velocity increases, more heat can be transferred to the PCM, and therefore increases the possible

amount of energy that can be stored in the PCM. This can be fundamentally related to the Reynolds number of the thermal fluid.

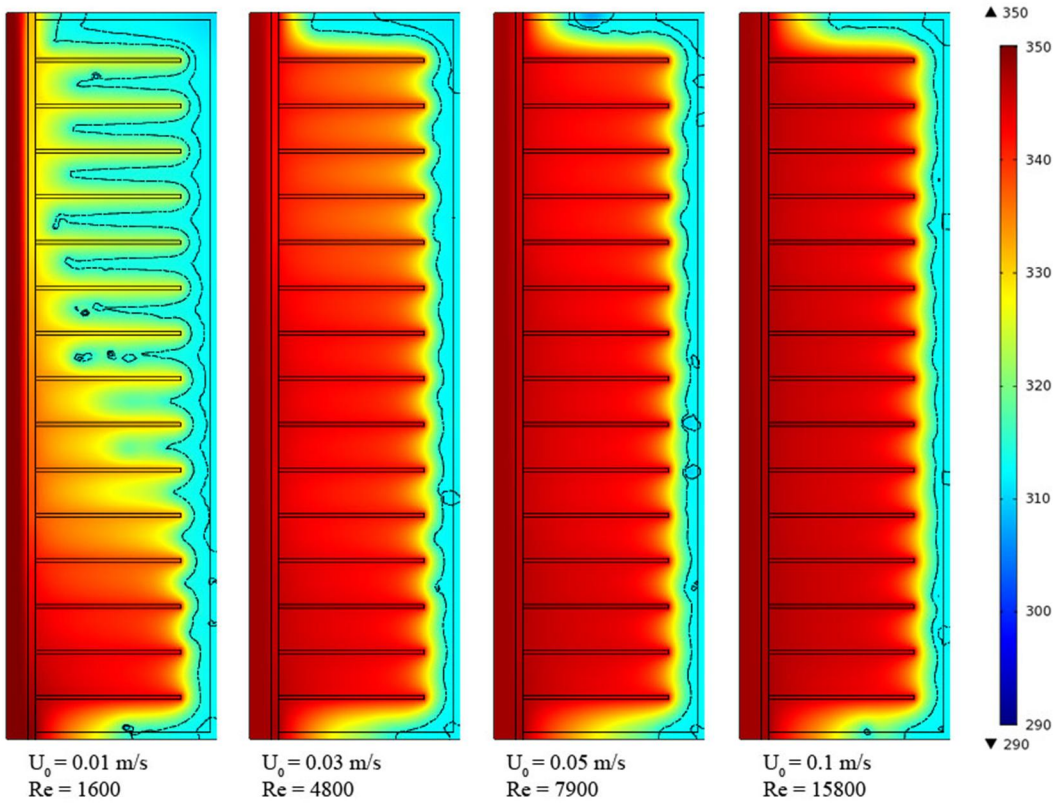

Fig. 5.5. Temperature distribution plots for the 15 fins configuration LHTES with various HTF velocities and their Reynolds numbers. Simulated time: 12 hours.

In Fig. 5.5, the higher number of fins contributed to the larger amount of heat distributed into the PCM when compared to the temperature distribution plots of Fig. 5.4. The results show that the possible amount of energy that can be stored increases with higher number of fins for corresponding velocities. For further clarification, the solid-liquid phase change interface can be indicated by the contour lines that represent the melting temperature (313 K – 316 K) of the paraffin wax. In Fig. 5.5, much of the PCM region is undergoing the melting phase, which is comparable to the contours in Fig. 5.4. This suggests higher amount of energy is being stored. During the charging process, there exists a slow heating

zone, or SHZ at which the PCM in this area is slower to receive heat due to the gap between the fins and the acrylic plastic container, as shown in Fig. 5.6. This area has a higher thermal resistance than the areas surrounding the fins. Therefore, the PCM in the SHZ is slower to melt, reducing the melting fraction of the phase change material. The SHZ area varies from one fin configuration to another, and it highly depends on the number of fins and the distance between the fins. For the current study, the effects of the distance between the fins and the enclosure are not in the scope of research, although the SHZ influences the thermal behavior of the PCM and the overall possible energy storage ability of the LHTES.

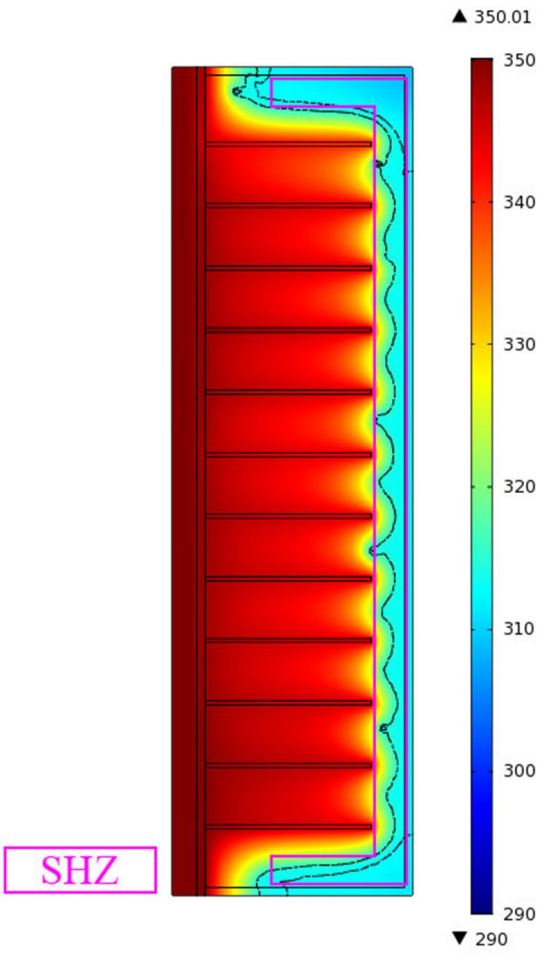

Fig. 5.6. Slow heating zone (SHZ) between the fins and the enclosure reduces the melting fraction of the PCM.

Figs. 5.7 to 5.14 show the total energy stored as a function of time for different LHTES fin configurations over a 12 hours of simulated charging time for various HTF velocities. The figures illustrated the variation of total energy stored for 0, 1, 6, 7, 12, 15, 21 and 24 fins configuration. The results of Fig. 5.7 for the 0 fin configuration show that there is no significant increase of the total energy stored in the PCM as the HTF velocities increases. This is due to the high thermal resistance of the PCM. With the addition of fins, the thermal resistance on the PCM reduces, and the higher thermal energy of the HTF initiates the heat transfer process into the PCM with the help of the fins. Thus, more energy can be stored in the PCM and by increasing the HTF velocities; the amount of energy that can be stored is more evident as clearly shown in the following figures.

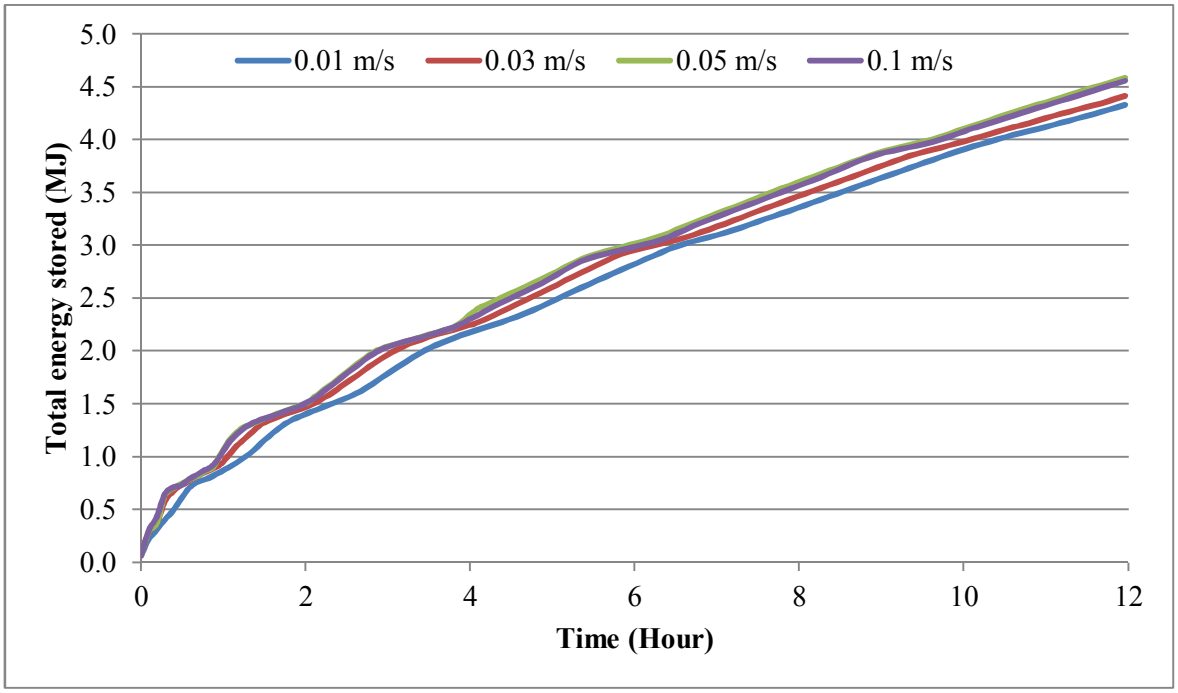

Fig. 5.7. Total energy stored for the 0 fin configuration LHTES over 12 hours of simulated time for various HTF velocities.

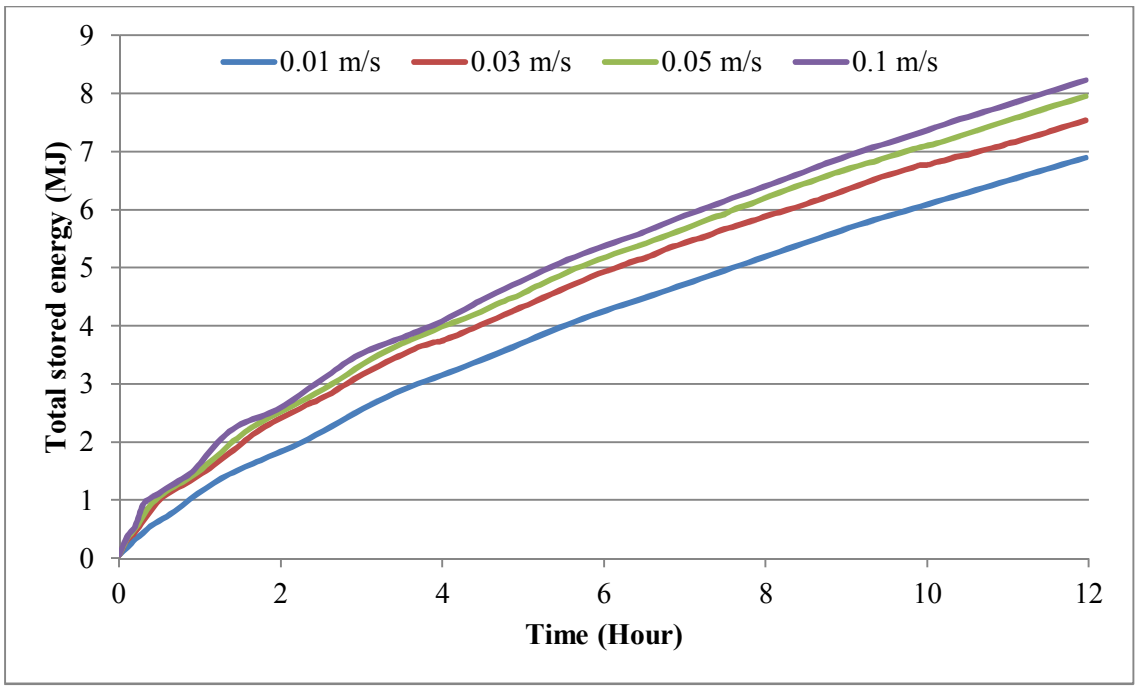

Fig. 5.8. Total energy stored for the 1 fin configuration LHTES over 12 hours of simulated time for various HTF velocities.

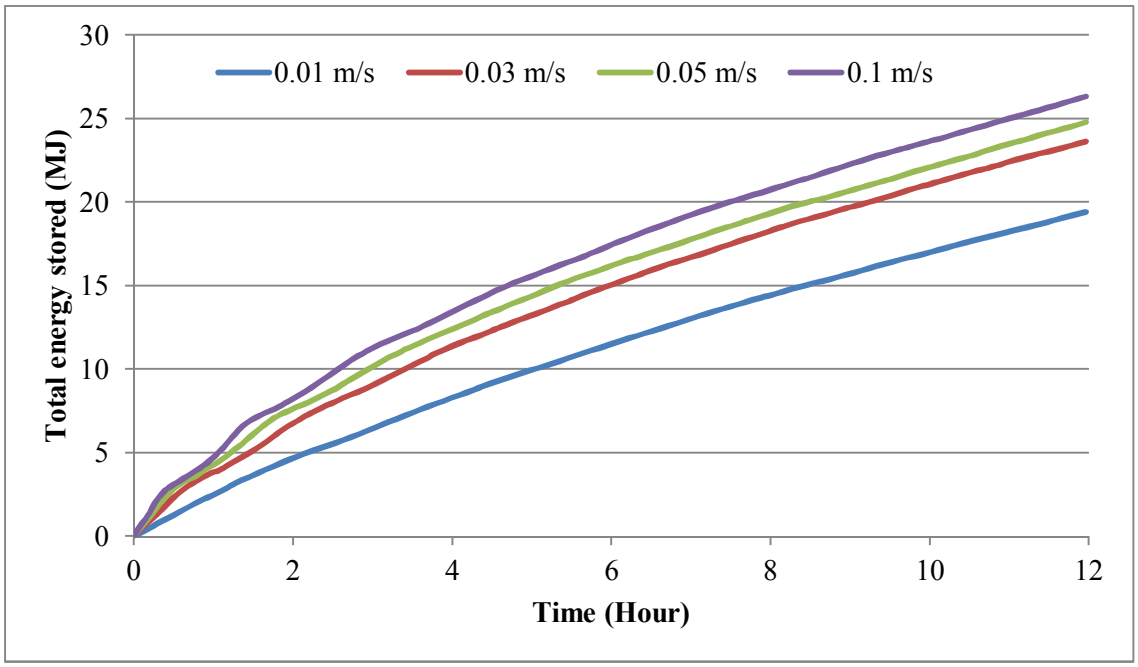

Fig. 5.9. Total energy stored for the 6 fins configuration LHTES over 12 hours of simulated time for various HTF velocities.

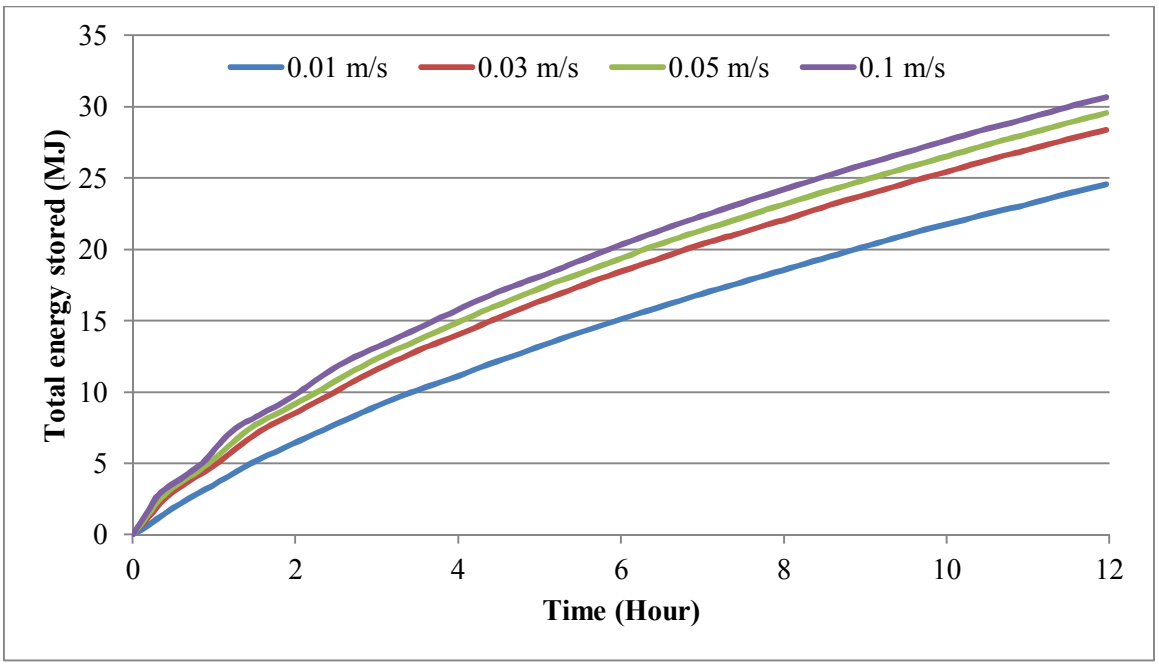

Fig. 5.10. Total energy stored for the 7 fins configuration LHTES over 12 hours of simulated time for various HTF velocities.

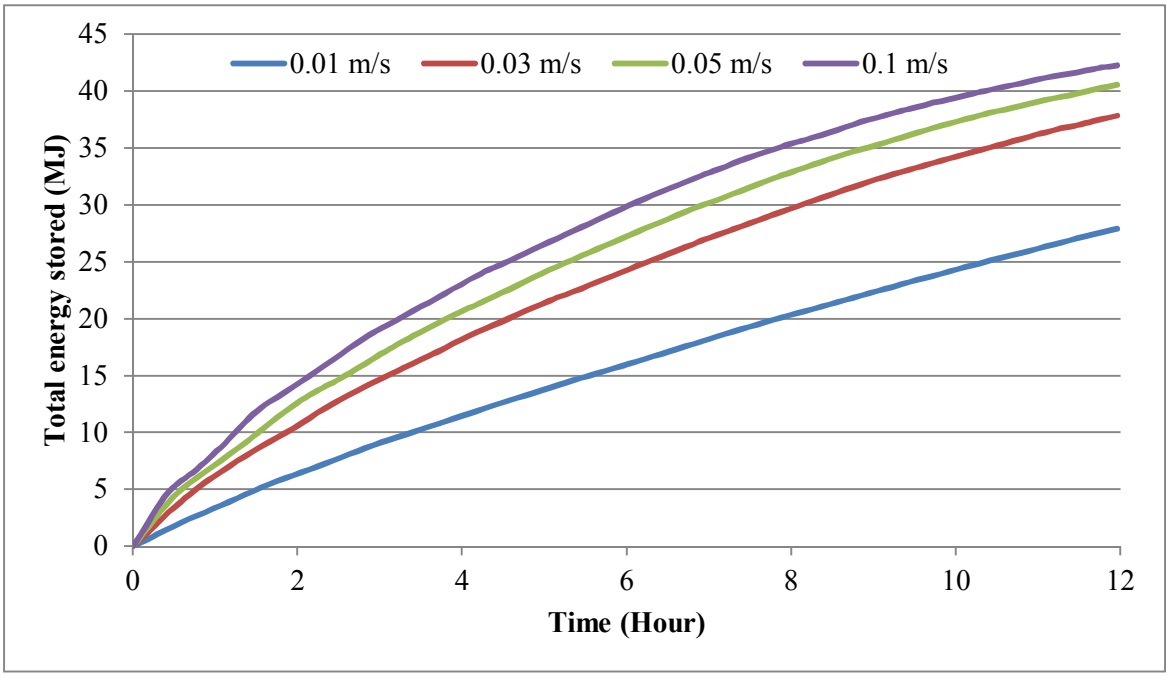

Fig. 5.11. Total energy stored for the 12 fins configuration LHTES over 12 hours of simulated time for various HTF velocities.

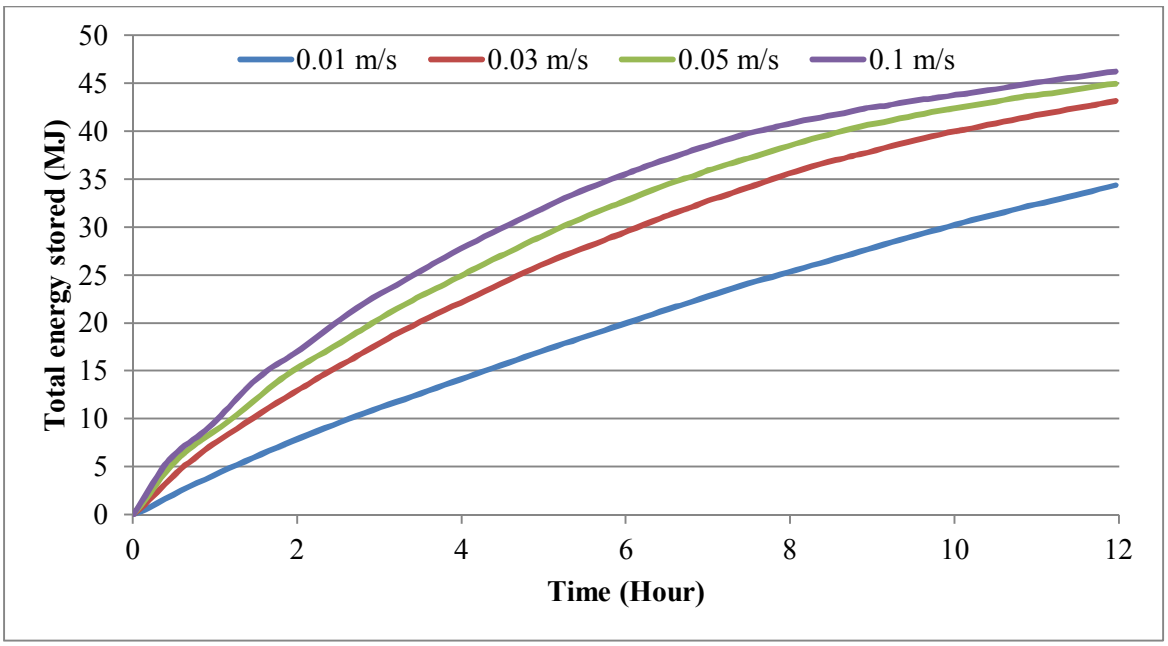

Fig. 5.12. Total energy stored for the 15 fins configuration LHTES over 12 hours of simulated time for various HTF velocities.

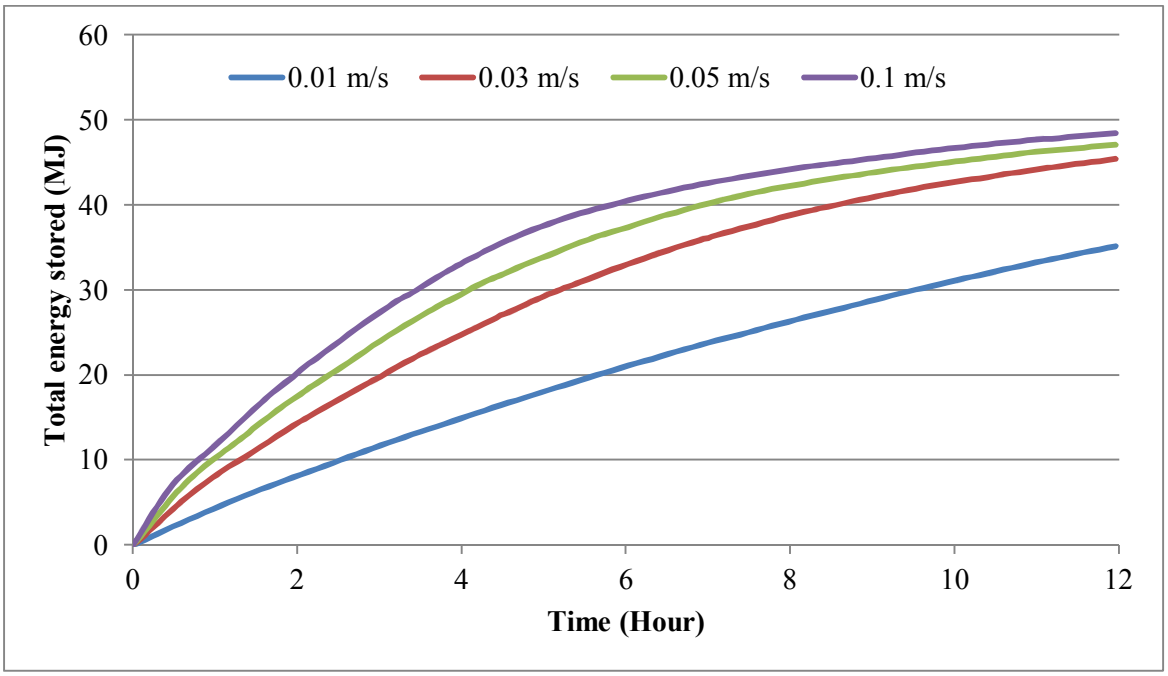

Fig. 5.13. Total energy stored for the 21 fins configuration LHTES over 12 hours of simulated time for various HTF velocities.

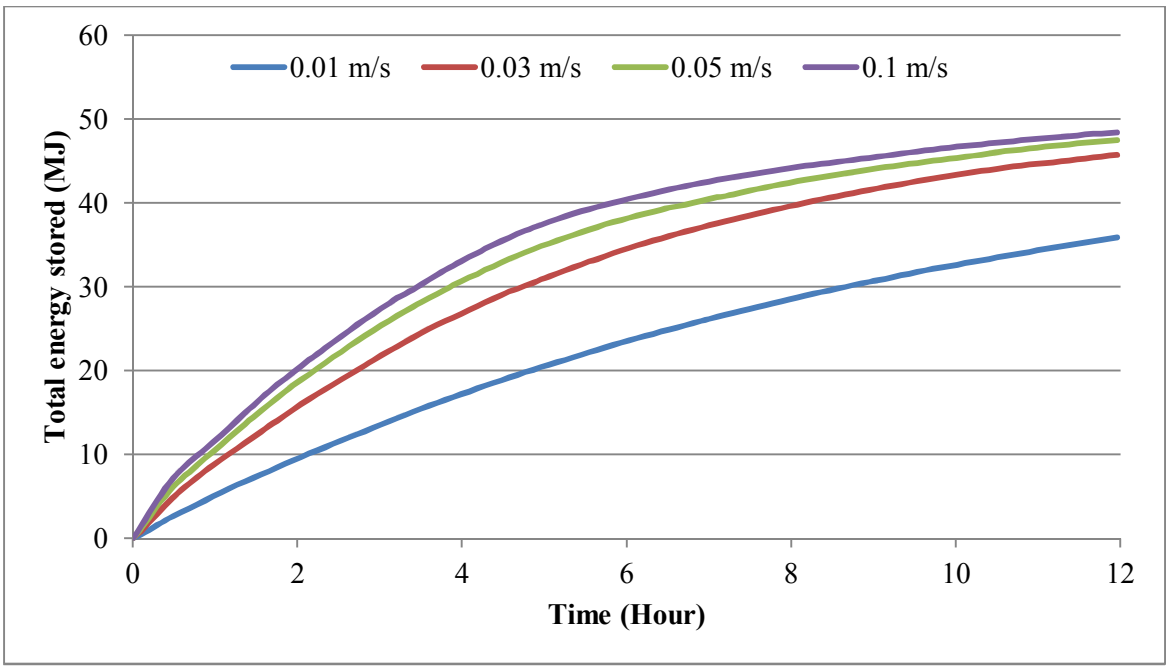

Fig. 5.14. Total energy stored for the 24 fins configuration LHTES over 12 hours of simulated time for various HTF velocities.

The 2D column chart shown in Fig. 5.15 illustrates the sensible energy stored in the PCM with different fin configurations and fluid inlet velocities. Table 5.3 tabulates the percentage of sensible energy increase for various numbers of fins as the HTF velocity increases (0.01 m/s to 0.1 m/s). The ratio of increase is given by:

$$Energy\ increase\ \% = \frac{E_{u=0.1m/s} - E_{u=0.01m/s}}{E_{u=0.1m/s}} \text{ x } 100 \tag{5.5}$$

Table 5.3: Sensible energy increase in the LHTES for various numbers of fins as the HTF velocity increases.

No. of fins	**0**	**1**	**2**	**3**	**4**	**5**	**6**
Energy increase (%)	3.5	11.7	12.9	13.0	13.5	17.8	15.7
	7	**9**	**12**	**15**	**18**	**21**	**24**
Energy increase (%)	12.4	18.3	35.9	33.5	23.3	26.5	28.4

The calculations demonstrate that there exists a steady increase of sensible heat contribution from 0 to 9 fins configuration with their percentage difference across the different HTF velocities varies between 3 to 18%. The majority of the PCM is not yet fully melted for these configurations and the thermal resistance of the phase change material is hindering the influence of the HTF velocities to distribute heat into the PCM efficiently. The percentage difference jumps to the highest percentage increase of 36% in the 12 fins configuration due to the larger fraction of the PCM has been melted, increasing the penetration of thermal energy into the SHZ areas and thus storing larger sensible heat in the liquid PCM. As the number of fins increases, the effects of increasing HTF velocities on the thermal resistance of the PCM are more evident as shown in Fig. 5.15.

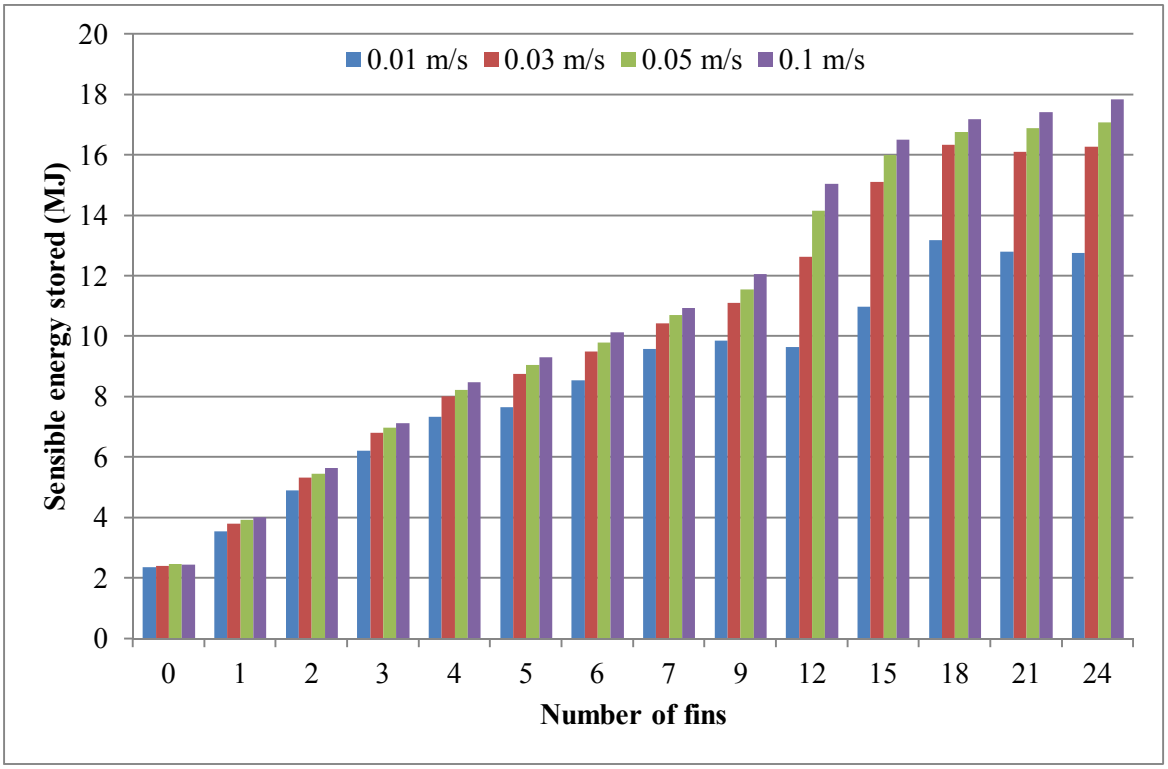

Fig. 5.15. Sensible thermal energy stored in various numbers of fins configuration for HTF velocities of 0.01 m/s, 0.03 m/s, 0.05 m/s and 0.1 m/s. Simulated time: 12 hours.

The 2D column chart shown in Fig. 5.16 illustrates the latent energy stored in the PCM with different fin configurations and fluid inlet velocities. Table 5.4 tabulates the percentage of latent energy increase for various numbers of fins as the HTF velocity increases.

Table 5.4: Latent energy increase in the LHTES for various numbers of fins as the HTF velocity increases.

No. of fins	**0**	**1**	**2**	**3**	**4**	**5**	**6**
Energy increase (%)	6.8	20.5	23.1	23.9	25.9	39.5	32.9
	7	**9**	**12**	**15**	**18**	**21**	**24**
Energy increase (%)	24.1	31.1	32.9	21.3	16.6	24.8	25.4

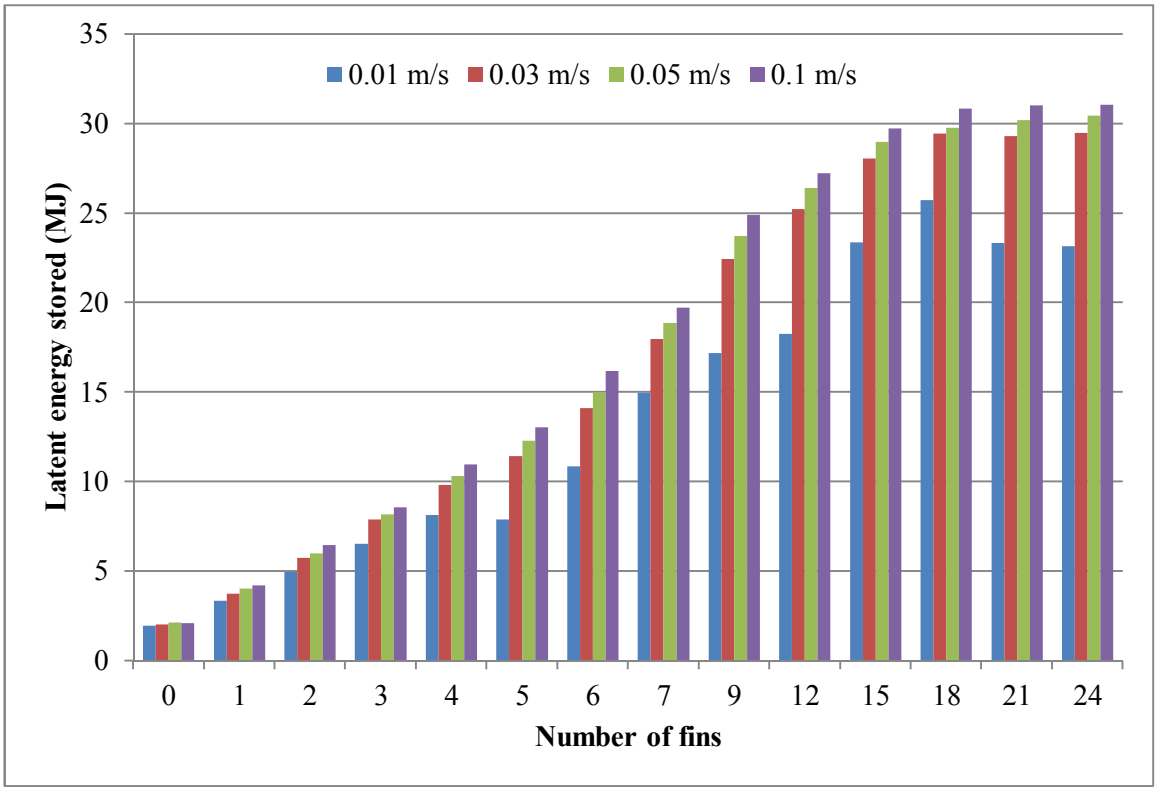

Fig. 5.16. Latent thermal energy stored in various numbers of fins configuration for HTF velocities of 0.01 m/s, 0.03 m/s, 0.05 m/s and 0.1 m/s. Simulated time: 12 hours.

The overall results shown in Fig. 5.16 illustrates that there is a progressive increase of latent energy percentage difference from the 0 to 12 fin configurations across the increasing HTF velocities. As the number of fins increases from 15 to 24, the rate of increase of the latent thermal energy stored in the PCM declines until it appears to be constant for 0.03 m/s to 0.1 m/s HTF velocities, whereas the 0.01 m/s HTF velocity shows an obvious reduction in latent heat contribution. This is due to most of the PCM volume has been melted and changed into the liquid state, reducing the contributions of latent thermal energy. Furthermore, with the increase of the number of fins, the volume of PCM reduces, hence reducing the possible amount of latent thermal energy contribution.

The total thermal energy stored in the various fin configurations for various HTF velocities after simulated charging time of 12 hours are shown in Fig. 5.17. As described in Eq. (5.4), the total thermal energy stored is the accumulation of the sensible and latent thermal energy stored in the LHTES. The results shown in Fig. 5.17 illustrates that the total thermal energy stored in the PCM increases as the number of fins and HTF velocity increases. Table 5.5 shows the percentage difference of the total thermal energy stored for various numbers of fins as the HTF velocity increases from 0.01 m/s to 0.1 m/s.

Table 5.5: Total energy percentage increase in the LHTES for various numbers of fins as the HTF velocity increases.

No. of fins	**0**	**1**	**2**	**3**	**4**	**5**	**6**
Energy increase (%)	5.0	16.2	18.3	18.9	20.5	30.5	26.3
	7	**9**	**12**	**15**	**18**	**21**	**24**
Energy increase (%)	19.9	26.9	34.0	25.7	19.0	27.4	26.5

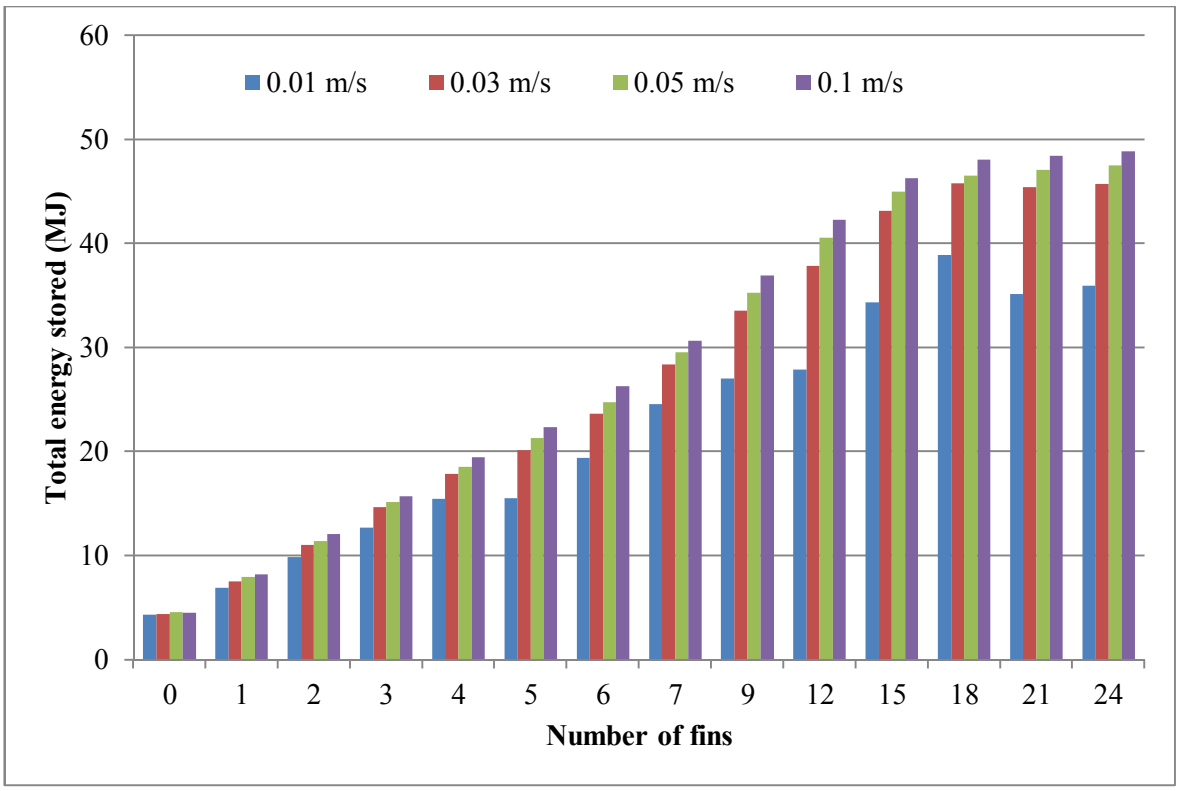

Fig. 5.17. Total thermal energy stored in various numbers of fins configuration for HTF velocities of 0.01 m/s, 0.03 m/s, 0.05 m/s and 0.1 m/s. Simulated time: 12 hours.

From 0 to 5 fins configuration, the velocity of HTF influences the increase of percentage difference which starts from 5.0 to 30.5%. However, the percentage difference declines from the 5 to 7 fins configuration. This is mainly due to the drop in latent heat contribution which is caused by the melting of the PCM as more areas of the PCM are melted and turned into the liquid state. This is also apparent in Table 5.4 which shows a reduction of latent energy difference across the HTF velocities from 5 to 7 fins configuration. Furthermore, a slow heating zone or SHZ created by the gap between the fins and the container reduces the contribution of both the sensible and latent heats as the thermal resistance of the SHZ area is high; creating inconsistencies in the total energy that can be possibly stored. Therefore, higher number of fins with higher HTF velocity may penetrate the SHZ in order for them to

melt, as will be discussed and shown in the next section. Additionally, from 7 to 12 fins configuration, the percentage difference increases again due to the increase of fin numbers which reduces the PCM thermal resistance, thus increasing the storage of total thermal energy. This cycle continues until the 24 fins configuration, where the maximum percentage difference was recorded for 12 fin configurations with 34% of difference across the HTF velocity variable.

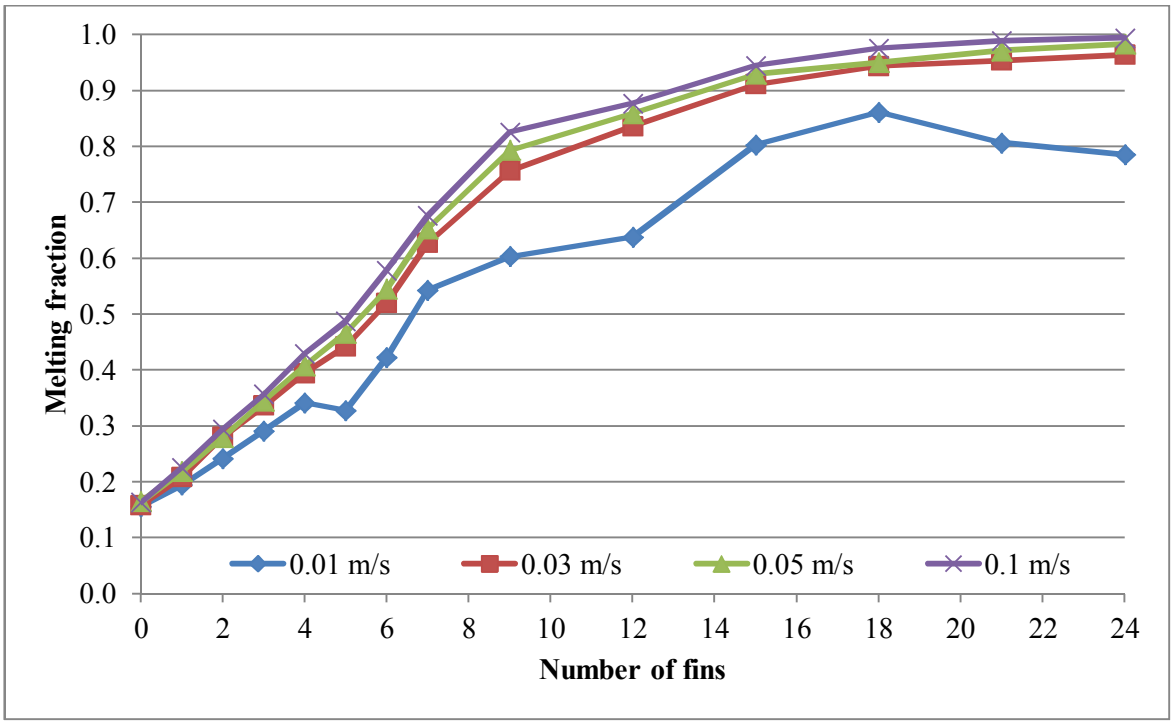

Fig. 5.18. Melting fraction for various HTF velocities from 0 to 24 fins configuration. Simulated time: 12 hours.

The plots shown in Fig. 5.18 illustrate the melting fractions of the PCM for different HTF velocities with various numbers of fins. Similar in Chapter 4, the middle temperature of the solid-liquid phase change interface (T = 314.5 K) is chosen for the calculation of the melting fraction. The results describe the melting fraction increases as the number of fins

increases for all the HTF velocities. For example, the 12 fins configuration recorded an increase in the melting fraction from 0.64, 0.84, 0.86 and finally 0.88 for 0.01, 0.03, 0.05 and 0.1 m/s HTF velocities respectively. A melting fraction of 0.99 ≈ 1 (or a nearly completed melt) was recorded for the 24 fins configuration at HTF velocity of 0.1 m/s.

5.4 Effects of number of fins as thermal enhancers

To investigate the effects of the number of fins on the thermal behavior of the PCM inside the latent heat thermal energy storage device, numerical studies were carried out on the 0 to 24 fins configuration of the system with fixed HTF velocities of 0.01 m/s and 0.1 m/s. Note that the velocity of 0.01 m/s translates into the mass flow rate of 0.0275 kg/s and Reynolds number of 1600, and therefore the flow in the tube is laminar. Whereas the velocity of 0.1 m/s translates into the mass flow rate of 0.275 kg/s with Reynolds number of 15800, which is a turbulent flow. The simulated time, time-steps, initial and boundary conditions are similar to those in the previous section.

5.4.1 Effects of the addition of fins at HTF velocity of 0.01 m/s

The temperature distribution plots for the 1, 6, 12, 18 and 24 fins configurations with HTF velocity of 0.01 m/s are shown in Fig. 5.19. From the figure, as the number of fins increases from 1 to 18 fins, the amount of possible thermal energy stored in the PCM increases. This is also demonstrated with the solid-liquid phase change interface or the melting front characterized by the two black contour lines. The interface denotes the temperature range of 313 K to 316 K and can be seen from 1 to 24 fins configuration. However, as the number of fins increases to 24, its temperature distribution plot shows a

reduction in the amount of energy stored in the PCM as the areas surrounding the fins are fully melted up to the 17th fin only. For other temperature distribution plots with the HTF velocity of 0.01 m/s, Appendix B can be referred to.

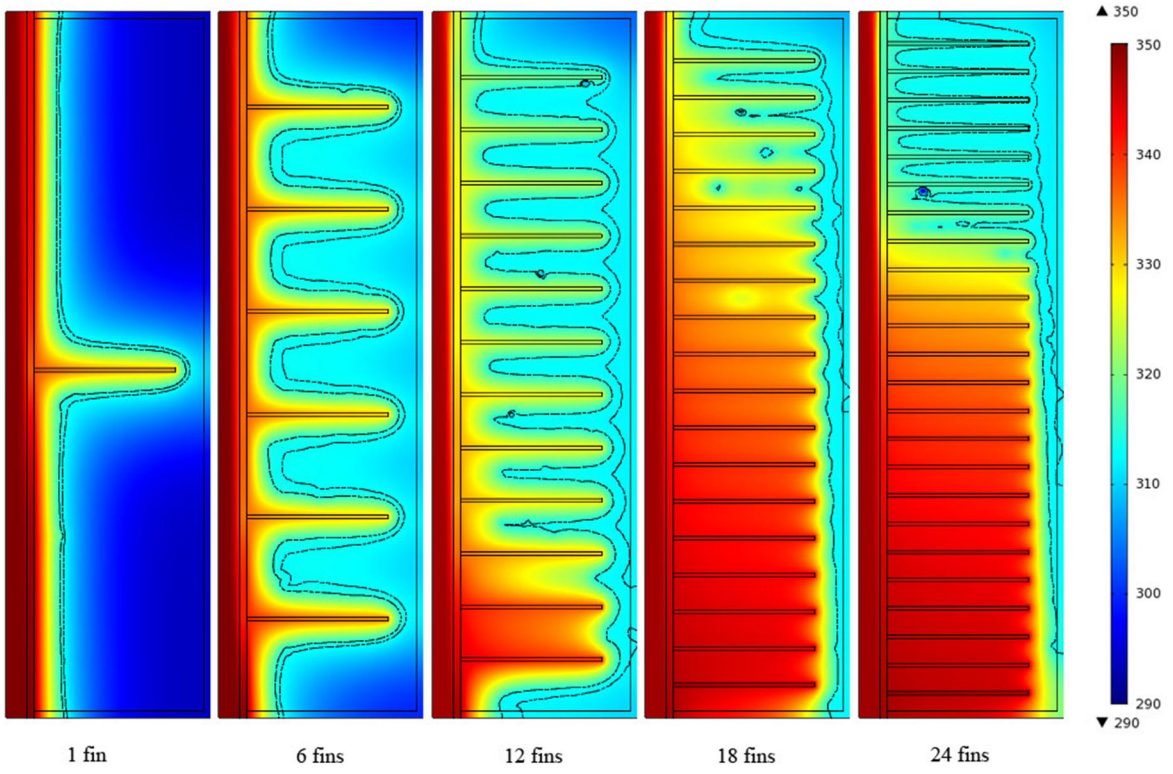

Fig. 5.19. Temperature distribution plots for the 1, 6, 12, 18 and 24 fins configuration LHTES after 12 hours of simulated charging time. u_0= 0.01 m/s.

Fig. 5.20 shows the total energy stored as a function of time for different fin configurations over a 12 hours of simulated charging time at HTF velocity of 0.01 m/s. The figure illustrates the variation of total energy stored for some of the 0 to 24 fins configuration of LHTES. As shown, the amount of total energy stored increases from 0 to 18 fins configuration. But, as previously noted; the total energy stored reduces from 18 to 24 fins configuration. This is because most of the heat supplied into the PCM congregate in the fins nearer to the inlet, and as the length of the tube increases much of the thermal energy in the HTF has been stored in most of the fins' surrounding regions up to the 17th fin; leaving

the subsequent areas to receive much less thermal energy from the HTF. The reduction of the total energy stored in the PCM is also influenced by the reduction of the PCM's volume as the number of fins increases. After the simulated charging time of 12 hours is completed, the highest and lowest energy stored in the PCM are 38.8 MJ and 4.3 MJ for 0 and 18 fins configuration respectively.

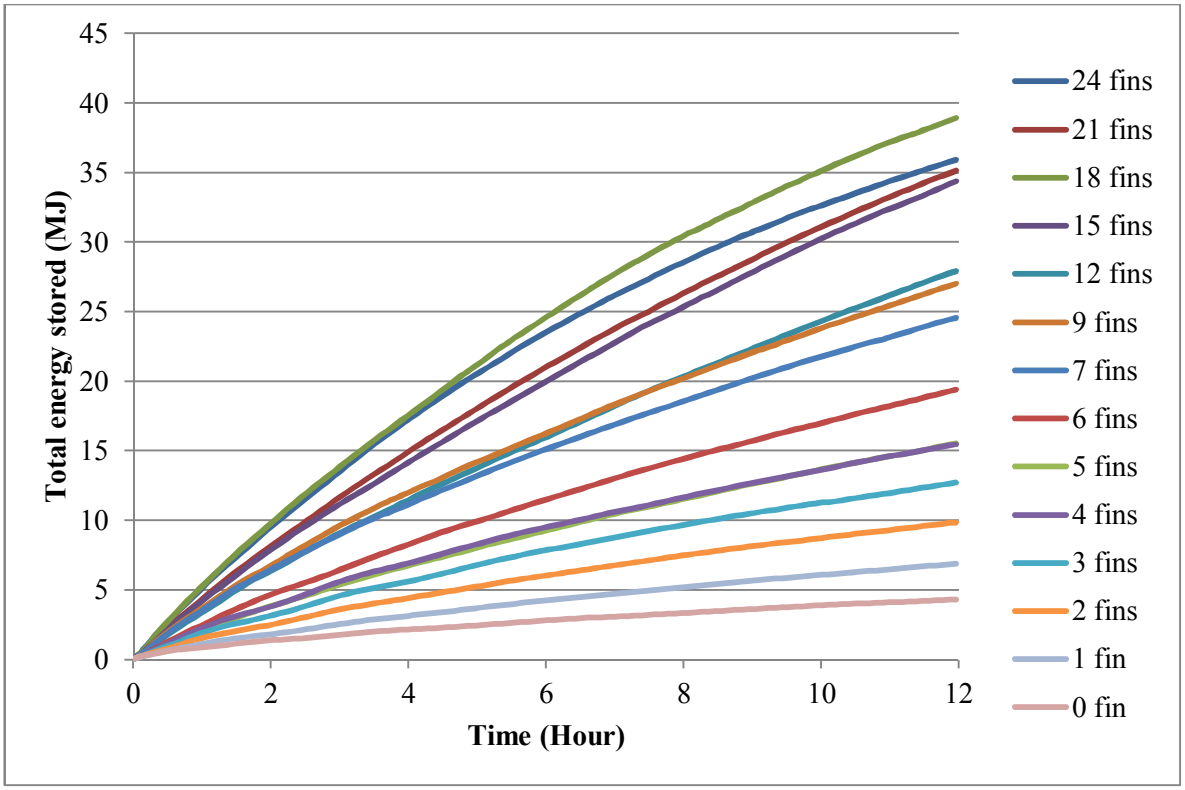

Fig. 5.20. Total energy stored in 0 to 24 fins configuration of the LHTES after 12 hours of simulated charging time. u_0 = 0.01 m/s.

The chart shown in Fig. 5.21 illustrates the amount of sensible and latent thermal energy stored in 0 to 24 fins configuration for HTF velocity of 0.01 m/s. The latent thermal energy stored in the PCM shows a progressive increase from 1.97 MJ for 0 fin configuration to a maximum of 25.73 MJ for 18 fins configuration, and reduces in the higher number of fins. The rate for sensible thermal energy storage also increases as the number of fins increases.

The minimum amount of sensible energy stored is 2.36 MJ for 0 fin configuration and the maximum was recorded for the 18 fins configuration in which 13.19 MJ of sensible energy has been stored. Evidently, the amount of energy stored reduces when the number of fins increases from 18 to 24 fins. This is because of the low HTF velocity which in turn lowers the rate of energy transfer to the PCM and therefore reducing the amount of total energy stored in the system.

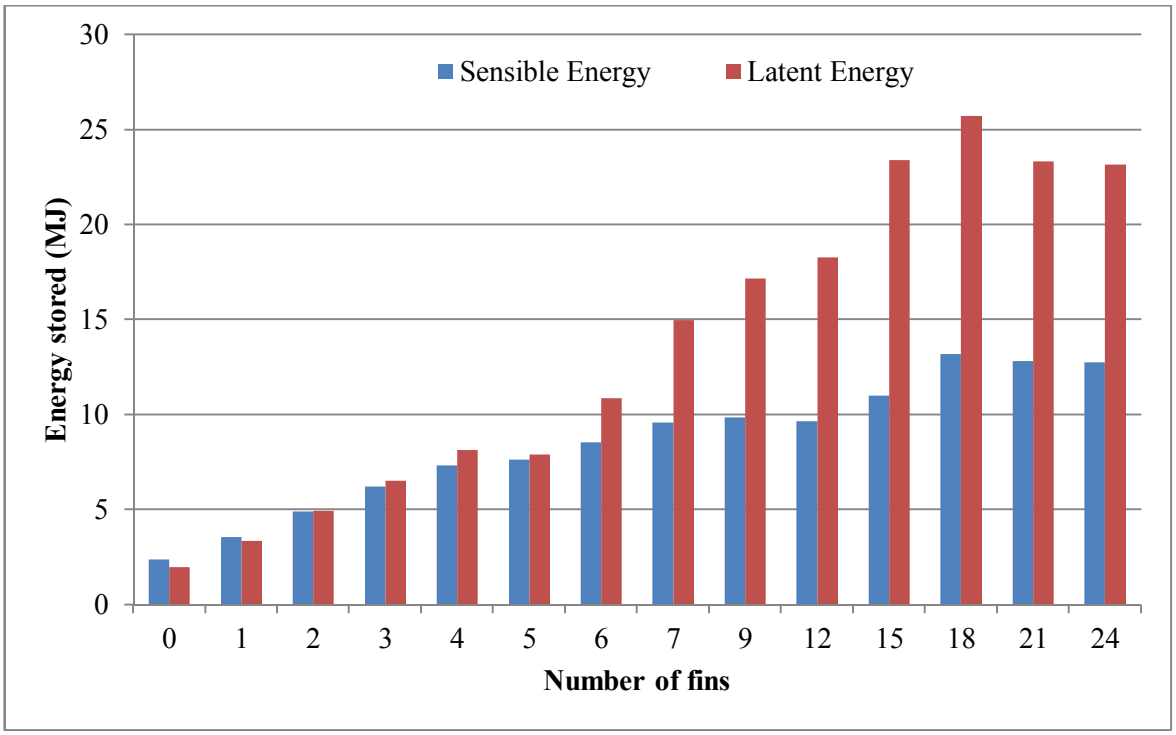

Fig. 5.21. Sensible and latent thermal energy stored in 0 to 24 fins configuration after 12 hours of simulated charging time. u_0 = 0.01 m/s.

5.4.2 Effects of the addition of fins at HTF velocity of 0.1 m/s

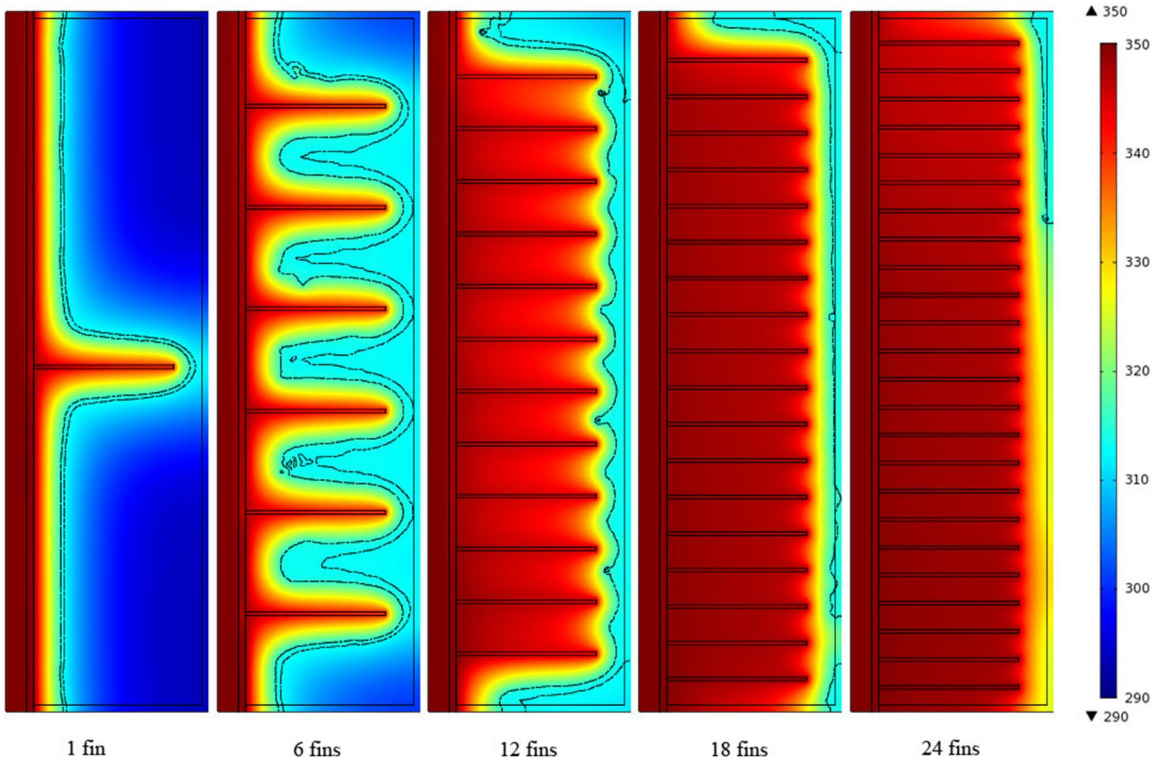

Fig. 5.22. Temperature distribution plots for the 1, 6, 12, 18 and 24 fins configuration LHTES after 12 hours of simulated charging time. u_0= 0.1 m/s.

The temperature distribution plots for the 1, 6, 12, 18 and 24 fins configurations with HTF velocity of 0.1 m/s are shown in Fig. 5.22. Similar to the previous subsection, as the number of fins increases, the amount of possible thermal energy stored in the PCM correspondingly increases. This is also can be demonstrated with the solid-liquid phase change interface or the melting front characterized by the two black contour lines. The interface denotes the temperature range of 313 K to 316 K and can be seen from 1 to 24 fins configuration. The contours can be clearly seen in the 1 and 6 fins configuration. But as the number of fins increased to 12 and 18 fins configuration, the contour line of 316 K has partially disappeared. With the 24 fins configuration, almost all of the PCM has been

melted and the 316 K contour line has disappeared completely, leaving a fraction of the melting front in the regions surrounding the fins nearer to the outlet where only the 313 K temperature contour line can be seen. For other temperature distribution plots with the HTF velocity of 0.1 m/s, Appendix C can be referred to.

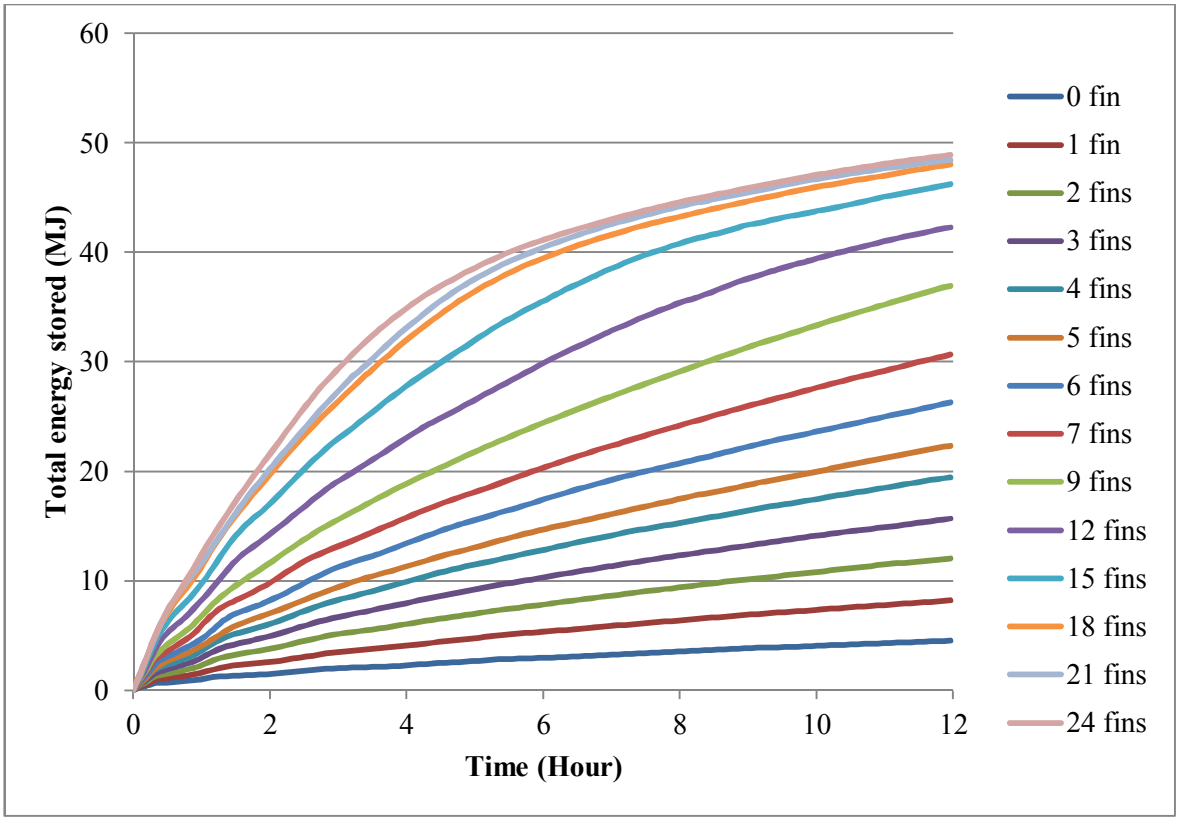

Fig. 5.23. Total energy stored in 0 to 24 fins configuration of the LHTES after 12 hours of simulated charging time. u_0 = 0.1 m/s.

Fig. 5.23 shows the total energy stored as a function of time for different LHTES's fin configurations over a 12 hours of simulated charging time at HTF velocity of 0.1 m/s. The figure illustrated the variation of total energy stored for some of the 0 to 24 fins configuration of LHTES. Similar to Fig. 5.20, the amount of total energy stored increases steadily as the number of fins increases. However, as the number of fins increases from 15

to 24 fins configuration, the rate of increase reduces significantly. As shown in Fig. 5.22, almost all of the PCM volume has been melted into the liquid phase in the LHTES with higher number of fins arrangement, reducing the latent thermal energy contribution to the overall total energy stored. The minimum and maximum total energy stored according to the results are 4.6 MJ and 48.9 MJ for 0 and 24 fins configurations respectively.

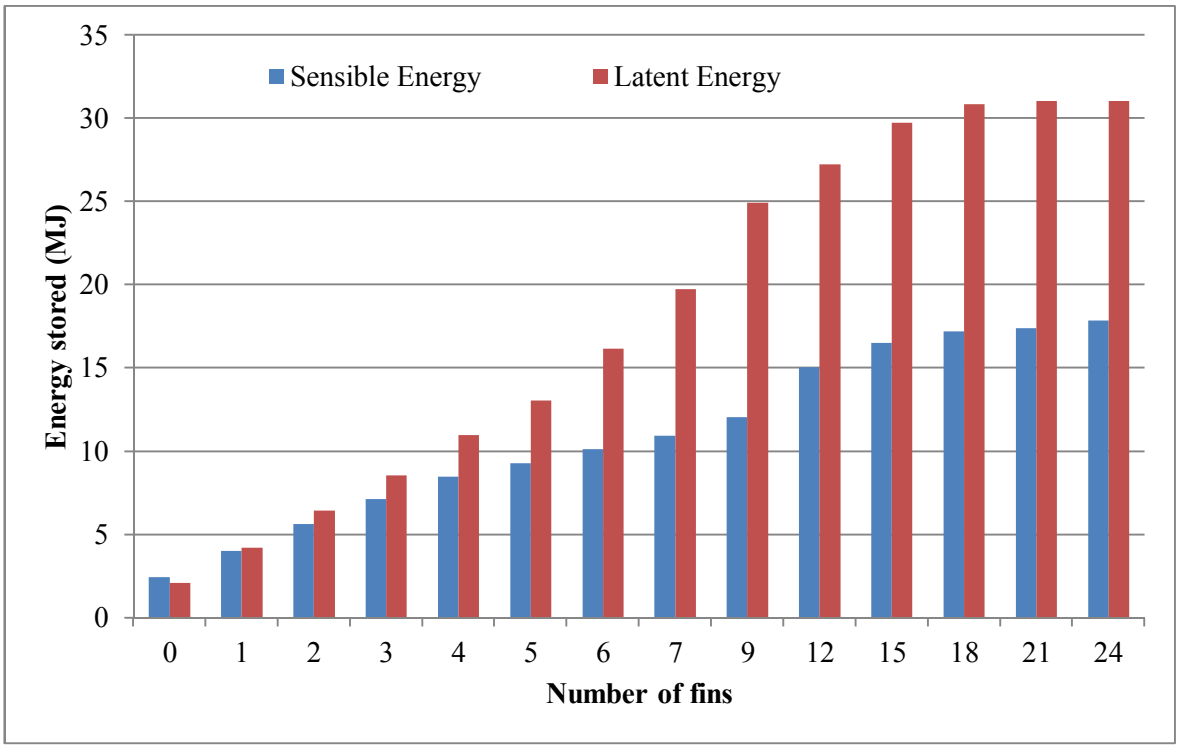

Fig. 5.24. Sensible and latent thermal energy stored in 0 to 24 fins configuration after 12 hours of simulated charging time. u_0 = 0.1 m/s.

The chart shown in Fig. 5.24 illustrates the amount of sensible and latent thermal energy stored in 0 to 24 fins configuration for HTF velocity of 0.1 m/s. The latent thermal energy stored in the PCM shows a progressive increase from 2.1 MJ for 0 fin configuration to a maximum of 31.1 MJ for 24 fins configuration. The rate of increase for sensible thermal energy storage shows a progressive growth from 0 to 18 fins configuration, from which the

increase rate seems to have slowed down as the number of fins increases. This is due to most of the PCM has been melted as a result of the reduced PCM volume with increasing number of fins.

5.5 LHTES maximum storage capacity and efficiency

As shown in the following Fig. 5.25, the plots for comparing between the maximum possible energy storage capacities with actual energy stored in the PCM for various fins configuration across the four different HTF velocities are presented. The maximum capacity of energy stored in the PCM can be calculated by using the following equation in which the whole PCM volume is assumed to be at the temperature of 350 K, which is the inlet fluid temperature:

$$E_{maximum} = \rho[(C_p * (313 - 293)[1/K]) + (C_{p,eff} * (316 - 313)[1/K]) + (C_p * (350 - 316)[1/K])] \quad (5.6)$$

The equation described in Eq. (5.6) is a COMSOL function which is used in the volume integration of the PCM domain. In Fig. 5.25, the highest maximum energy storage capacity that the entire PCM volume can store is 57.4 MJ for the 0 fin configuration. However, the lowest maximum energy storage capacity is obtained for the LHTES with 24 fins configuration with 52.3 MJ of possible thermal energy stored. The linear decrease of the maximum storage capacity of the PCM shown in Fig. 5.25 is mainly due to gradual reduction of the phase change material's available volume. As the number of fins increases, some of the phase change materials are displaced by the copper fins, reducing the possible amount of energy that can be stored.

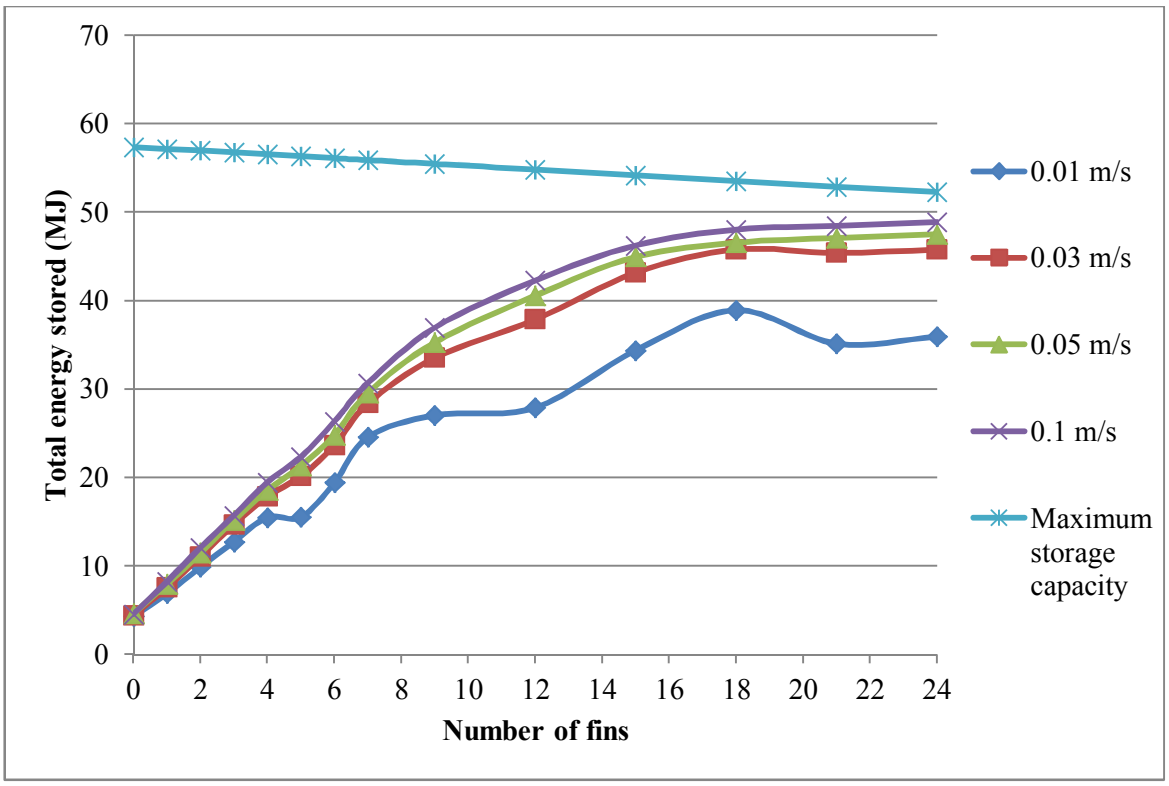

Fig. 5.25. Total energy stored for various HTF velocities as compared to the maximum storage capacity for 0 to 24 fins configuration of LHTES after simulated charging time of 12 hours.

The highest total energy that can be stored in the LHTES for the HTF of 0.05 and 0.1 m/s velocities are 47.5 MJ and 48.9 MJ respectively in the 24 fins configuration LHTES. While for HTF velocities of 0.01 and 0.03 m/s, their highest total energy stored is achieved in the 18 fins configuration with 38.9 MJ and 45.8 MJ respectively. The reason for the declining of total energy increase rate as the number of fins increases from 18 to 24 fins, as shown in Fig. 5.25 can be explained by referring to the melting fraction figure of Fig. 5.18 which illustrates that almost all of the PCM has been melted starting with the 18 fins configuration LHTES. Additionally, as expected the energy storage rate and the amount of melted PCM of the low HTF velocity of 0.01 m/s is smaller than the other higher HTF velocities.

Fig. 5.26 shows the LHTES performance efficiency for some of the 0 to 24 fins configuration for HTF of 0.01 m/s and 0.1 m/s velocities calculated by using the following equation:

$$\eta = \frac{E_{actual}}{E_{maximum}} \text{ x } 100\ \% \tag{5.7}$$

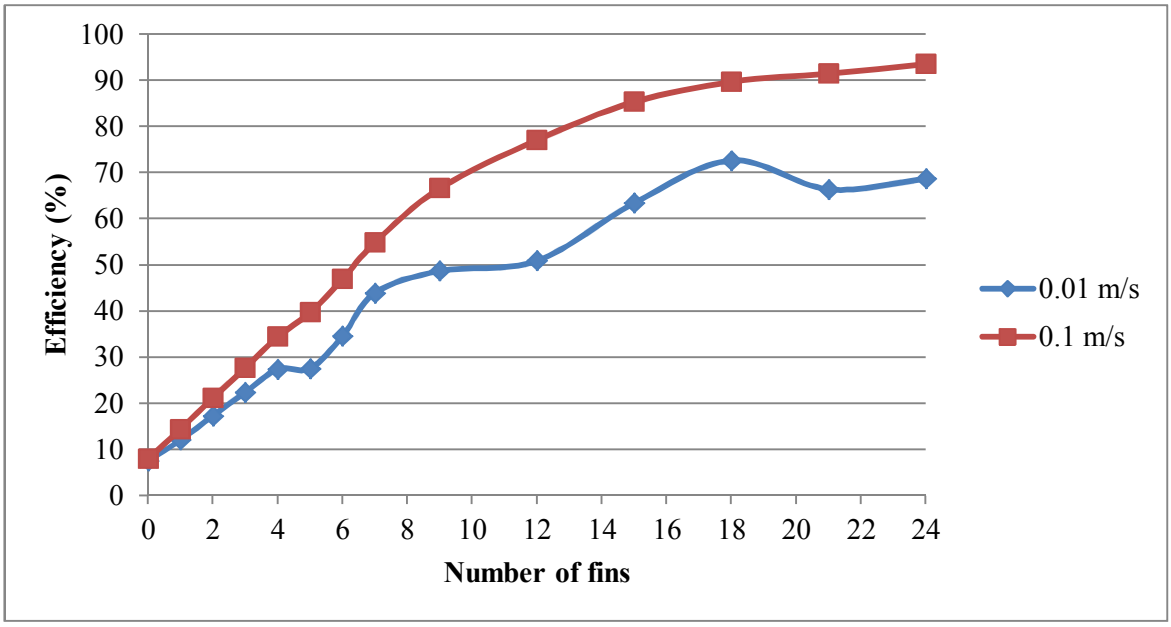

Fig. 5.26. Thermal energy storage efficiencies for various numbers of fins after 12 hours of simulated charging time. HTF velocities: 0.01 m/s and 0.1 m/s.

As shown, the efficiency for both of the HTF velocities increases with the addition of fins. The 0 fin configuration evidently has the lowest storage efficiencies having resulted to achieve only about 7.5 and 7.9% efficiencies for HTF velocities of 0.01 and 0.1 m/s respectively. Whereas, the highest recorded efficiency for both of the velocities is 93.5% efficiency for 0.1 m/s in the 24 fins configuration LHTES and 72.7% efficiency for 0.01 m/s obtained in the 18 fins configuration.

Referring to Fig. 5.25, for the LHTES that uses HTF velocity of 0.01 m/s; the device achieves the highest energy stored of 38.9 MJ with 18 fins configuration, which translates to 72.7% of storage efficiency. Increasing the number of fins does not result in any increase of total energy stored and storage efficiency, but the addition of fins shows that both plots in Figs. 5.25 and 5.26 suffered reductions.

In LHTES device that uses HTF velocity of 0.1 m/s, the numerical results show a gradual increase in total energy stored and storage efficiency. Furthermore, the addition of fins from 18 to 24 shows that the rates of increase for both plots in Figs. 5.25 and 5.26 are declining as the number of fins increases. Additionally, the total energy stored for 18 fins configuration with HTF velocity of 0.1 m/s is 48.1 MJ which translates to 89.7% of storage efficiency. Adding the total number of fins to 24 (33.33% increase), increases the total energy stored by only 0.9 MJ, or 1.8% of increase.

Thus, from the discussion and results shown, a latent heat thermal energy storage device with 18 fins configuration demonstrates a good balance between the storage performance efficiency, the total thermal energy storage capacity and the cost of material needed to manufacture the latent heat thermal energy storage system that uses paraffin wax as the medium.

CHAPTER 6

CONCLUSION

6.1 Conclusion

The effective heat capacity method has been studied and showed that it can be used to characterize the melting process of a phase change material. By using the modified heat capacity that changes its value when the temperature of the PCM is in the melting range of the paraffin wax (313K to 316K); the numerical problem of defining the non-linear characteristic of PCM heat capacity can be solved. The modified heat capacity has been incorporated successfully into the COMSOL software in order to study the effects of fins and heat transfer fluid velocities on the thermal behavior of the PCM. On the other hand, a slow heating zone (SHZ) was identified during the charging process. This area of the PCM volume is slower to receive heat due to the gap between the fins and the container. The higher thermal resistance of the SHZ area causes the PCM to melt slower which reduces the melting fraction of the PCM.

The HTF velocities of 0.01, 0.03, 0.05 and 0.1 m/s were used in the numerical analysis of LHTES for fin configurations of 0 to 24. After 12 hours of charging time, the sensible energy stored in the solid and liquid phase of the PCM demonstrates a steady increase as the HTF velocity increases. The results show that the minimum energy stored was recorded for the 0 fin configuration and HTF velocity of 0.01 m/s with 2.37 MJ. Whereas, the maximum sensible energy stored was achieved by the 24 fins configuration LHTES and HTF velocity of 0.1 m/s with 17.84 MJ. The latent energy stored during the melting process

of the PCM shows a steady increase as the number of fins increases from 0 to 12 and also across the various HTF velocities. However, the rate of increase of the latent energy stored in the PCM from 15 to 24 fins configurations declines and appears to be constant for 0.03 m/s to 0.1 m/s HTF velocities. LHTES with 0.01 m/s HTF velocity however shows an obvious reduction in latent heat contribution. This is caused by the increasing melted fraction of the PCM volume as the number of fins increases. The minimum latent energy stored was recorded for the 0 fin configuration and HTF velocity of 0.01 m/s with 1.97 MJ. Whereas, the maximum latent energy stored was achieve by the 24 fins configuration LHTES and HTF velocity of 0.1 m/s with 31.07 MJ. Overall, the effect of increasing HTF velocities on the thermal behavior of the PCM shows that the amount of energy that can be stored increases as the HTF velocity increases.

In the case pertaining to the effect of increasing the number of fins from 0 to 24 with HTF velocities of 0.01 m/s and 0.1 m/s, generally the total energy that can be stored increases as the number of fins increases. For the LHTES device that uses HTF velocity of 0.01 m/s, the minimum energy stored was recorded for the 0 fin configuration with 4.33 MJ. Whereas, the maximum energy stored was achieved for the 18 fin configuration LHTES with 38.93 MJ. The total energy stored in the higher number of fins shows a reduction due to the low HTF velocity which in turn lowers the heat transfer rate to the PCM, congregating most of the heat nearer to the inlet of the LHTES. Additionally, the minimum and maximum total energy stored for HTF velocity of 0.1 m/s are 4.6 MJ and 48.9 MJ for 0 and 24 fins configurations respectively.

The 0 fin configuration LHTES has the lowest storage efficiencies with only about 7.5 and 7.9% efficiencies for HTF velocities of 0.01 and 0.1 m/s respectively. The highest recorded

efficiency was recorded for the 24 fins configuration LHTES with 93.5% at HTF velocity of 0.1 m/s. The highest efficiency for HTF velocity of 0.01 m/s was achieved by the 18 fins configuration LHTES with 72.7%.

6.2 Recommendations

Future research studies may include the following recommendations:

1. The current study focuses only on the charging process of the PCM. Future studies can include the discharging or solidification process of the PCM.
2. The current study assumes that the effects of free convection during the melting process of the PCM are negligible. Further studies on employing free convection during the charging process of the PCM using simpler geometry can be explored.
3. Other types of fin geometries can be further explored to study their effects on the thermal behavior of the PCM.
4. The effects of fin thickness, height and gap between the fins and the container have a good research values and can be further explored using COMSOL software.
5. Experimental works on the LHTES can be carried out in order to validate the numerical analysis.

REFERENCES

ABHAT, A. 1983. Low temperature latent heat thermal energy storage: heat storage materials. *Solar Energy,* 30**,** 313-332.

ABHAT, A. et al., 1981. Development of a modular heat exchanger with an integrated latent heat storage. Report no. BMFT FBT 81-050. Germany Ministry of Science and Technology Bonn.

AGYENIM, F., HEWITT, N., EAMES, P. & SMYTH, M. 2010. A review of materials, heat transfer and phase change problem formulation for latent heat thermal energy storage systems (LHTESS). *Renewable and Sustainable Energy Reviews,* 14**,** 615-628.

AINSWORTH, M. & ODEN, J. T. 2000. A posteriori error estimation in finite element analysis, pure and applied mathematics. Wiley-Interscience.

ALEXIADES, V. & SOLOMON, A. D. 1992. Mathematical modeling of melting and freezing process. Washington, DC: Hemisphere Publishing Corporation.

ANICA, T. 2005. Experimental and numerical investigations of heat transfer during technical grade paraffin melting and solidification in a shell and tube latent thermal energy storage unit. *Solar Energy,* 79**,** 648-660.

AZPIAZU, M. N., MORQUILLAS, J. M. & VAZQUEZ, A. 2003. Heat recovery from a thermal energy storage based on the Ca(OH)2/CaO cycle. *Applied Thermal Engineering,* 23**,** 733-741.

BAYLIN, F. 1979. Low temperature thermal energy storage: a state of the art survey. Report no. SERI/RR/-54-164. Golden, Colorado, USA: Solar Energy Research Institute.

BECKETT, G., MACKENZIE, J. A. & ROBERTSON, M. L. 2001. A Moving Mesh Finite Element Method for the Solution of Two-Dimensional Stefan Problems. *Journal of Computational Physics,* 168**,** 500-518.

BENARD, C., GOBIN, G. & MARTINEZ, F. 1985. Melting in rectangular enclosures: experiments and numerical simulations. *J Heat Transfer,* 107**,** 794-802.

BENENSON, W., HARRIS, J. W. & STOCKER, H. 2000. Handbook of physics. New York: Springer-Verlag Inc.

BENLI, H. & DURMUS, A. 2009. Performance analysis of a latent heat storage system with phase change material for new designed solar collectors in greenhouse heating. *Solar Energy,* 83**,** 2109-2119.

BERTRAND, O., BINET, B., COMBEAU, H., COUTURIER, S., DELANNOY, Y., GOBIN, D., LACROIX, M., LE QUÉRÉ, P., MÉDALE, M., MENCINGER, J., SADAT, H. & VIEIRAF, G. 1999. Melting driven by natural convection. A comparison exercise: first results. *Int J Therm Sci,* 38**,** 5-26.

BINET, B. & LACROIX, M. 1998. Numerical study of natural-convection dominated melting inside uniformly and discretely heated rectangular cavities. *Numer Heat Transfer Part A,* 33**,** 207-224.

BISWAS, R. 1977. Thermal storage using sodium sulfate decahydrate and water. 99**,** 99-100.

BRENT, A. D., VOLLER, V. R. & REID, K. J. 1988. Enthalpy-porosity technique for modeling convection–diffusion phase change: application to the melting of a pure metal. *Numer Heat Transfer,* 13**,** 297-318.

BUDDHI, D. et al., 1988. Solar thermal storage systems using phase change materials. *Int J Energy Res,* 12**,** 547-555.
BUDDHI, D. & SAWHNEY, R. L. 1994. Proceedings on thermal energy storage and energy conversion, School of Energy and Environmental Studies, Devi Ahilya University, Indore, India.
CARSLAW, H. S. & JAGER, J. C. 1973. Conduction of heat in solids. Second ed. London: Oxford University Press.
CHARLSSON, B., STYMME, H. & WATTERMARK, G. 1979. An incongruent heat of fusion system CaCl26H2O made congruent through modification of chemical composition of the system. *Solar Energy,* 23**,** 333-350.
CHENG, W. L., MEI, B. J., LIU, Y. N., HUANG, Y. H. & YUAN, X. D. 2011. A novel household refrigerator with shape-stabilized PCM (Phase Change Material) heat storage condensers: An experimental investigation. *Energy,* 36**,** 5797-5804.
COMSOL 2011. COMSOL Multiphysics User's Guide. Version 4.2.
DEBORAH, A. K. & MICHAEL, K. J. 2005. Introduction to thermal and fluid engineering. New Jersey: John Wiley and Sons.
DUTIL, Y., ROUSSE, D. R., SALAH, N. B., LASSUE, S. & ZALEWSKI, L. 2011. A review on phase-change materials: Mathematical modeling and simulations. *Renewable and Sustainable Energy Reviews,* 15**,** 112-130.
ESEN, A. & KUTLUAY, S. 2004. A numerical solution of the Stefan problem with a Neumann-type boundary condition by enthalpy method. *Applied Mathematics and Computation,* 148**,** 321-329.
ETTOUNEY, H., ALATIQI, I., AL-SAHALI, M. & AL-HAJIRIE, K. 2006. Heat transfer enhancement in energy storage in sphericalcapsules filled with paraffin wax and metal beads. *Energy Conversion and Management,* 47**,** 211-228.
ETTOUNEY, H., EL-DESSOUKY, H. & AL-ALI, A. 2005. Heat transfer during phase change of paraffin wax stored in spherical shells. *J Sol Energy Eng,* 127**,** 357-366.
FARID, M. M. 1986. Solar energy storage with phase change. *J Sol Energy Res,* 4**,** 11-29.
FARID, M. M., HAMAD, F. A. & ABU-ARABI, M. 1998. Phase change cool storage using dimethyl-sulfoxide. *Energy Conversion and Management,* 39**,** 819-826.
FARID, M. M. & HUSIAN, R. M. 1990. An electrical storage heater using phase change method of heat storage. *Energy Conversion and Management,* 30**,** 219-230.
FARID, M. M. & KANZAWA, A. 1989. Thermal performance of a heat storage module using PCM's with different melting temperatures: mathematical modeling. *J Sol Energy Eng,* 111**,** 152-157.
FARID, M. M., KIM, Y. & KANZAWA, A. 1990. Thermal performance of heat storage module using PCM's with different melting temperatures: experimental. *J Sol Energy Eng,* 112**,** 125-131.
FLANDRO, G. A., MCMAHON, H. M. & ROACH, R. L. 2011. Basic aerodynamics: incompressible flow. Cambridge University Press.
FREUND, M., MÓZES, G. & JAKAB, E. 1982. Paraffin products: properties, technologies, applications. Amsterdam: Elsevier.
GARG, H. P., MULLICK, S. C. & BHARGAVA, A. K. 1985. *Solar thermal energy storage*, D. Reidel Publishing Co.
GEORGE, A. 1989. Hand book of thermal design. In: Guyer C, editor. Phase change thermal storage materials. McGraw Hill Book Co.
GHONEIM, A. A. 1989. Comparison of theoreticalmodels of phase-change and sensible heat storage for air and water-based solar heating systems. *Solar Energy,* 42**,** 209-220.

GO, Z., LIU, H. & LI, Y. 2004. Thermal energy recovery of air-conditioning system heat recovery system calculation and phase change material development. *Applied Thermal Engineering,* 24**,** 2511-2526.

GOODMAN, T. R. 1958. The heat balance integral and its application in problems involving a change. *Trans ASME,* 80**,** 335-342.

GROULX, D. & LACROIX, M. 2007. Study of the effect of convection on close contact melting of high Prandtl number substances. *International Journal of Heat and Mass Transfer,* 46**,** 213-220.

GROULX, D. & OGOH, W. 2009. Solid-liquid phase change simulation applied to a cylindrical latent heat energy storage system. *Proceedings of the COMSOL Conference 2009*.

GUPTA, S. C. 2003. The classical Stefan problem: Basic concepts, modelling and analysis.: Elsevier Science B.V.

HALAWA, E., BRUNO, F. & SAMAN, W. 2005. Numerical analysis of a PCM thermal storage system with varying wall temperature. *Energy Conversion and Management,* 46**,** 2592-2604.

HAMDAN, M. A. & ELWERR, F. A. 1996. Thermal energy storage using a phase change material. *Solar Energy,* 56**,** 183-189.

HASNAIN, S. 1998. Review on sustainable thermal energy storage technologies, Part I: heat storage materials and techniques. *Energy Conservation and Management,* 39**,** 1127-1138.

JIAN-YOU, L. 2008. Numerical and experimental investigation for heat transfer in triplex concentric tube with phase change material for thermal energy storage. *Solar Energy,* 82**,** 977-985.

JIJI, L. M. 2009a. Heat conduction. Third ed.: Springer-Verlag.

JIJI, L. M. 2009b. Heat convection. Second ed.: Springer-Verlag.

JONES, B. J., SUN, D., KRISHNAN, S. & GARIMELLA, S. V. 2006. Experimental and numerical study of melting in a cylinder. *international Journal of Heat and Mass Transfer,* 49**,** 2724-2738.

KEUNG, C. S. 1980. The use of sources and sinks in solving two dimension conduction problem with change of phase in arbitrary domains. Ph.D. dissertation, Columbia University, New York.

KUZNIK, F., VIRGONE, J. & NOEL, J. 2008. Optimization of a phase change material wall-board for building use. *Applied Thermal Engineering,* 28**,** 1291-1298.

LACROIX, M. 1989. Computation of heat transfer during melting of a pure substance from an isothermal wall. *Numer Heat Transfer Part B,* 15**,** 191-210.

LACROIX, M. 2001. Contact melting of a phase change material inside a heated parallelepedic capsule. *Energy Conversion and Management,* 42**,** 35-44.

LACROIX, M. & BENMADDA, M. 1998. Analysis of natural convection melting from a heated wall with vertically oriented fins. *Int J Numer Methods Heat Fluid Flow,* 8**,** 465-478.

LACROIX, M. & VOLLER, V. R. 1990. Finite different solutions of solidification phase change problems: transformed versus fixed grids. *Numer Heat Transfer Part B,* 17**,** 25-41.

LAMBERG, P., LEHTINIEMI, R. & HENELL, A. M. 2004. Numerical and experimental investigation of melting and freezing processes in phase change material storage. *International Journal of Thermal Sciences,* 43**,** 277-87.

LAMBERG, P. & SIREN, K. 2003. Analytical model for melting in a semi-infinite PCM storage with an internal fin. *Heat Mass Transf,* 39**,** 167-176.

LANE, G. A. 1983. Solar heat storage-latent heat materials. Boca Raton, FL: CRC Press Inc.

LANE, G. A. et al., 1978. Macro-encapsulation of PCM. Report no. ORO/5117-8. Midland, Michigan: Dow Chemical Company.

LANE, G. A. & ROSSOW, H. E. 1976. Encapsulation of heat of fusion storage materials. In: Proceedings of the second south eastern conference on application of solar energy. 442-455.

LAUARDINI, V. J. 1981. Heat transfer in cold climates New York: Pub. Van Nostrand.

LIU, C. & GROULX, D. 2011. Numerical study of the effect of fins on the natural convection driven melting of phase change material. In: Proceedings of COMSOL conference. Boston.

LIU, Z. & CHUNG, D. D. L. 2005. Calorimetric evaluation of phase change materials use as thermal interface materials. *Thermo Chemical Acta,* 366**,** 135-147.

LIU, Z., SUN, X. & MA, C. 2005. Experimental study of the characteristics of solidification of stearic acid in an annulus and its thermal conductivity enhancement. *Energy Conversion and Management,* 46**,** 971-984.

MACKENZIE, J. A. & MEKWI, W. R. 2007. Adaptive computations: theory and algorithms. *In:* TANG, T. & XU, J. (eds.) *On the use of moving mesh methods to solve PDEs.* Beijing: Science Press.

MASSOUD, K. 2002. Principles of heat transfer. New York: John Wiley and Sons.

MORISSON & ABDEL-KHALIK 1978. Effects of phase-change energy storage on the performance of air-based and liquid-based solar heating systems. *Solar Energy,* 20**,** 57-67.

NATERER, G. F. 2003. Heat transfer in single and multiphase systems. Boca Raton, Florida: CRC Press LLC.

NAYAK, K. C., SAHA, S. K. & DUTTA, P. 2006. A numerical model for heat sinks with PCMs and thermal conductivity enhancers. *international Journal of Heat and Mass Transfer,* 49**,** 1833-1844.

PRAKASH, J., GARG, H. P. & DATTA, G. 1985. A solar water heater with a built-in latent heat storage. *Energy Conversion and Management,* 25**,** 51-56.

PROVATAS, N., GOLDENFELD, N. & DANTZIG, J. 1999. Adaptive mesh refinement computation of solidification microstructures using dynamic data structures. *J Comput Phys,* 148**,** 265-290.

REDDY, K. S. 2007. Thermal modeling of PCM-based solar integrated collector storage water heating system. *J Sol Energy Eng,* 129**,** 458-464.

REGIN, A. F., SOLANKI, S. C. & SAINI, J. S. 2008. Heat transfer characteristics of thermal energy storage system using PCM capsules: A review. *Renewable and Sustainable Energy Reviews,* 12**,** 2438-2458.

ROSEN, M. A. & DINCER, I. 2003. Energy methods for assessing and comparing thermal storage systems. *International Journal of Energy Research,* 27**,** 415-430.

SAITOH, T. S. & MOON, J. H. 1998. An experimental study for combined close-contact and natural convection melting in a spherical capsule. *International Journal of Fluid Mechanics Research,* 25**,** 220-229.

SAMAN, W., BRUNO, F. & HALAWA, E. 2005. Thermal performance of PCM thermal storage unit for a roof integrated solar heating system. *Solar Energy,* 78**,** 341-349.

SCHWARTZ, M. M. 2002. Encyclopedia of Materials, Parts, And Finishes. Second ed.: CRC Press.

SEENIRAJ, R. V., VELRAJ, R. & NARASIMHAN, N. L. 2002. Thermal analysis of a finned-tube LHTS module for a solar dynamic power system. *Heat Mass Transf,* 38**,** 409-417.

SHAMSUNDAR, N. & SPARROW, E. M. 1975. Analysis of multidimensional conduction phase change via the enthalpy model. *J Heat Transfer,* 97**,** 333-340.

SHAMSUNDAR, N. & SPARROW, E. M. 1976. Effect of density change on multidimensional conduction phase change. *J Heat Transfer,* 98**,** 550-557.

SHARMA, A., TYAGI, V. V., CHEN, C. R. & BUDDHI, D. 2009. Review on thermal energy storage with phase change materials and applications. *Renewable and Sustainable Energy Reviews,* 13**,** 318-345.

SHUKLA, A., BUDDHI, D. & SAWHNEY, R. L. 2009. Solar water heaters with phase change material thermal energy storage medium: a review. *Renewable and Sustainable Energy Reviews,* 13**,** 2119-2125.

SIMPSON, J. E. & GARIMELLA, S. V. 1998. An investigation of the solutal, thermal and flow fields in unidirectional alloy solidification. *International Journal of Heat and Mass Transfer,* 41**,** 2485-2502.

SPARROW, E. M. & HSU, C. F. 1981. Analysis of two-dimensional freezing on the outside of a coolant-carrying tube. *International Journal of Heat and Mass Transfer,* 24**,** 1345-1357.

STEFAN, J. 1891. Uber die theorie der eisbildung imbesondee uber die eisbindung im polarmeere. *Ann. Phys. U. Chem.,* 42**,** 269-286.

STRITIH, U. 2004. An experimental study of enhanced heat transfer in rectangular PCM thermal storage. *International Journal of Heat and Mass Transfer,* 47**,** 2841-2847.

SUNA, D., ANNAPRAGADAB, S. R. & GARIMELLA, S. V. 2009. Experimental and numerical study of melting of particle-laden materials in a cylinder. *International Journal of Heat and Mass Transfer,* 52**,** 2966-2978.

SUWONDO, A., MANSOORI, G. & HIRAN, S. 1994. Characterization of alkanes and paraffin waxes for application as phase change energy storage medium. *Energy Sources,* 16**,** 117-128.

TAN, Z., LIM, K. M. & KHOO, B. C. 2007. An adaptive mesh redistribution method for the incompressible mixture flows using phase-field model. *J Comput Phys,* 225**,** 1137-1158.

TELKES, M. 1975. Thermal storage for solar heating and cooling. In: Proceedings of the workshop on solar energy storage sub-systems for heating and cooling of buildings. University of Virginia, Charlottesville.

TYAGI, V. V. & BUDDHI, D. 2007. PCM thermal storage in buildings: a state of art. *Renewable and Sustainable Energy Reviews,* 11**,** 1146-1166.

VOLLER, V. R. 1990. Fast implicit finite-difference method for the analysis of phase change problems. *Numer Heat Transfer Part B,* 17**,** 155-169.

WANG, Y., AMIRI, A. & VAFAI, K. 1999. An experimental investigation of the melting process in a rectangular enclosure. *International Journal of Heat and Mass Transfer,* 42**,** 3639-3642.

YEH, L. T. & CHUNG, B. T. 1975. Solidification and melting of material subjected to convection and radiation. *J Space Cr Rockets,* 12**,** 329-334.

ZALBA, B., MARIN, J. M., CABEZA, L. F. & MEHLING, H. 2003. Review on thermal energy storage with phase change: materials, heat transfer analysis and applications. *Applied Thermal Engineering,* 23**,** 251-283.

ZHANG, Y. & FAGHRI, A. 1996. Heat transfer enhancement in latent heat thermal energy storage system by using the internally finned tube. *International Journal of Heat and Mass Transfer,* 39**,** 3165-3173.

APPENDIX A

Temperature Distribution Plots as a Function of Heat Transfer Fluid Velocities

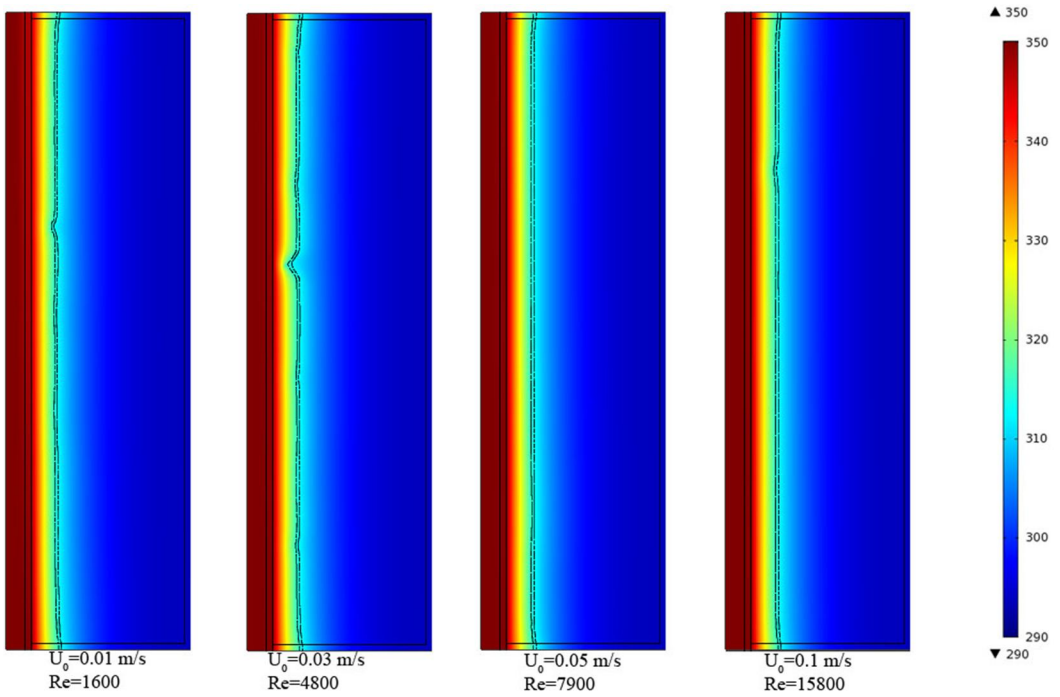

Fig. A.1. Temperature distribution plots for 0 fin configuration LHTES with various HTF velocities and their Reynolds numbers. Simulated time: 12 hours.

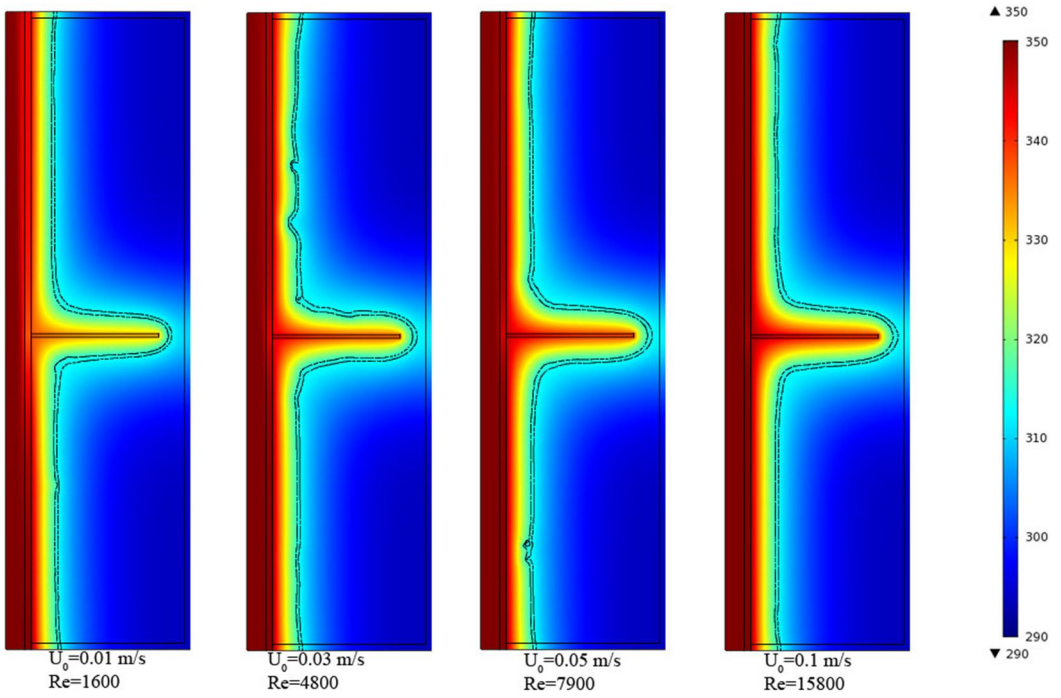

Fig. A.2. Temperature distribution plots for 1 fin configuration LHTES with various HTF velocities and their Reynolds numbers. Simulated time: 12 hours.

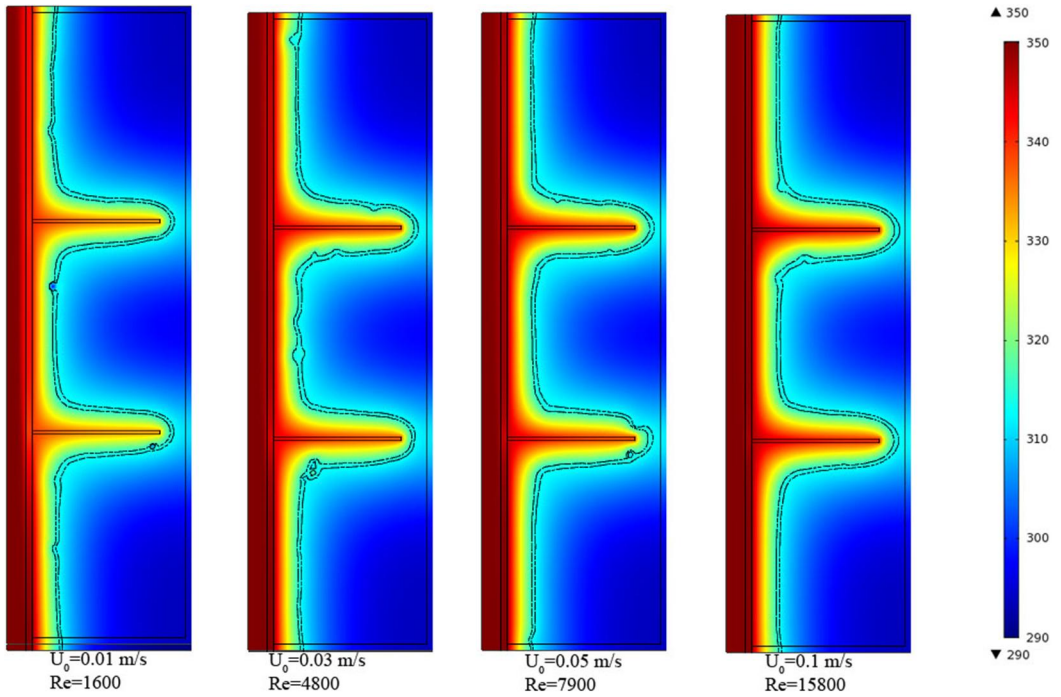

Fig. A.3. Temperature distribution plots for 2 fins configuration LHTES with various HTF velocities and their Reynolds numbers. Simulated time: 12 hours.

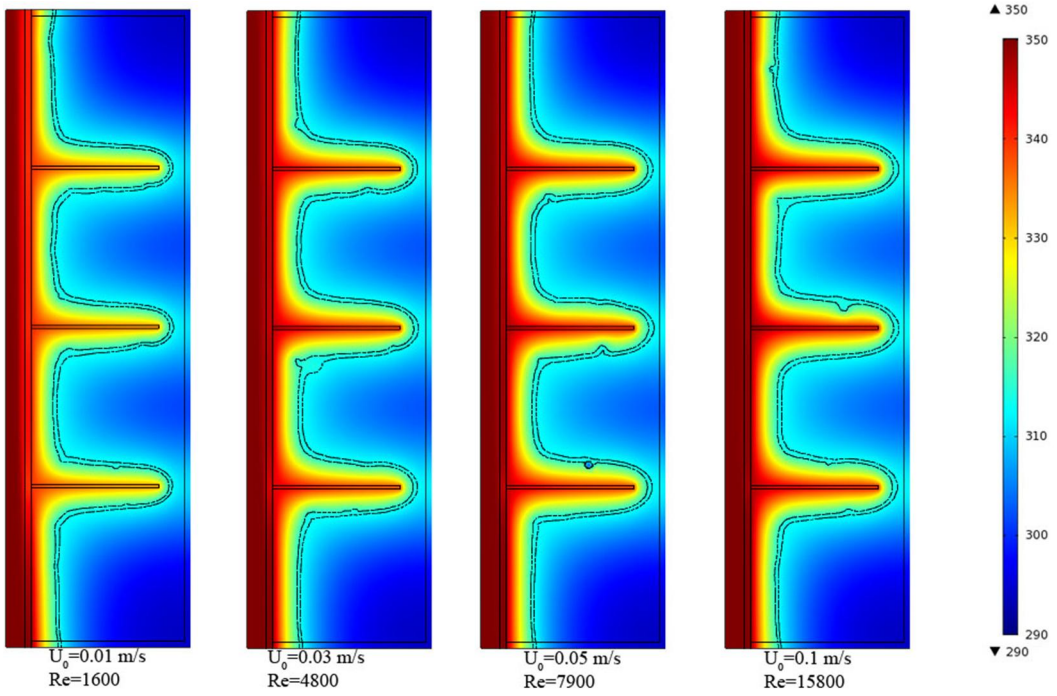

Fig. A.4. Temperature distribution plots for 3 fins configuration LHTES with various HTF velocities and their Reynolds numbers. Simulated time: 12 hours.

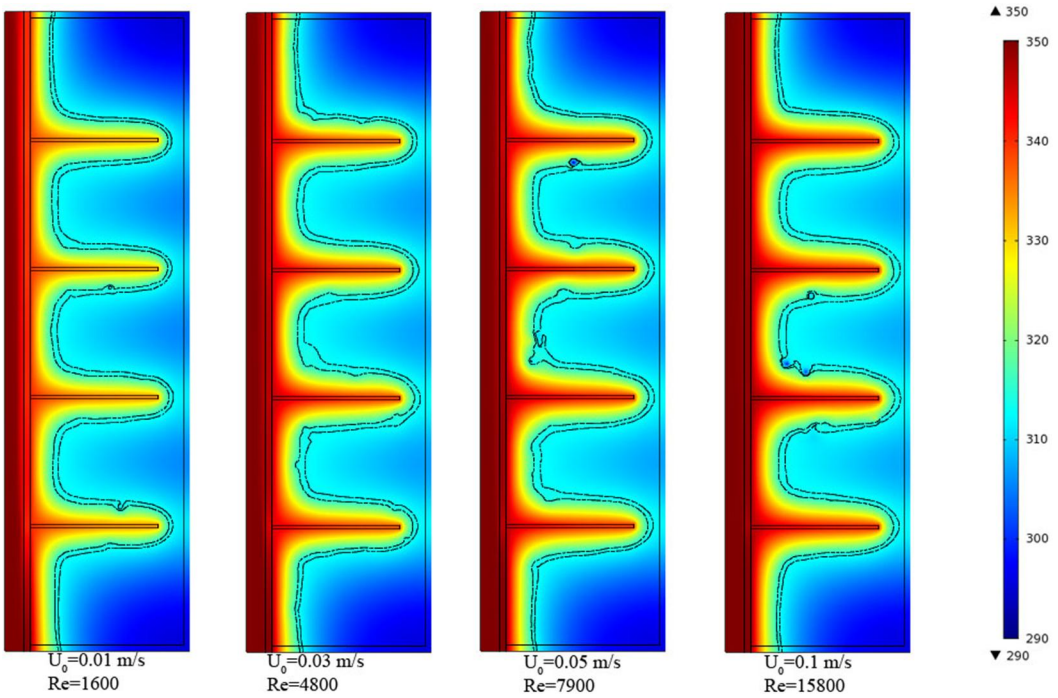

Fig. A.5. Temperature distribution plots for 4 fins configuration LHTES with various HTF velocities and their Reynolds numbers. Simulated time: 12 hours.

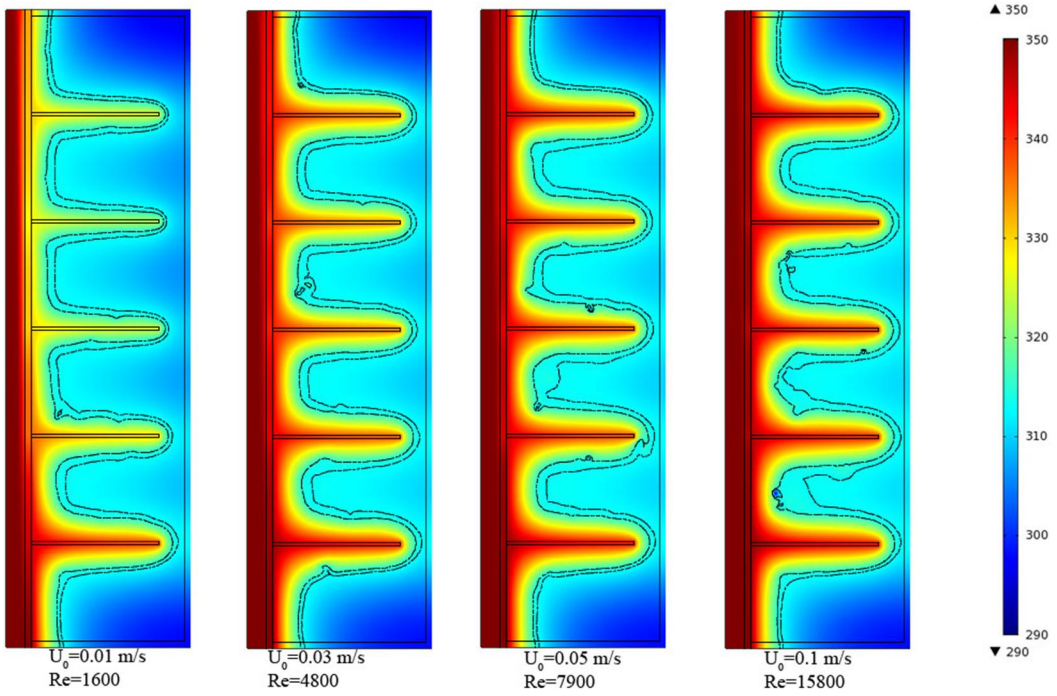

Fig. A.6. Temperature distribution plots for 5 fins configuration LHTES with various HTF velocities and their Reynolds numbers. Simulated time: 12 hours.

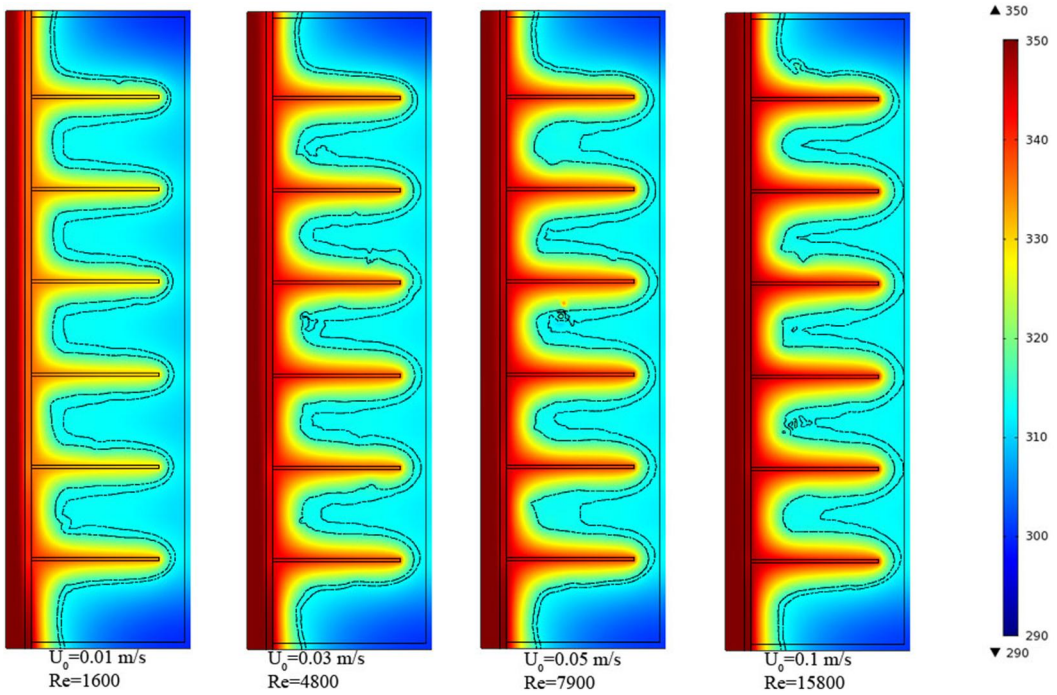

Fig. A.7. Temperature distribution plots for 6 fins configuration LHTES with various HTF velocities and their Reynolds numbers. Simulated time: 12 hours.

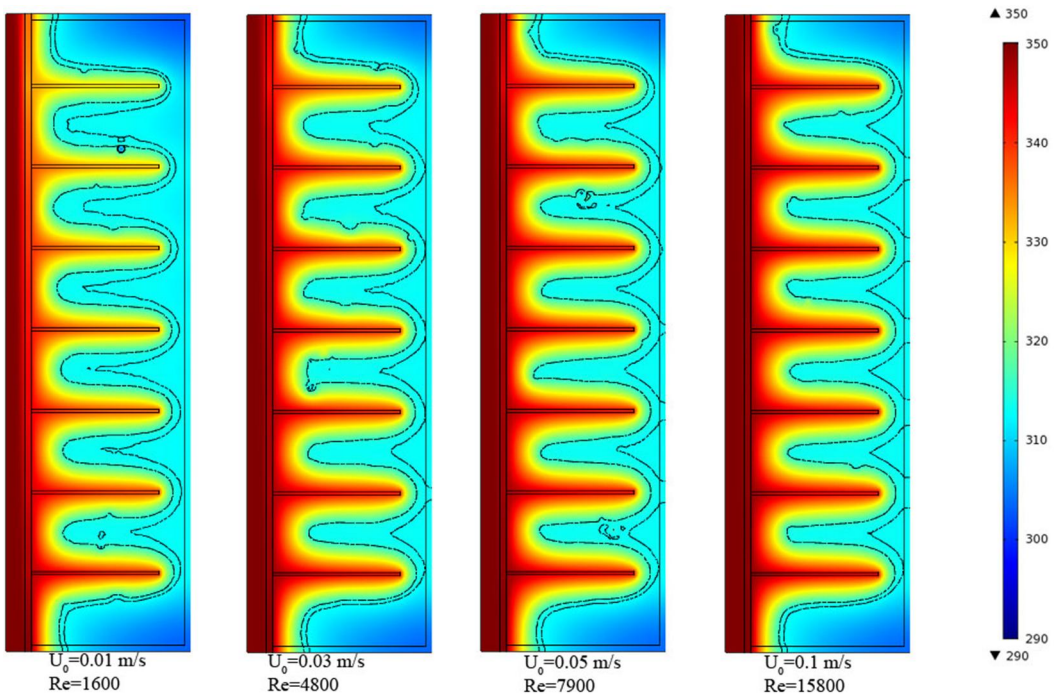

Fig. A.8. Temperature distribution plots for 7 fins configuration LHTES with various HTF velocities and their Reynolds numbers. Simulated time: 12 hours.

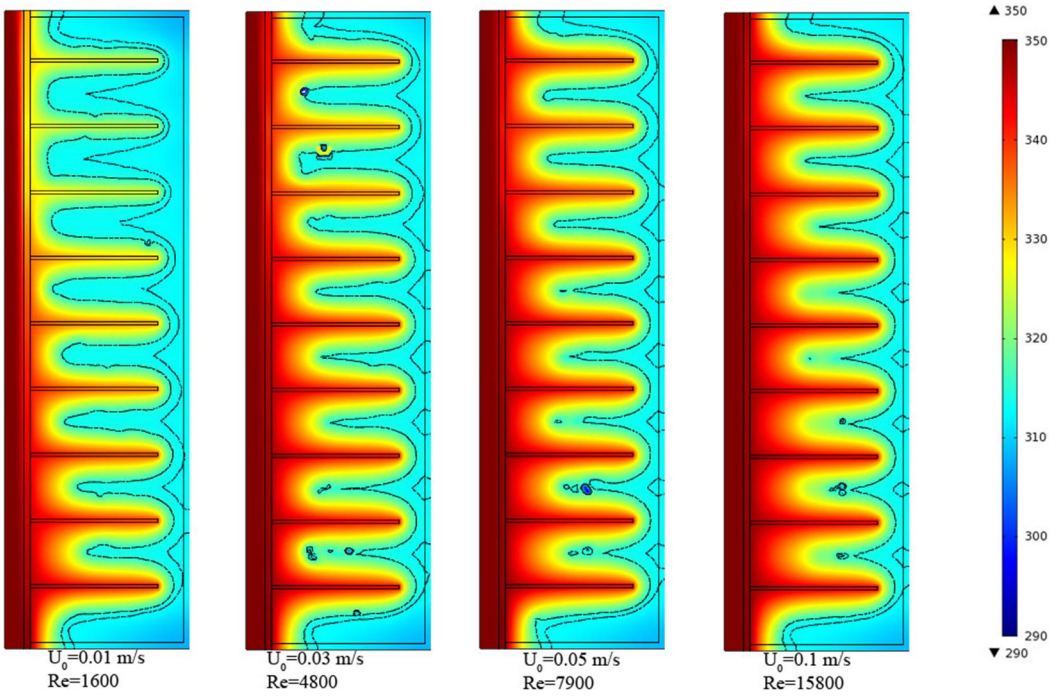

Fig. A.9. Temperature distribution plots for 9 fins configuration LHTES with various HTF velocities and their Reynolds numbers. Simulated time: 12 hours.

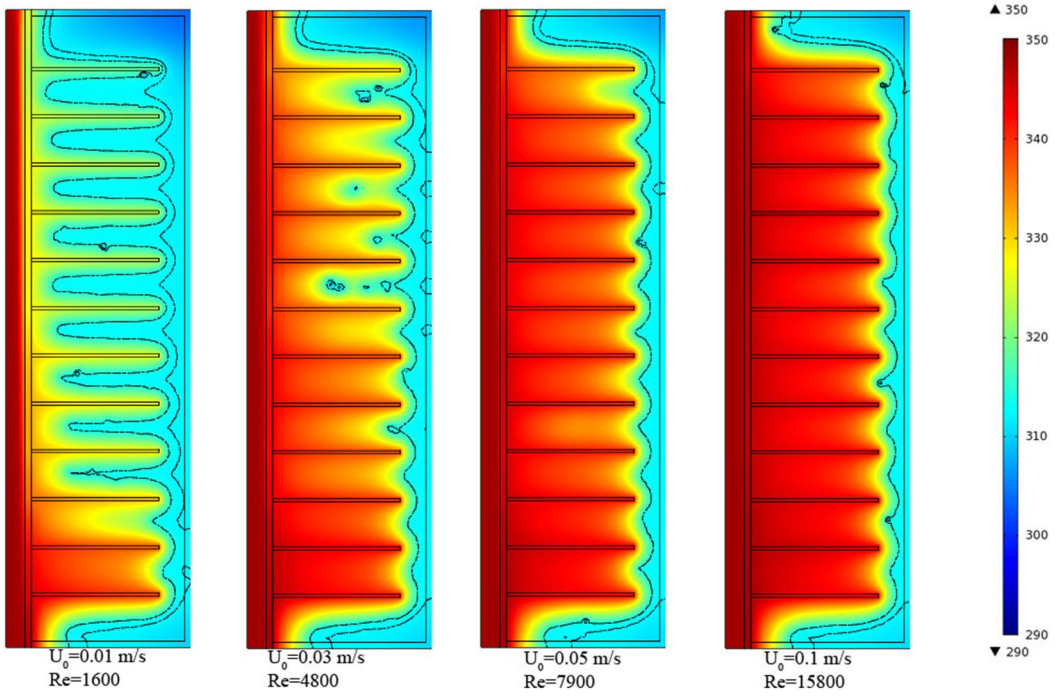

Fig. A.10. Temperature distribution plots for 12 fins configuration LHTES with various HTF velocities and their Reynolds numbers. Simulated time: 12 hours.

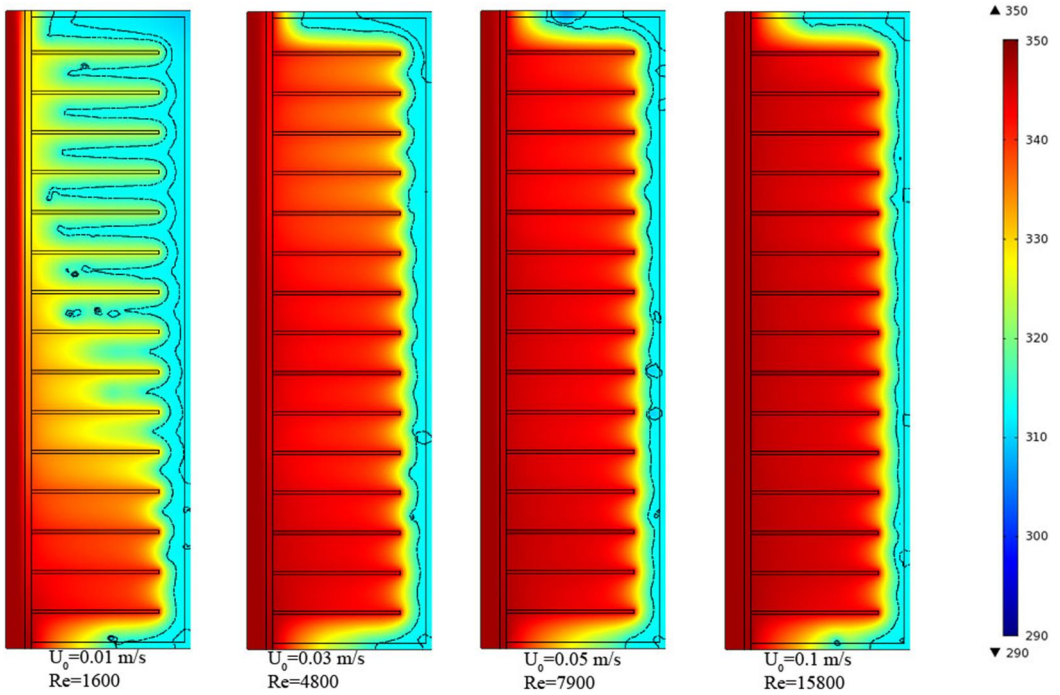

Fig. A.11. Temperature distribution plots for 15 fins configuration LHTES with various HTF velocities and their Reynolds numbers. Simulated time: 12 hours.

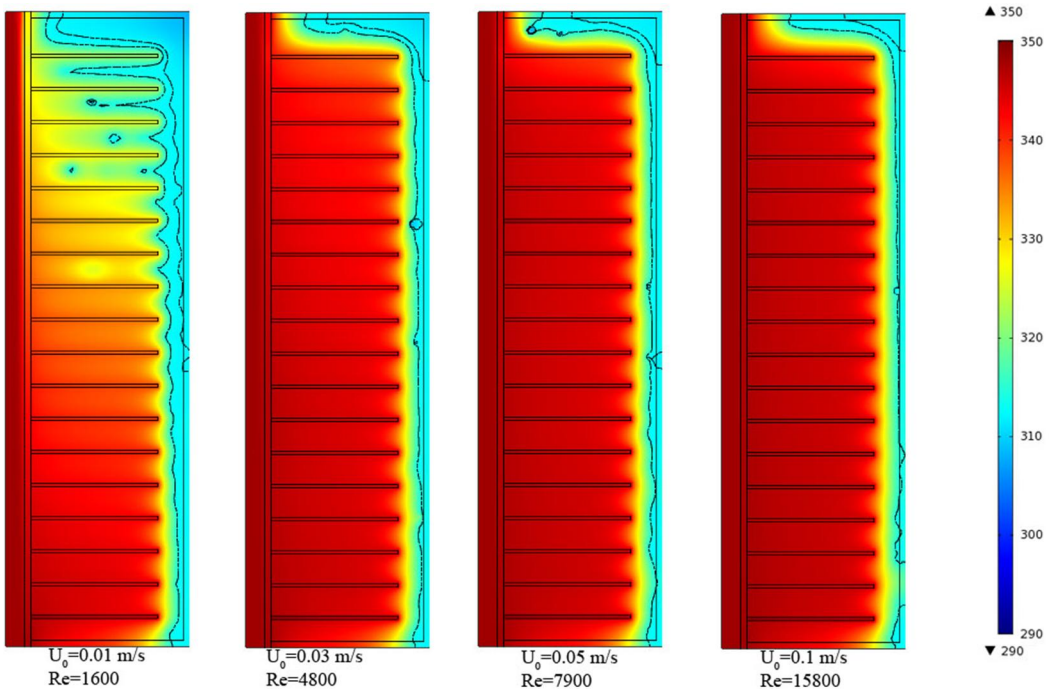

Fig. A.12. Temperature distribution plots for 18 fins configuration LHTES with various HTF velocities and their Reynolds numbers. Simulated time: 12 hours.

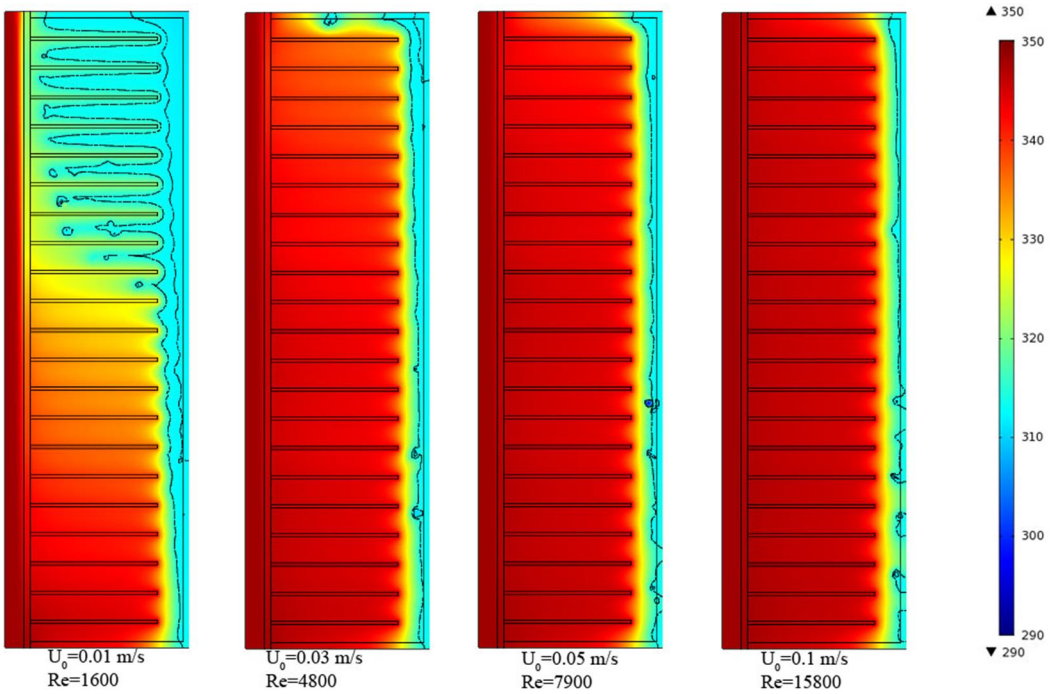

Fig. A.13. Temperature distribution plots for 21 fins configuration LHTES with various HTF velocities and their Reynolds numbers. Simulated time: 12 hours.

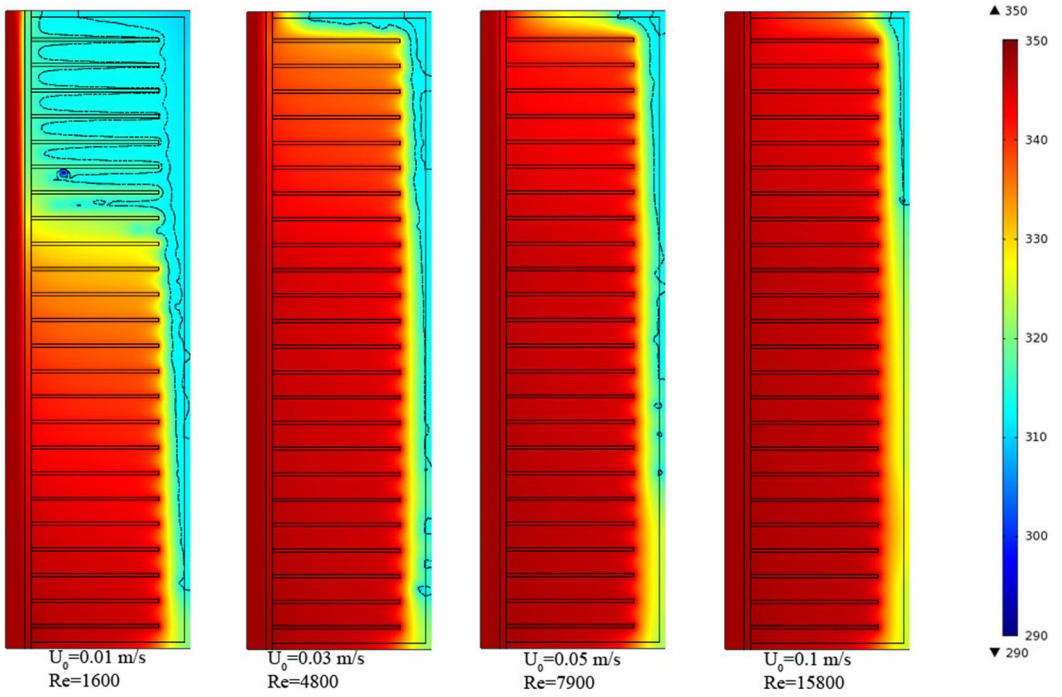

Fig. A.14. Temperature distribution plots for 24 fins configuration LHTES with various HTF velocities and their Reynolds numbers. Simulated time: 12 hours.

APPENDIX B

Temperature Distribution Plots as a Function of Number of Fins for HTF Velocity of 0.01 m/s

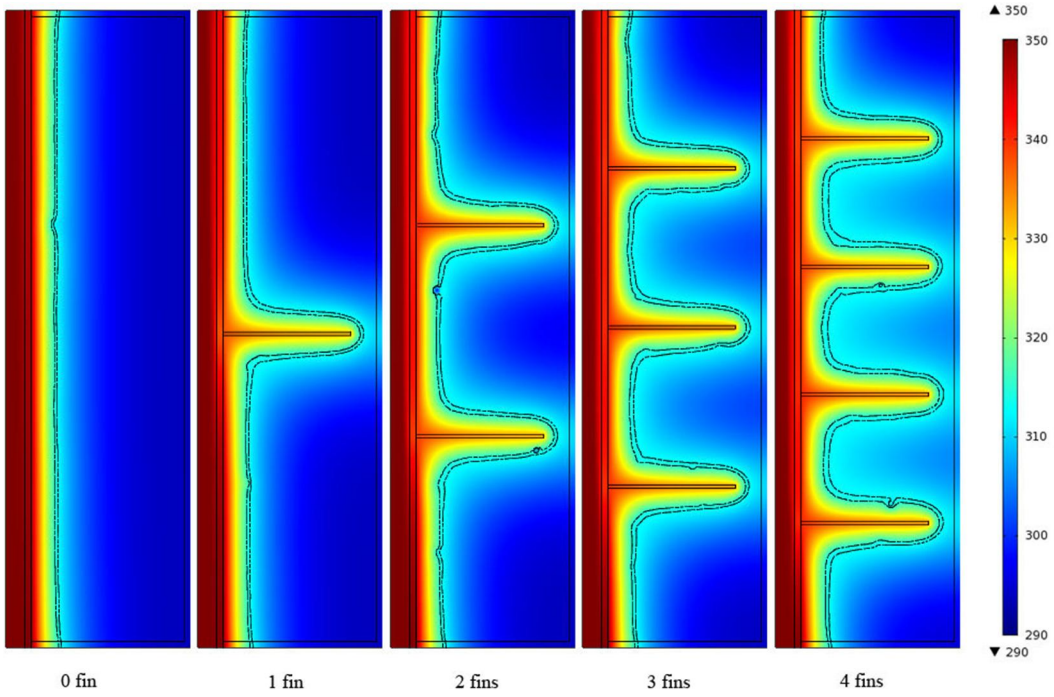

Fig. B.1. Temperature distribution plots for the 0, 1, 2, 3 and 4 fins configuration LHTES after 12 hours of simulated charging time. u_0= 0.01 m/s.

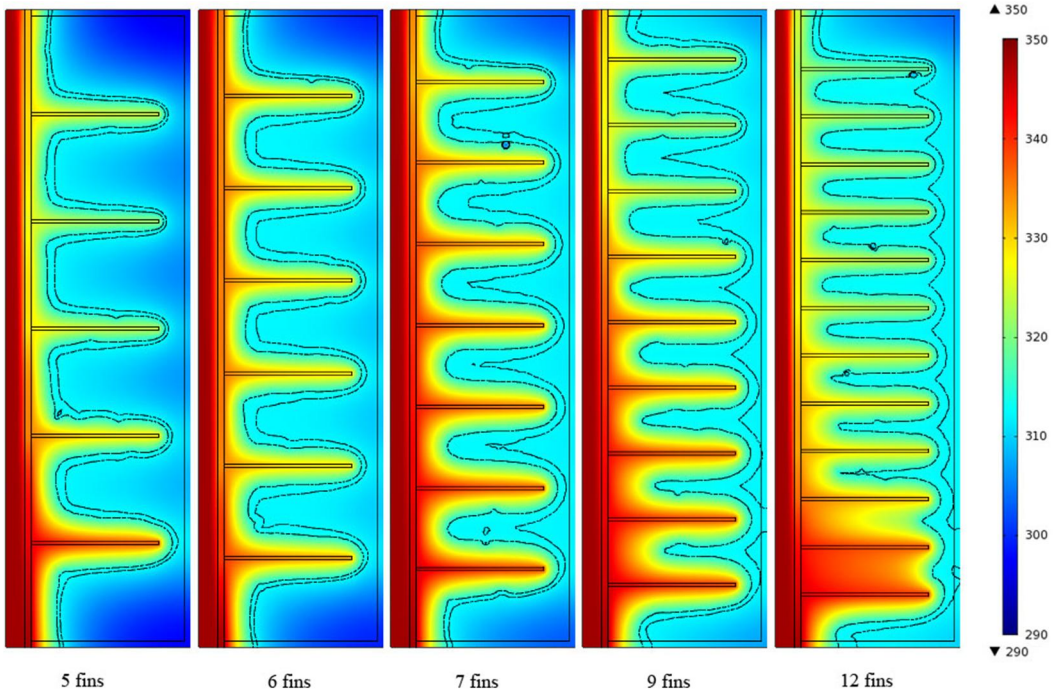

Fig. B.2. Temperature distribution plots for the 5, 6, 7, 9 and 12 fins configuration LHTES after 12 hours of simulated charging time. u_0= 0.01 m/s.

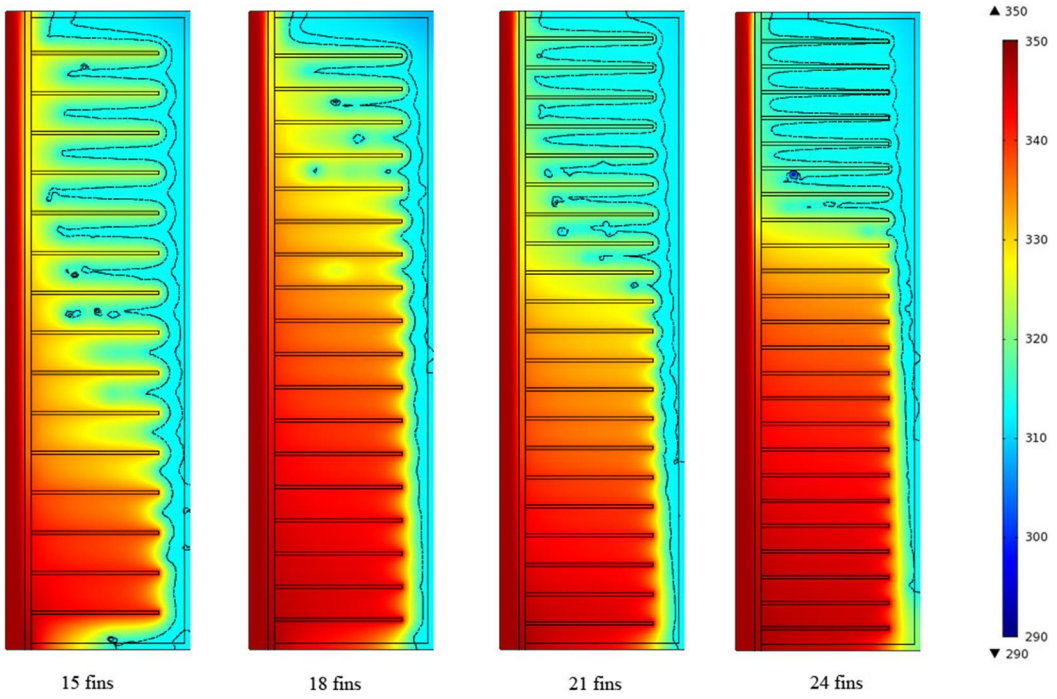

Fig. B.3. Temperature distribution plots for the 15, 18, 21 and 24 fins configuration LHTES after 12 hours of simulated charging time. u_0= 0.01 m/s.

APPENDIX C

Temperature Distribution Plots as a Function of Number of Fins for HTF Velocity of 0.1 m/s

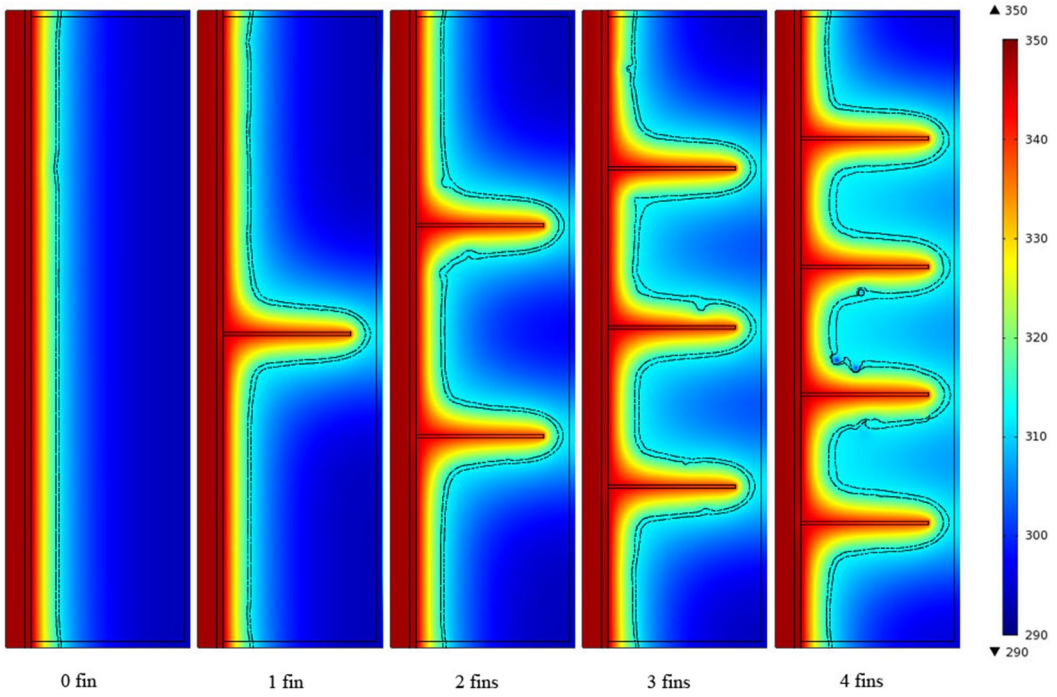

Fig. C.1. Temperature distribution plots for the 0, 1, 2, 3 and 4 fins configuration LHTES after 12 hours of simulated charging time. u_0= 0.1 m/s.

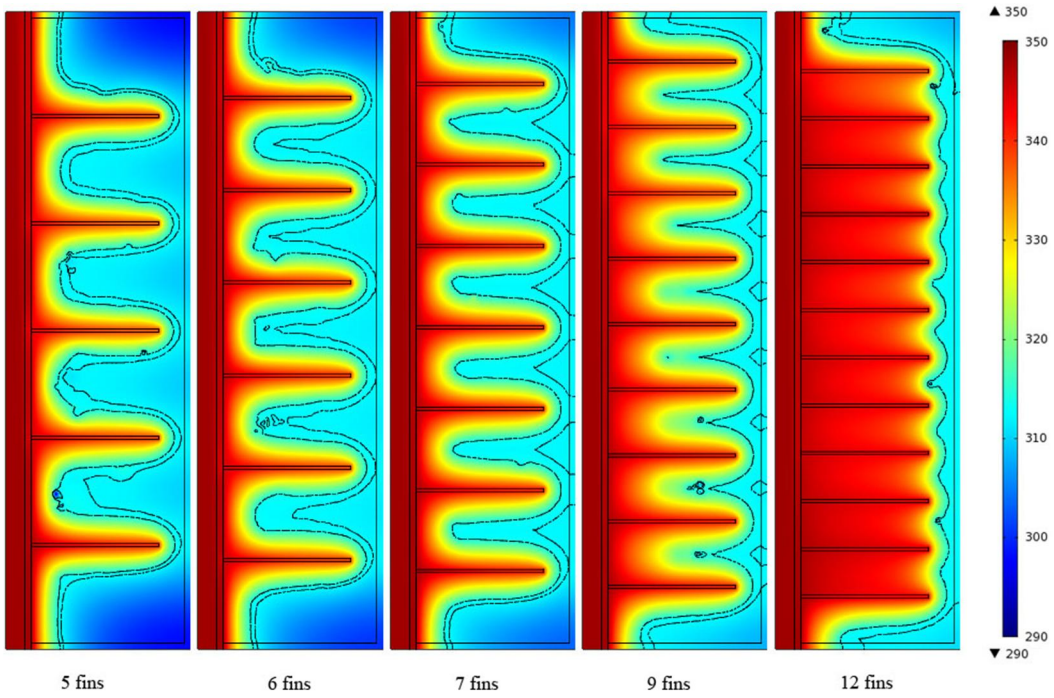

Fig. C.2. Temperature distribution plots for the 5, 6, 7, 9 and 12 fins configuration LHTES after 12 hours of simulated charging time. u_0= 0.1 m/s.

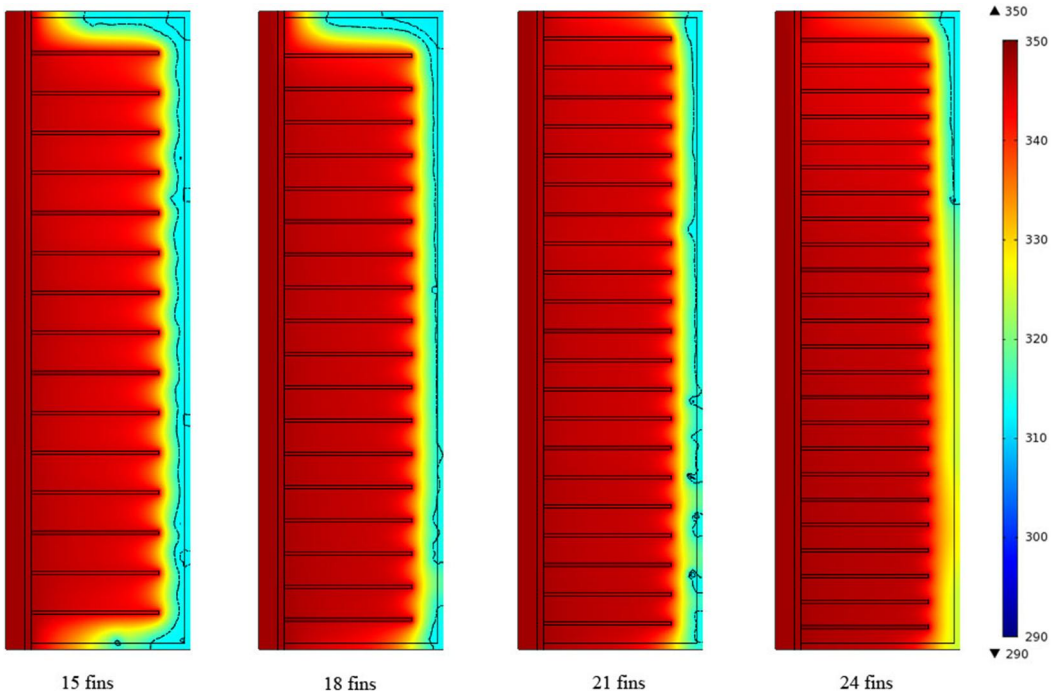

Fig. C.3. Temperature distribution plots for the 15, 18, 21 and 24 fins configuration LHTES after 12 hours of simulated charging time. u_0= 0.1 m/s.